JULIENE DOS REIS MOREIRA

CLONING AND FUNCTIONAL CHARACTERIZATION OF THE *OBSCURAVENOSA* GENE IN TOMATO (*Solanum lycopersicum* L.)

Thesis submitted to the Plant Physiology Graduate Program of the Universidade Federal de Viçosa as part of the requirements for obtaining the degree of *Doctor Scientiae*.

Adviser: Agustin Zsögön

VIÇOSA - MINAS GERAIS
2020

Ficha catalográfica elaborada pela Biblioteca Central da Universidade Federal de Viçosa - Campus Viçosa

T
M838c
2020

Moreira, Juliene dos Reis, 1992-
Cloning and functional characterization of the *OBSCURAVENOSA* gene in tomato (*Solanum lycopersicum* L.) / Juliene dos Reis Moreira. – Viçosa, MG, 2020.
1 tese eletrônica (126 f.): il. (algumas color.).

Inclui anexos.
Orientador: Agustin Zsögön.
Tese (doutorado) - Universidade Federal de Viçosa.
Inclui bibliografia.
DOI: https://doi.org/10.47328/ufvbbt.2021.137
Modo de acesso: World Wide Web.

1. Folhas - Fisiologia. 2. Análise foliar. 3. Auxinas. 4. Clonagem molecular. I. Universidade Federal de Viçosa. Departamento de Biologia Vegetal. Programa de Pós-Graduação em Fisiologia Vegetal. II. Título.

CDD 22. ed. 575.573952

Bibliotecário(a) responsável: Renata de Fátima Alves CRB6/2578

JULIENE DOS REIS MOREIRA

CLONING AND FUNCTIONAL CHARACTERIZATION OF THE *OBSCURAVENOSA* GENE IN TOMATO (*Solanum lycopersicum* L.)

Thesis submitted to the Plant Physiology Graduate Program of the Universidade Federal de Viçosa as part of the requirements for obtaining the degree of *Doctor Scientiae*.

APPROVED: December 22th, 2020.

Assent:

Juliene dos Reis Moreira
Juliene dos Reis Moreira
Author

Agustin Zsögön
Adviser

ACKNOWLEDGMENTS

I thank God for my life, for always being by my side showing me that I will never be alone.

I thank my family for support, especially my grandmother and mother, who are for me an example and inspiration of strength and dedication.

To my laboratory friends: Emmanuel, Suzy, Jessenia, Bruno, and João Victor for the company at all times, for the good laughs and advice.

To all my colleagues from the plant physiology graduate program, for the conversations, help and companionship, especially in the last few months.

To the Universidade Federal de Viçosa and the Plant Physiology Program, for the infrastructure for the development of this work. Thanks also to CAPES, for my scholarship. This study was financed in part by the Coordenação de Aperfeiçoamento de Pessoal de Nível Superior – Brasil (CAPES) – Finance Code 001.

To Prof. Agustin Zsögön for the guidance and teachings during project development.

To all the collaborating professors involved in this project, Prof. Wagner Otoni, Prof. Joni Lima and Prof. Lázaro Peres.

I especially thank Prof. Magdalena Rossi and Dr. Bruno Lira for receiving me in their laboratory to perform a part of this work, for the attention and for all I learned with them.

ABSTRACT

MOREIRA, Juliene dos Reis, D.Sc., Universidade Federal de Viçosa, December, 2020. **Cloning and Functional Characterization of the *OBSCURAVENOSA* Gene in Tomato (*Solanum lycopersicum* L.)**. Adviser: Agustin Zsögön.

Heterobaric and homobaric leaves are found in many plant families and have a remarkable distribution in nature. What differentiates these two types of leaves is the presence or absence of bundle sheath extensions (BSEs), a structural trait which produces different physiological responses. Leaves with BSEs (heterobaric) have greater hydraulic integration and greater photosynthetic performance, on the other hand, leaves without BSEs (homobaric) have uniform photosynthesis along the blade and probably an improved mechanism to control water loss under stress conditions. Tomatoes currently cultivated were selected after long years of crop breeding. Originally, tomato is a heterobaric crop, however, most field cultivars have a spontaneous recessive mutation known as *obscuravenosa* (*obv*) and, as a consequence, have lost the BSEs. For several years, this mutation was unconsciously selected in conjunction with other traits of agronomic interest. This suggests that the variation between homobaric and heterobaric characters has agronomic value in tomato. The first step to better understand the impacts of BSE at the plant level and to be able to manipulate it within the tomato crop and in other crops is knowing the genes involved in its formation. For this, we use tomato as a model to elucidate the molecular bases that control the development of BSEs. Using publicly available resources combined with *in silico* analysis, we identified a strong candidate gene for the *obv* mutation. Solyc05g054030 has a SNP (A→G) in the third exon, which leads to the exchange of a histidine residue for arginine at position 135 of the protein. The gene encodes a zinc finger transcription factor C2H2 type. We have shown through predictions that the OBV protein has three classic zinc finger domains, which allow interaction with DNA. In the *obv* mutant, the exchange of histidine for arginine caused the loss of a zinc finger motif, which may have led to the interruption of the protein functionality. We complemented the *obv* mutant with the functional *OBV* allele recovering the clear vein phenotype. *OBV* further regulates the leaf insertion angle, leaf serration, vein density and fruit shape. *OBV* appears to coordinate the development of BSEs through an auxin-mediated mechanism, specifically by changes in some members involved in auxin signaling (ARFs and Aux/IAAs). We have identified a link

between *OBV* and *AUXIN RESPONSE FACTOR 4* (*ARF4*). The findings reported here will give support for identification of other components linked to the molecular pathway that directs the formation of BSEs in leaves.

Keywords: Bundle Sheath Extension. Heterobaric leaf. Molecular cloning. Auxin.

RESUMO

MOREIRA, Juliene dos Reis, D.Sc., Universidade Federal de Viçosa, dezembro de 2020. **Clonagem e Caracterização Funcional do Gene *OBSCURAVENOSA* em Tomate (*Solanum lycopersicum* L.)**. Orientador: Agustin Zsögön.

Folhas heterobáricas e homobáricas são encontradas em muitas famílias de plantas e têm uma interessante distribuição na natureza. O que diferencia esses dois tipos de folhas é a presença ou ausência de extensões de bainha do feixe (BSEs), essa diferença estrutural confere respostas fisiológicas distintas. Folhas com BSEs (heterobáricas) apresentam maior integração hidráulica e maior desempenho fotossintético, por outro lado, folhas sem BSEs (homobáricas) possuem fotossíntese uniforme ao longo da lâmina e provavelmente um mecanismo aprimorado para controlar a perda de água em condições de estresse. Os tomates cultivados atualmente foram selecionados após longos anos de melhoramento genético. Originalmente o tomate é uma cultura heterobárica, porém, a maioria das cultivares de campo possuem uma mutação recessiva espontânea conhecida como *obscuravenosa* (*obv*) e, como consequência, perderam a BSE. Por vários anos essa mutação foi selecionada inconscientemente em conjunto com outras características de interesse agronômico. Isso sugere que a variação entre os caracteres homobárico e heterobárico tem valor agronômico em tomateiro. O primeiro passo para entender melhor os impactos da BSE a nível de planta e poder manipula-la dentro da cultura do tomateiro e em outras culturas é conhecendo os genes envolvidos na sua formação. Para isso, utilizamos o tomate como cultura modelo para elucidar as bases moleculares que controlam o desenvolvimento de BSEs. Utilizando recursos disponíveis publicamente combinados com análises *in silico*, identificamos um forte gene candidato para a mutação *obv*. O locus solyc05g054030 possui um SNP (A→G) no terceiro exon, que leva à troca de um resíduo histidina por arginina na posição 135 da proteína. O gene codifica um fator de transcrição zinc finger do tipo C2H2. Mostramos por meio de predições que a proteína OBV tem três domínios zinc finger clássicos, que permitem a interação no DNA. No mutante *obv*, a troca da histidina por arginina ocasionou a perda de um motivo zinc finger, o que pode ter levado à interrupção na funcionalidade da proteína. Complementamos o mutante *obv* com o alelo *OBV* funcional, recuperando o fenótipo de veia clara. Além de ser um controlador chave na formação das BSEs, *OBV* regula o ângulo de inserção da folha, serrilhamento foliar, densidade de veias e formato do fruto. *OBV* coordena o

desenvolvimento de BSEs por meio de um mecanismo mediado por auxina, especificamente por mudanças em alguns membros envolvidos na sinalização de auxina (ARFs e Aux/IAAs). Identificamos uma ligação entre *OBV* e *AUXIN RESPONSE FACTOR 4* (*ARF4*). As descobertas aqui relatadas servirão de suporte para a identificação de outros componentes ligados à via molecular que direciona a formação de BSEs nas folhas.

Palavras-chave: Extensão da Bainha do Feixe. Folha heterobárica. Clonagem molecular. Auxina.

CONTENTS

GENERAL INTRODUCTION

Water movement in plants along the continuum soil-plant-atmosphere follows the gradient of water potential, where the water is transported through the plant body in an analogous way to an electric circuit, with a series of additive resistances between soil and atmosphere (Cowan, 1965; Cowan, 1972). In this system, the leaf represents a 'hydraulic bottleneck' and a central determinant of water movement in the whole plant (Tyree et al., 1993; Yang and Tyree, 1994; Nardini and Salleo, 2000). Water flow in the stem occurs through xylem conduits within the vascular bundles, which, when entering the leaf blade, reorganize into major and minor veins. The central (primary), secondary and tertiary veins are those with the major diameter and participate mainly in the water supply to the leaf, while the minor diameter veins (quaternary and above) are involved in water distribution throughout the blade (Sack and Scoffoni, 2013).

The structure and distribution of veins have a central role in the leaf hydraulic architecture, directly affecting the leaf hydraulic conductivity (K_{leaf}) (Brodribb et al., 2007). When leaving xylem conduits, the water transits through a layer of parenchyma cells in compact arrangement, the cells of the sheath that surround the vascular bundles (Esau, 1977). Many species of eudicots display an extension of this sheath, forming a connection of the vascular region with the epidermis of the leaf (Haberlandt, 1882; Neger, 1918). Classical studies described such bundle sheath extensions (BSEs) as compact columns of parenchymatous or sclerenchymatous cells, extending from major or minor veins to the upper, lower or both epidermis (Haberlandt, 1882; Neger, 1918). These extensions lack intercellular spaces and chloroplasts, resulting in translucent areas in the leaf blade, identified as a network of bright lines on a dark green background (Wylie, 1943, 1952; McClendon, 1992).

BSEs act as structural barriers, dividing the mesophyll into compartments and precluding lateral diffusion of water vapor and CO_2 (Neger, 1918; Terashima, 1992). The partial pressure of these gases can vary independently between compartments, so these leaves are functionally classified as *heterobaric* (Terashima, 1992). On the other hand, leaves devoid of BSEs are *homobaric*, as the free lateral diffusion of gases in the mesophyll results in more uniform partial pressures (Terashima, 1992; Pieruschka et al., 2006).

Some roles attributed to BSEs suggest that this structure has an important ecological value. By acting as guides for visible light, BSEs can function as "transparent windows" enriching neighbouring mesophyll cells with high levels of photosynthetically active radiation (400-700 nm). The optimization of light distribution in the mesophyll innermost layers contributes to an enhanced photosynthetic performance and provides adaptive advantages for species of xeromorphic environments (Vogelmann, 1989; Karabourniotis et al., 2000). Other hypothetical functions, although not experimentally demonstrated so far, include mechanical support (Read and Stokes, 2006), or restriction of pathogen propagation (Lawson and Morison, 2006). BSEs can also improve hydraulic integration within the leaf blade. In heterobaric leaves, the epidermis and mesophyll are hydraulically bound to vascular tissues through BSE, providing an additional extra-xylematic route of lower resistance for the flow of liquid water, which is not observed in homobaric leaves (Zwieniecki et al., 2007; Buckley et al., 2011). Thus, K_{leaf} is higher in heterobaric than in homobaric leaves, but this can be dynamically affected by irradiance level (Scoffoni et al., 2015).

The BSEs have a particular ecological distribution in nature. In a climax forest, most species from the upper strata tend to have translucent leaf veins, whereas those dwelling in the understory and ground strata have opaque leaf veins (Kenzo et al., 2007; Inoue et at., 2015). This suggests that leaf vein translucence could have an ecological function by promoting adaptation to different levels of light intensity. In agricultural settings, BSEs are found in many sun-loving crops (*e.g.* tomato, soybean, barley, grapevine), but are absent in other species (*e.g.* tobacco, coffee, cocoa, chili peppers) that have been domesticated from shade-loving ancestors.

Due to the potential role of BSEs in light distribution across the canopy (BSE can improves photosynthetic assimilation; Karabourniotis et al., 2000; Nikolopoulos et al., 2002) and in water availability across the leaf blade (BSE can increases the hydraulic conductivity in leaves; Zwieniecki et al., 2007; Buckley et al., 2011); BSEs manipulation might be a strategy for improve water-use efficiency and crop yield. The first step toward this goal is to unveil the genetic control of BSEs development. The tomato is an ideal model for BSEs study, since wild species and some commercial cultivars are heterobaric and there are cultivars such as M82, VFN8 and Heinz that are homobaric due to the presence of the *obscuravenosa* (*obv*) mutation. In addition to this phenotypic versatility (cultivars with and without BSEs), tomato has valuable resources and tools, such as freely

available annotated genome and well-established genetic transformation protocols, which facilitate its biotechnological manipulation.

Here, we seek to identify and characterize the gene underlying the *obscuravenosa* mutation, and thus the genetic basis of BSEs development in tomato. We further investigate the pleiotropic effects and the molecular mechanisms by which this gene controls BSEs development.

OBJECTIVES

General objective: to identify and functionally characterize a gene responsible for BSEs development in the tomato.

Specific objectives:

1- Mapping of the tomato genome for in silico identification and validation of the candidate gene.

2- Functional characterization of the target gene.

3- Identification of the gene role in the regulation of BSEs and evaluate possible pleiotropic effects.

4- Investigation of the impacts of the target gene on commercial tomato cultivars.

REFERENCES

Brodribb TJ, Feild TS, Jordan GJ (2007) Leaf maximum photosynthetic rate and venation are linked by hydraulics. Plant Physiology **144**: 1890-1898

Buckley TN, John GP, Scoffoni C, Sack L (2015) How does leaf anatomy influence water transport outside the xylem? Plant Physiology **168**: 1616-1635

Buckley TN, Sack L, Gilbert ME (2011) The role of bundle sheath extensions and life form in stomatal responses to leaf water status. Plant Physiology **156**: 962-973

Cowan IR (1965) Transport of water in the soil-plant-atmosphere system. Journal of Applied Ecology **2**: 221

Cowan IR (1972) An electrical analogue of evaporation from, and flow of water in plants. Planta **106**: 221-226

Esau K (1977) Anatomy of Seed Plants, 2nd ed. John Wiley & Sons, Inc., New York

Haberlandt G (1882) Vergleichende anatomie des assimilatorischen gewebesystems des pflanzens. Jahrbücher für Wissenschaftliche Botanie **13**: 74-188

Inoue Y, Kenzo T, Tanaka-Oda A, Yoneyama A, Ichie T (2015) Leaf water use in heterobaric and homobaric leafed canopy tree species in a Malaysian tropical rain forest. Photosynthetica **53**: 177-186

Karabourniotis G, Bornman JF, Nikolopoulos D (2000) A possible optical role of the bundle sheath extensions of the heterobaric leaves of *Vitis vinifera* and *Quercus coccifera*. Plant Cell and Environment **23**: 423-430

Kenzo T, Ichie T, Watanabe Y, Hiromi T (2007) Ecological distribution of homobaric and heterobaric leaves in tree species of Malaysian lowland tropical rainforest. American Journal of Botany **94**: 764-775

Lawson T, Morison J (2006) Visualising patterns of CO_2 diffusion in leaves. New Phytologist **169**: 641-643

Mcclendon JH (1992) Photographic survey of the occurrence of bundle-sheath extensions in deciduous dicots. Plant Physiology **99**: 1677-1679

Nardini A, Salleo S (2000) Limitation of stomatal conductance by hydraulic traits: sensing or preventing xylem cavitation? Trees: Structure and Function **15**: 14-24

Neger F (1918) Wegsamkeit der Laubblatter fur gase. Flora **111**: 152-161

Nikolopoulos D, Liakopoulos G, Drossopoulos I, Karabourniotis G (2002) The relationship between anatomy and photosynthetic performance of heterobaric leaves. Plant Physiology **129**: 235-243

Pieruschka R et al. (2006) Lateral diffusion of CO_2 from shaded to illuminated leaf parts affects photosynthesis inside homobaric leaves. New Phytologist **169**: 779-788

Read J, Stokes A (2006) Plant biomechanics in an ecological context. American Journal of Botany **93**: 1546-65

Sack LS, Coffoni C (2013) Leaf venation: structure, function, development, evolution, ecology and applications in the past, present and future. New Phytologist **198**: 983-1000

Scoffoni C (2015) Modelling the outside-xylem hydraulic conductance: towards a new understanding of leaf water relations. Plant Cell and Environment **38:** 4-6

Scoffoni C, Kunkle J, Pasquet-Kok J, Vuong C, Patel AJ, Montgomery RA, Sack L (2015) Light-induced plasticity in leaf hydraulics, venation, anatomy, and gas exchange in ecologically diverse *Hawaiian lobeliads*. New Phytologist **207**: 43-58

Terashima I (1992) Anatomy of non-uniform leaf photosynthesis. Photosynthesis Research **31**: 195-212

Tyree M, Sinclair BLP, Granier A (1993) Whole shoot hydraulic resistance in *Quercus* species measured with a new high-pressure flowmeter. Annales des Sciences Forestières **50**: 417-423

Vogelmann TC (1989) Penetration of light into plants. Photochemistry and Photobiology **50**: 895-902

Wylie RB (1943) The role of the epidermis in foliar organization and its relations to the minor venation. American Journal of Botany **30**: 273-280

Wylie RB (1952) The bundle sheath extension in leaves of dicotyledons. American Journal of Botany **39**: 645-651

Yang S, Tyree MT (1994) Hydraulic architecture of *Acer saccharum* and *A. rubrum*: comparison of branches to whole trees and the contribution of leaves to hydraulic resistance. Journal of Experimental Botany **45**: 179-186

Zwieniecki MA, Brodribb TJ, Holbrook NM (2007) Hydraulic design of leaves: insights from rehydration kinetics. Plant Cell and Environment **30**: 910-921

CHAPTER 1: *In silico* identification and validation of the candidate gene

1. INTRODUCTION

Leaves are organs that have an incredible variety of shapes, sizes, textures and colors. Many of these traits attract attention when they are very peculiar or distinctive. Some leaves, for example, have translucent veins, which stand out as a network of bright lines on a dark green background. This phenotype is produced by an anatomical structure that connects vascular bundle to the leaf epidermis, called bundle sheath extension (BSE) (Wylie, 1943, 1952; Mcclendon, 1992). BSEs are described as a column of cells without intercellular spaces and chloroplasts, and are composed of parenchymal cells (*e.g.* tomato), sclerenchymatic (*e.g.* maize and rice) or of the two cell types (*e.g. Myrcia tomentosa*) (Baresch et al., 2018). This structure is quite dynamic between species, can be found only in the main vein, in the main and secondary veins or even in all of them (Haberlandt, 1882; Neger, 1918).

BSEs act as a physical barrier and divide the mesophyll into small compartments, restricting the lateral diffusion of gases, especially water vapor and CO_2. The partial pressure of these gases varies differently between compartments and; therefore, these leaves are classified as *heterobaric* (Neger, 1918; Terashima, 1992). On the other hand, in leaves lacking BSEs the diffusion of gases occurs relatively freely, resulting in more uniform partial pressures along the blade, so these leaves are classified as *homobaric* (Terashima, 1992; Pieruschka et al., 2006).

The distribution of heterobaric and homobaric leaves in nature is very striking. In a climax forest, most species in the upper strata tend to have translucent veins leaf (heterobaric), while those that live in the understory and soil strata have opaque veins leaf (homobaric) (Kenzo et al., 2007; Inoue et al., 2015). This suggests that the presence of clear veins on the leaf does not occur merely as an attractive feature. Besides being flashy, BSEs can impact the functionality of the leaves and contribute to adaptation in environments with specific conditions of irradiance, humidity or temperature. Previous studies showed that BSEs can affect photosynthetic assimilation (e.g. in environments where light is limited to sunflecks) and hydraulic conductivity in response to changes in irradiance (Pieruschka et al., 2010; Scoffoni et al., 2008).

Taken together, these evidences show that BSEs can become a trait of great agricultural potential, improving crops performance under specific environmental conditions. However, to manipulate this trait in crops it becomes essential to understand the molecular bases of the control the BSEs development.

The tomato is an ideal model crop for studying BSEs, as it has wild species and some commercial cultivars that are heterobaric and others cultivars that are homobaric due the presence of recessive mutation *obscuravenosa* (*obv*). The *obv* mutation appeared spontaneously and was observed in numerous commercial tomato cultivars, suggesting its unconscious selection by breeding programs. A previous work identified the chromosomal region containing the *obv* mutation (Jones et al., 2007). This work used a collection of 76 introgression lines (ILs) containing chromosomal fragments from wild specie *Solanum pennellii* introgressed into *Solanum lycopersicum* (cv. M82) genetic background (Eshed and Zamir 1995). In each IL, the genomic fragment from *S. pennellii* was delimited by molecular markers and according to the overlap of the different fragments, the genome was segmented in smaller regions called *bins*. So, *obv* mutation was mapped to chromosome 5, bin d-5E. This genomic fragment was subsequently sequenced, delimiting the number of possible candidate genes for the *obv* mutation (Chitwood et al., 2013). Based on this list of candidates and the premise that the gene underlying *obv* mutation might be a key regulator of BSEs development, we performed a deep *in silico* characterization aiming to select the most likely candidate for *OBV* gene and validate your function *in vivo*.

2. MATERIAL AND METHODS

GWAS analysis

The online repository of genetics and genomics information Sol Genomics Network (https://solgenomics.net/locus/37560/view) was used to access the database of 360 genomes of tomato cultivars and wild species (Lin et al., 2014). In this platform, we searched for the desired region of chromosome 5 and analyzed genetic variations (SNPs or indels) present in all 37 listed genes in the bin d-5E. Then, we used the extensive database from the Tomato Genetics Resource Center, TGRC (http://tgrc.ucdavis.edu/) to access phenotypic data for a large number of tomato cultivars and wild species and conduct a genotype × phenotype association study.

The Genome-Wide Association Study (GWAS) was performed using data of 37 tomato accessions (25 wild-type and 12 mutants for *obv* phenotype, Supplemental Table 1) and the Plink (v.1.07) software (Purcell et al., 2007). A total of 3,218,302 SNPs with a minor allele frequency (MAF) greater than 5% were used for association analysis. The whole-genome significant cutoff was defined as P=1.554e-08 based on the Bonferroni correction method. A Manhattan plot was generated using the *R* package qqman (Turner, 2014). Gene annotation was obtained from International Tomato Annotation Group (ITAG, v.2.4) and visualized using the *R* package Gviz (Hahne and Ivanek, 2016).

Structural modeling analysis

The analysis of functional domains in OBV protein were done using the functional domain prediction tool from http://smart.embl-heidelberg.de/ and mutations predictions were obtained with the software: Protein Homology/analogY Recognition Engine V2.0 and http://www.sbg.bio.ic.ac.uk/phyre2/html.

OBV homologs identification and phylogenetic inference

To identify *OBV* homologs in tomato and other plant species, we firstly performed a BLAST search (BLASTP, Altschul et al., 1990) in proteomes of plant species using *OBV* sequences from *Arabidopsis thaliana* as query and setting the E-value threshold to 1e-10. The BLAST hits had their sequences retrieved and aligned together with OBVs and non-OBVs sequences from *A. thaliana* with MUSCLE (Edgar, 2004). The alignment was submitted to trimAl (Capella-Gutiérrez et al., 2009) for alignment trimming and then submitted to FastTree (Price et al., 2010) for tree inference. Trees were visually inspected using FigTree (Rambaut, 2012). Protein accessions which clustered together with *OBV*s from *A. thaliana* forming a monophyletic clade were considered as *OBV* homologs. Further phylogenetic inference using only *OBV* homologs were performed using MUSCLE, for sequence alignment, trimAl, for alignment trimming, SMS (Lefort et al., 2017), for evolutionary model selection, and PHYML (Guindon et al., 2010), for maximum likelihood tree inference. Final trees were annotated with taxonomic information from NCBI Taxonomy using TaxOnTree (http://bioinfo.icb.ufmg.br/taxontree). The plant proteomes used in this work were retrieved from Sol Genomics Network, for tomato (v.4.0, Hosmani et al., 2019), and from Uniprot (The UniProt Consortium, 2019), for other plants.

Molecular cloning

The fragment corresponding to the coding sequence of *OBV* gene from wild type and mutant was amplified, purified and cloned independently in the plasmids PCR8/GW/TOPO® (Invitrogen) using the primers listed in Supplementary Table 4. Subsequently, each fragment was recombined in the overexpression vector pK7WG2D,1 (Karimi et al., 2002). For silencing construct, a specific fragment of coding sequence of *OBV* gene was selected using BLAST queries against the Sol Genomics database (https://solgenomics.net/, ITAG release 2.40). The amplified fragment was cloned into the plasmids PCR8/GW/TOPO® (Invitrogen), and then recombined in the gene silencing vector pK7GWiWG2 (I) (Karimi et al., 2002). All constructs were confirmed by PCR and sequencing.

Plant transformation

MT and *obv* mutant seeds were sterilized by agitation in 30% (v/v) commercial bleach (2.7% [w/v] sodium hypochlorite) for 15 min followed by three rinses with sterile distilled water. Approximately 30 seeds were inoculated into flasks containing MS salts (Murashige and Skoog, 1962) half-strength, vitamins B5, sucrose 30 g L^{-1} and agar 4 g L^{-1}. The pH of the medium was adjusted to 5.7± 0,05 and autoclaved for sterilization. The seeds were kept during four days in the dark, 25 ± 1 °C, followed by four days under photoperiod of 16-h/8-h day/night and intensity 45 ± 3 µmol m^{-2} s^{-1}. Transgenic plants were generated by transformation mediated by *Agrobacterium tumefaciens* strain EHA105 according to Pino et al. (2010), with few modifications. Cotyledons of 8-day-old seedlings were sectioned and used in co-cultivation with *Agrobacterium* in Root Inducing Medium (RIM), for two days, 25 ± 1 °C in the dark. Then, explants were transferred to Shoot Inducing Medium (SIM), where were kept under photoperiod of 16-h/8-h and light intensity of 10-20 µmol m^{-2} s^{-1}, for four weeks. Two medium exchanges were performed during this period. Shoots Well developed (above 5 cm) were transferred to flasks containing MS medium without hormones. At all stages *in vitro*, the medium was supplemented with kanamycin 100 mg L^{-1} and timentin 300 mg L^{-1}.

Selection of transgenic lines

T0 plants regenerated *in vitro* were acclimatized under controlled conditions, photoperiod 16-h/8-h day/night, irradiance of 150 µmol m^{-2} s^{-1} and temperature of 25 ± 1 °C, using Tropostrato® substrate autoclaved and vermiculite (1:1) for 4 weeks.

Posteriorly, T0 plants were transferred to pots (350 ml) containing the same formulation described above and kept in the greenhouse for phenotyping and seed production.

For confirmation of transgenics, DNA genomic was extracted from young leaves following Dellaporta et al. (1983). The presence of the resistance gene *nptII* (*Neomicina fosfotransferase II*) was confirmed by PCR using specific primers. For identification of the insert, a second PCR was performed using the primer forward *pCaMV 35S* and specific reverse (Supplementary Table 4). To obtain homozygous plants, transgenics T1 and T2 were screened with spray of kanamycin (400 mg L^{-1}) for five days. The lines that showed 100% of surviving plants was considered homozygous.

Real-time quantitative PCR (qRT)

Young leaves ~2.0 cm were collected for extraction of total RNA using Trizol® (Ambion, Life Technology), according to the manufacturer's recommendations. The cDNA synthesis was performed with SuperScript™ III First-Strand Synthesis System (Invitrogen). Real-time quantitative PCR reactions (qRT) were performed in a thermocycler Real-Time da StepOnePlus PCR (Applied Biosystems) with a final volume of 14µl using reagent SYBR Green Master Mix (Thermo Fisher Scientific). The melting curves were analyzed for nonspecific amplifications and dimerization of primers. Absolute fluorescence data were analyzed using the software LinRegPCR (Ruijter et al., 2009) to obtain the values of quantification cycle (Cq) and calculate the primer efficiency. The abundance of transcripts was normalized against the geometric mean of two reference genes, *TIP4* and *EXPRESSED* (Expósito-Rodriguez et al., 2008). Primers used are listed in Supplementary Table 4.

Anatomical analysis

The expanded leaflets from 4^{th} or 5^{th} leaf were used for anatomical analyzes. To obtain cross sections, a 1×0.5 cm fragment in the center of the leaflet was removed and fixed in FAA70 (alcohol-formalin-acetic acid 70%) during 24 h. Subsequently, the samples were transferred to ethanol 70% (v/v) and dehydrated in ethanol series (70%, 85% e 95%), 2 h in each series under vacuum (-20 polHg) (Kraus and Arduim, 1997). Pre-infiltration was performed with resin and ethanol 95% (1:1) for 2 h under vacuum (-20 polHg). The infiltration was done in resin for one week. The cross-sections of 5µm thickness were mounted on blades and stained with toluidine blue 0,05% (SAKAI, 1973). The images were analyzed in the photomicroscope (Zeiss AxioScope A1).

3. RESULTS AND DISCUSSION

3.1 Identification of the *OBV* gene

In a previous work, we showed that the monogenic recessive *obscuravenosa* (*obv*) mutant lacks BSEs in tomato leaves (Zsögön et al., 2015). Through mapping of *S. pennellii* introgression lines (ILs), *OBV* was localized within a 1.5 cM interval on chromosome 5 (Jones et al., 2007) and subsequently fine-mapped into the bin d-5E, which spans 37 genes (Chitwood et al., 2013). We first analyzed the relative expression for most of the genes in the bin d-5E in wild-type (cv. Micro-Tom) and *obv* mutant plants, and we did not find clear results that could direct our search (Supplementary Figure 1). Next, using publicly available genomic information, we conducted a comparison of gene sequences between 25 wild-type and 12 *obv* mutant tomato cultivars (Supplementary Table 1). The SNP-GWAS analysis revealed multiple SNPs (Single Nucleotide Polymorphism) in coding and non-coding regions, and thirteen were consistently different between phenotypic categories (Supplementary Table 2). Improving our search, we found three genomic regions with SNPs strongly associated with the *obv* phenotype within bin d5-E (Figure 1A, B). In addition, we reinforced the analysis using gene annotations (Gene Ontology) and arrived at three candidates: Solyc05g053870, encoding a Copine I-like protein; Solyc05g053930, encoding an ATP-binding serine/threonine kinase and Solyc05g054030, encoding a Zinc finger transcription factor, C2H2-type (Figure 1C).

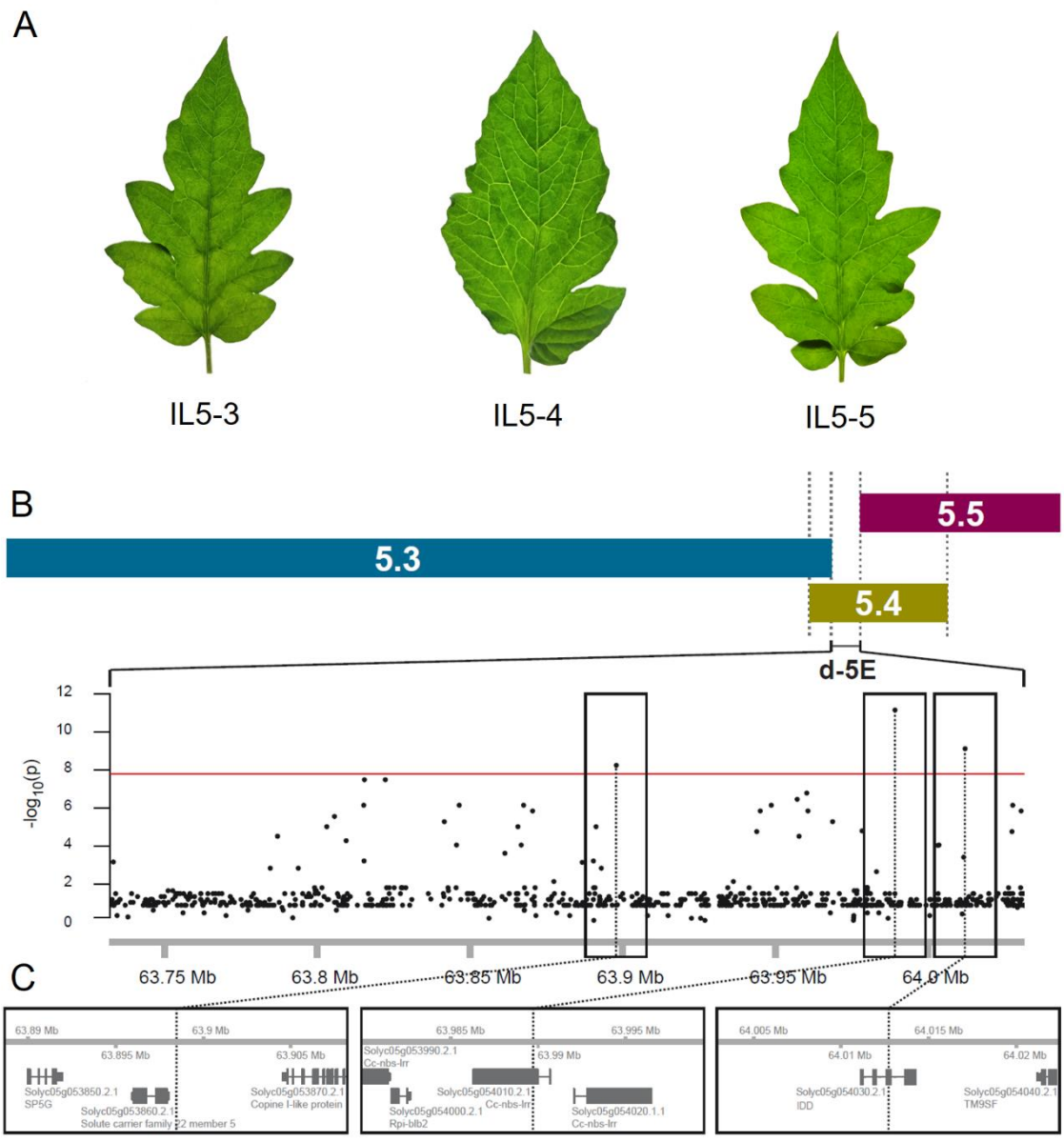

Figure 1. Distribution of SNPs-GWAS in the genetic bin d-5E (spanning 37 genes) of tomato chromosome 5 - *Solanum pennellii* introgression lines (IL). (A) Leaflets phenotype of the introgression lines IL 5-3 (dark veins), IL 5-4 (clear veins) and IL 5-5 (dark veins). (B) Manhattan plot of the GWAS for *obv* phenotype on d-5E region (63.73 to 64.03 Mb of chromosome 5). X-axis represents the chromosome position and the Y-axis represents the negative log10 of P-values per SNP derived from the association analysis. The red horizontal line represents the Bonferroni-corrected genome-wide significance threshold (P=1.554e-08). Gene annotations surrounding SNPs with P-value below the significance threshold are shown in boxes. (C) The three highest points correspond to genomic regions with a strong association with the *obv* phenotype. Magnification of these regions showing the genes associated with these SNPs: Solyc05g053870; Solyc05g053930 and Solyc05g054030.

Our *in silico* analyses revealed that many homobaric tomato cultivars (including the reference genome of Heinz 1706) harbor a SNP (A→G) in the third exon of the Solyc05g054030 locus (Figure 2A), resulting in a predicted histidine to arginine substitution in the 135 amino acid residue (H135R). We cloned and Sanger-sequenced the full cDNA (1149 bp) from wild-type MT and *obv* mutant plants and confirmed that the respective sequences matched those of heterobaric (A) and homobaric (G) cultivars (Figure 2B). A comprehensive exploration among tomato cultivars showed that distribution of clear and dark veins is strongly linked with the presence of histidine or arginine in 135 position respectively. (Figure 2C).

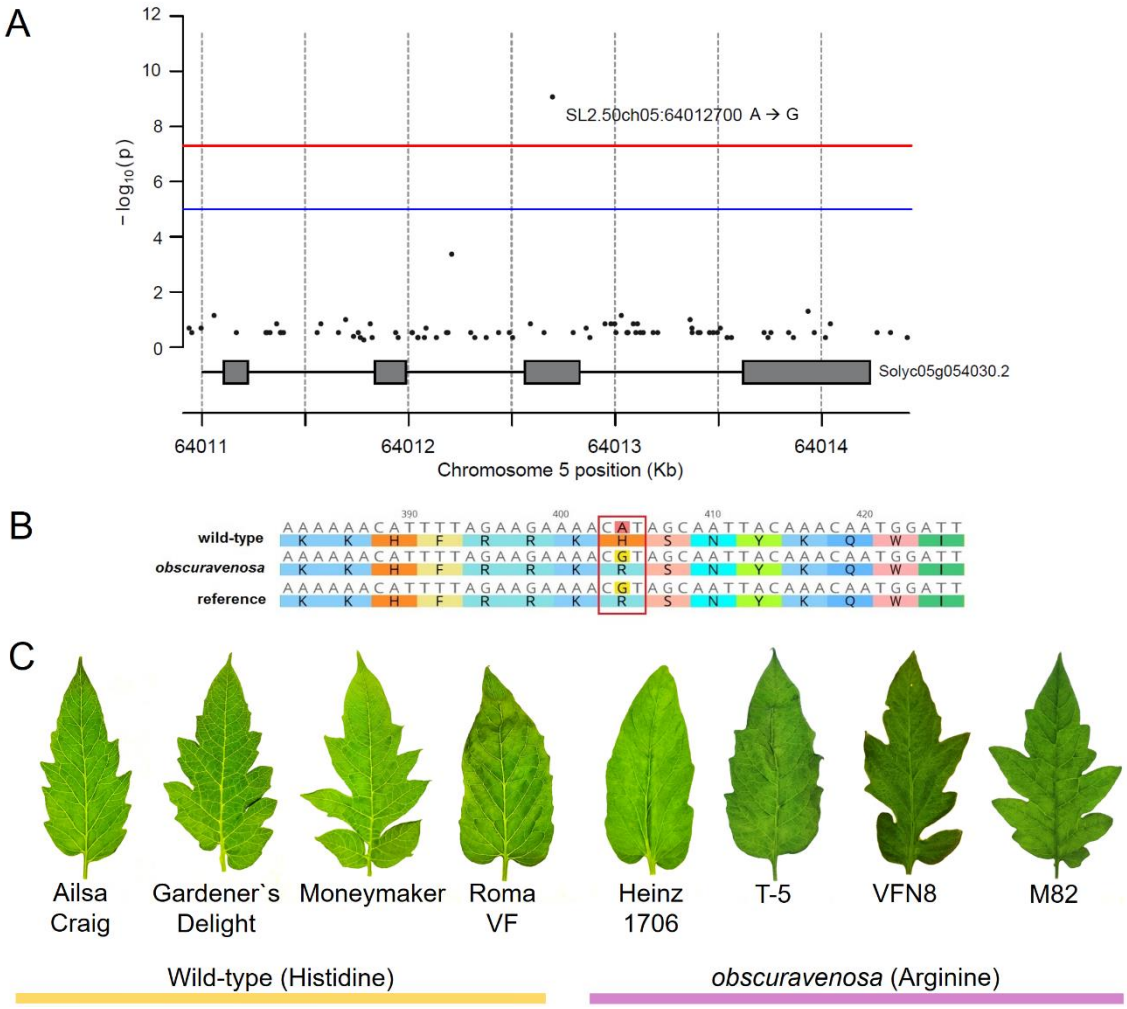

Figure 2. Characterization of the Solyc05g054030 gene. (A) Gene structure showing exons (boxes) and introns (lines). GWAS analysis shows all the SNPs found in the Solyc05g054030 gene for 25 wild-type and 12 *obv* mutant tomato cultivars. The SNP (A→G) located in the third exon this gene is strongly associated with the *obv* phenotype. In the Manhattan plot the X-axis represents the chromosome position and the Y-axis represents the negative log10 of P-values per SNP derived from the association analysis.

The red horizontal line represents the Bonferroni-corrected genome-wide significance threshold (P=1.554e-08). (B) Alignment of nucleotide and amino acid sequences comparing the wild-type, *obv* mutant and the reference genotype (Heinz 1706). The SNP (A→G) is marked with a red box and results in substitution to histidine for arginine in the protein. (C) Leaflets of cultivars with clear veins (wild-type) and cultivars with dark veins (*obscuravenosa*). Heterobaric cultivars has a predicted histidine and homobaric has an arginine in 135 position.

3.2 Sequence comparison and structural modeling of the OBV protein

Zinc finger proteins constitute an abundant family of transcriptional regulatory proteins. In *Arabidopsis*, 176 proteins containing zinc finger domains were predicted, 143 of which showed to be exclusive to plants (Englbrecht et al., 2004). In *S. lycopersicum*, 112 zinc finger proteins have been recently identified, and 30 reported as unique from tomato (Ming et al., 2020; Liao et al., 2020). The classic zinc finger domain (C2H2) consists of one α-helix and two β-sheets antiparallel harbouring two cysteines (C2) and two histidines (H2) that coordinate the binding of a zinc ion (Zn^{2+}), on a conserved pattern described as Cys-X_{2or4}-Cys-X_{12}-His-X_{3or5}-His, where X represents any amino acid (Luchi, 2001; Pabo et al., 2001). Cysteine and histidine residues are essential for the configuration and activity of the zinc finger domain. The side chain charges of both residues maintain a link stable with Zn^{2+} and the spatial arrangement of the chains allows a perfect docking with the larger DNA groove. Therefore, changes in any of the zinc binding residues (Cys or His) can impair or even eliminate the ability of the interaction with DNA (Pabo et al., 2001; Razin et al., 2012).

Functionally, C2H2 class of transcription factors (TFs) participate in the regulation of diverse physiological processes along plant development from germination to flowering (Lu et al., 2012; Kim et al., 2006; Morita et al., 2006; An et al., 2012). The recognition and interaction with DNA are done by four amino acid residues located in the *N*-terminal portion of the α-helix. These residues confer specificity during interaction and allow each zinc finger domain to recognize three or four nucleotides. Thus, modifications in amino acids located in the recognition region or in nearby residues can lead to the domain destabilization or functional loss (Razin et al., 2012; Pabo et al., 2001).

The complete sequence of the *OBV* gene encodes a 381 amino acid protein containing three predicted C2H2 zinc finger domains. Instead, *obv* mutant allele displays only two

zinc finger domains (Figure 3A). The loss of the second domain in the mutant occurred because histidine at position 135 is a key amino acid and necessary for the binding of Zn^{2+} in the domain structure. According to the *in silico* protein structure prediction, the residue 135 is in a loop that connects two β-strands (Figure 3B). Although it is a subtle change because histidine and arginine are both chemically similar residues, the protein sequence profile indicated that histidine is the only amino acid able to ensure protein stability in this region. Analyzing other possible mutations for this same region, we found that all other amino acids showed a high intolerance level for position 135, that is, none could replace histidine in this context (Figure 3C). Our results reinforce what is reported in the literature, some residues can be exchanged for similar ones without changing structure or functioning of the zinc finger, while others are critics and mutations in these amino acids certainly disrupt the domain function (Pabo et al., 2001; Razin et al., 2012). This suggests that *obv* mutation may have promoted loss of function in *OBV* protein.

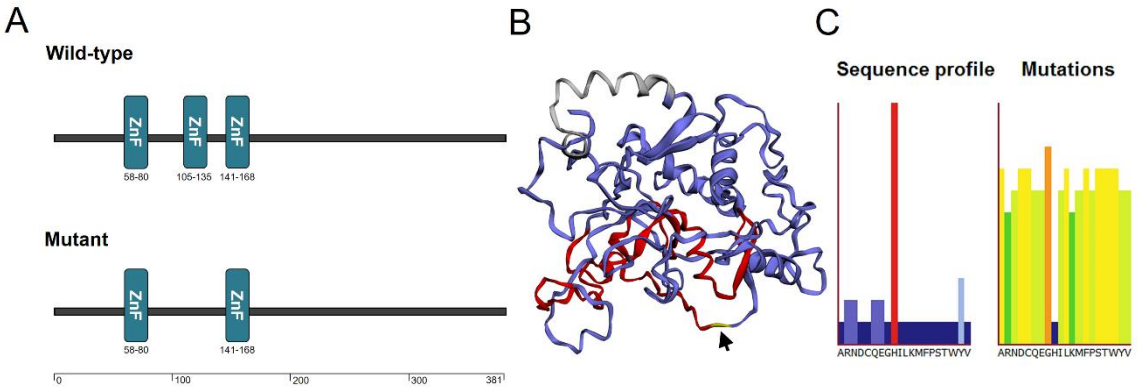

Figure 3. Functional domains prediction in the OBV protein. (A) Wild-type protein sequence showing the presence of three conserved zinc finger domains and position of each domain. Below, *obv* mutant protein sequence showing only two Zinc finger domains. The analysis were done using the functional domain prediction tool from http://smart.embl-heidelberg.de/ and http://www.sanger.ac.uk/Software/Pfam/ (Bateman et al., 2004). (B) Mutant 3D protein model highlighting in yellow (arrow) the position of the *obv* mutation. (C) Analysis of the protein sequence profile and predictions of possible mutations for position 135. These analyzes were obtained with the software: Protein Homology/analogY Recognition Engine V2.0 and http://www.sbg.bio.ic.ac.uk/phyre2/html.

A survey for *OBV* homologous loci in tomato genome retrieved 18 paralogs distributed in all chromosomes except 12 (Figure 4A). To better understand the diversity of the *OBV* gene, a member of C2H2 TFs, we performed a phylogenetic analysis combining 19 sequences of tomato, 16 sequences from genetic model *Arabidopsis thaliana* and 6 sequences from basal bryophyte *Physcomitrella patens* (Figure 4B). The tree topology showed two clades, both of which displayed *P. patens* sequences clustered together in a basal position. *OBV* (solyc05g054030 in red) was grouped in a monophyletic clade with three tomato paralogs (Solyc01g005060; Solyc06g072360 and Solyc03g098070) and three *Arabidopsis* orthologs (*SHOOT GRAVITROPISM 5/*INDETERMINATE DOMAIN - *SGR5*/*IDD*15; *IDD*16 and *IDD*14), forming a brother group with both. The phylogenetic positioning of *OBV* suggests that this gene does not have a direct ortholog and the closest putative ortholog is a *SGR5*/*IDD*15.

The putative *Arabidopsis thaliana* ortholog gene, *SGR5*/*IDD15*, is involved in shoot gravitropism through changes in the sheath cell gravity sensors (Morita et al., 2006). Together with *IDD*15, *IDD*14 and *IDD*16 cooperatively control shoot morphogenesis and shoot gravitropic responses through regulation of biosynthesis and auxin transport (Cui et al., 2013). An expression profile analysis suggested that three out of the 18 *OBV* tomato paralogs are involved in stress responses, two of which (Solyc07g053570 and Solyc11g069240) were specifically related to drought, and another (Solyc03g121660) related to salt stress (Zhao et al., 2020). Unfortunately, biological functions for the three *OBV* closest paralogs (Solyc01g005060; Solyc06g072360 and Solyc03g098070) remains unknown.

To evaluate the level of sequence conservation, *OBV* protein was compared to related Solanaceae species, *A. thaliana*, *Glycine max* and *Oryza sativa*. The percentage of identity was from 94% with potato (*Solanum tuberosum*), 85% with eggplant (*Solanum melongena*), 79% with pepper (*Capsicum annuum*), 69% with tobacco (*Nicotiana tabacum*), 67% with *Nicotiana benthamiana*, 58% with *Arabidopsis thaliana*, 58% with soybean (*Glycine max*) and 51% with rice (*Oryza sativa*) (Supplementary Table 3). For all sequences analyzed, with the exception of the reference tomato Heinz, the histidine remained preserved in position 135 (Supplementary Figure 2). The conservation of specific sequences in the OBV protein, especially functional domains regions, suggest maintenance of your biological function among species and reinforce the importance of Cys and His residues in zinc-finger domain.

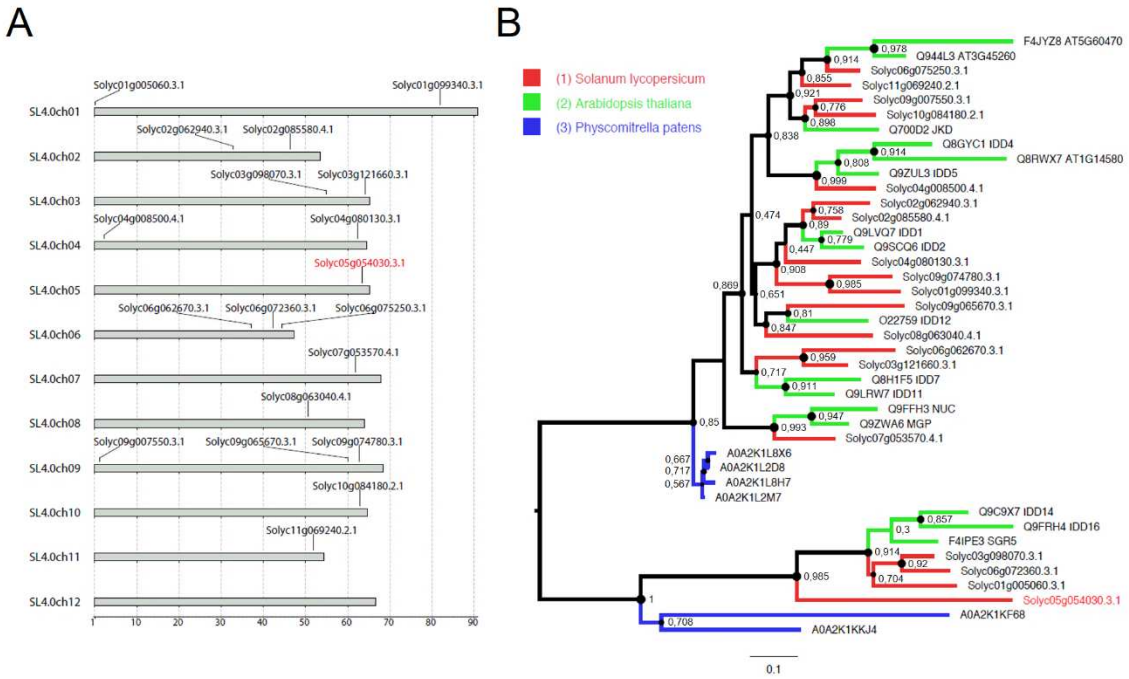

Figure 4. Paralogs of the *OBV* gene and phylogenetic reconstruction of OBV protein family. (A). Distribution of 18 paralogs of the *OBV* found in all chromosomes from tomato, except 12. (B) Phylogenetic reconstruction of OBV protein family. Maximum likelihood tree of the OBV family, subclade comprising the tomato *OBV* (in red) with its paralogs and orthologs in *Arabidopsis thaliana* and the basal angiosperm *Physcomitrella patens*, used as external group. The tree was inferred with PHYML (substitution model: JTT+G+I, bootstrap replicates: 1000). Nodes with branch support > 80% have larger size.

3.3 Target gene validation by complementation

In vivo validation of the target gene was performed through complementation the *obv* mutant. For this, we created an overexpression vector containing cDNA sequence of *OBV* functional driven by a *35S* promoter and transformed into the *obv* mutant, Micro-Tom (MT) background (Figure 5A). We recovered 21 independent transformation events in T0 (confirmed by PCR and q-PCR) and observed translucent veins in all 21 regenerants harboring the *OBV* functional sequence. Additionally, we transformed the MT (wild-type) with same construction, which was used as a transformation control (Supplementary Figures 3-6).

We confirmed that insertion of functional *OBV* allele into *obv* complemented the mutant, recovering the BSEs. Then, three overexpression lines (*obv*-*OBV*^{OE} #5, #10 and #12) were selected for further analysis. We first confirmed that the expression level of *OBV* was increased (5-20 fold) compared to wild-type plants (Figure 5B) and produced cross-sections of leaves to verify the presence of BSEs in mid-veins. Lastly, we allowed T0 plants to self-pollinate and produced fruits to harvest T1 seeds of all three lines (#5, #10 and #12). From individual T1 lines, we screened T2 and T3 families and identified individuals harbouring a homozygous transgene insertion. We confirmed the presence of BSEs and the increased expression levels in at least ten T3 individuals from each event (Figure 5C-G). These results suggest that the defect in BSE development in the *obv* mutant could be caused by a genetic alteration in *OBV* gene.

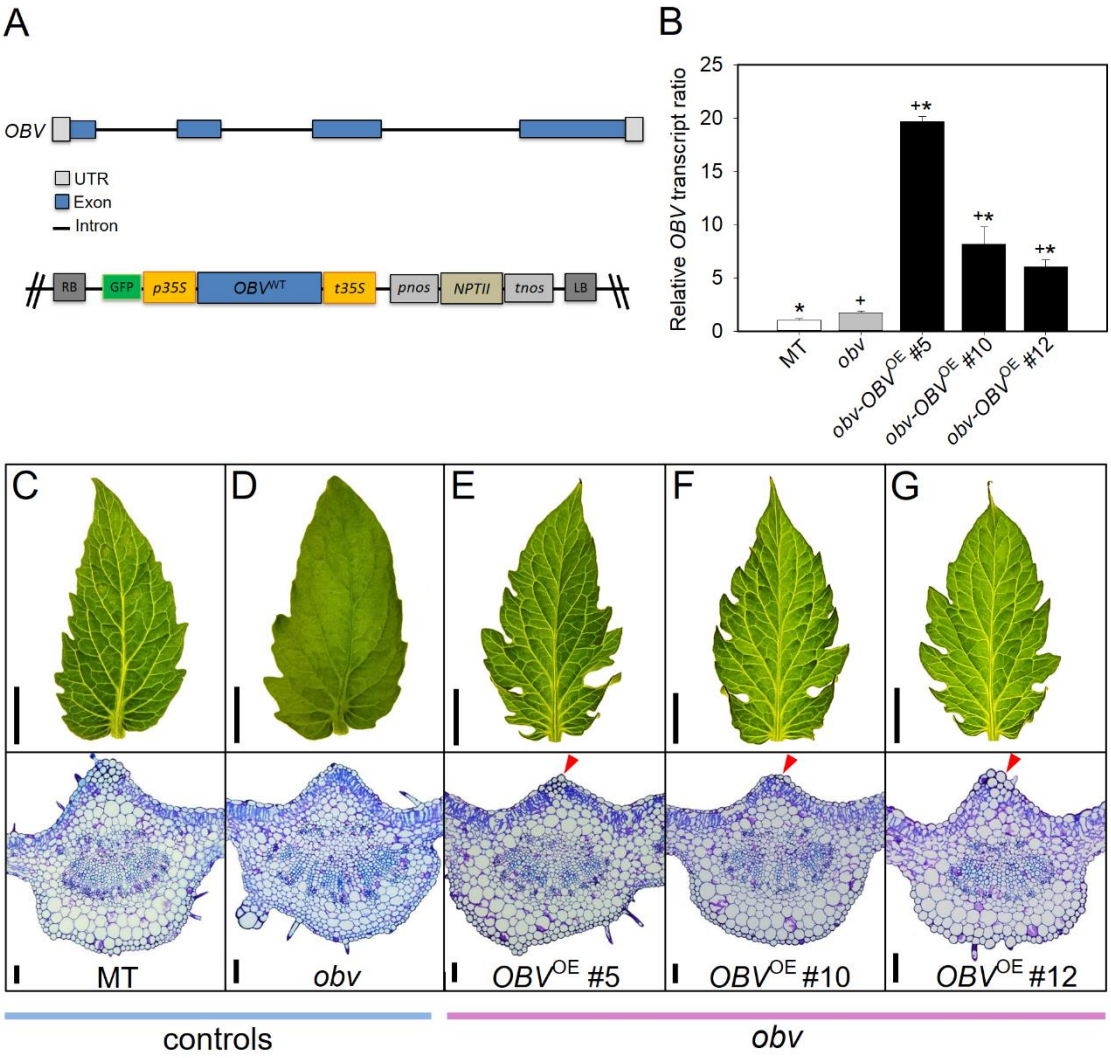

Figure 5. Complementation of the *obv* mutant with the *OBV* functional allele. (A) Gene structure showing exons (boxes), introns (lines) and a schematic of the construction used. (B) Relative *OBV* mRNA levels in leaves of MT, *obv* and three complemented lines (*obv*-*OBV*^{OE} #5, #10 and #12) transformed with overexpression construction. Values were normalized against the MT (wild-type) sample. Asterisk indicates statistical difference in relation to the *obv* and sum sign shows statistical difference in relation to the MT. (C-G) Representative leaflets and cross-sections of MT, *obv* mutant and *obv* complemented lines (#5, #10 and #12) in T3 generation. Red arrows show the recovery of BSEs in all *OBV*^{OE} lines. Bars = 1 cm and 100 µm for cross-sections.

To confirm that a single amino acid substitution in *OBV* gene is responsible for the loss of BSEs in tomato, we next constructed an overexpression vector containing mutant cDNA sequence under control of a *35S* promoter and transformed into the *obv* mutant. We retrieved 15 transgenic events and in all of them the mutant phenotype was not reverted. A control transformation experiment using the same vector on MT plants yielded five confirmed transgenic events, all presenting wild-type phenotype (Supplementary Figures 7 and 8). Then, we selected two lines from MT background (MT-*obv*^{OE} #2 and #4) and two *obv* mutant (*obv*-*obv*^{OE} #1 and #3) and confirmed the increase expression of the mutant allele (Figure 6A).

As the expression of the *obv* allele in mutant is greater than expression of the functional *OBV* allele in wild-type (Figure 6A), we wondered if obv protein could be performing its functions in the cell, but with reduced efficiency. However, our results discarded this hypothesis, because even increasing the mutant allele expression BSEs were not recovered in *obv* mutant. Furthermore, we did not observe any other visible effect in leaves or plants from MT and *obv* overexpressing the mutant allele, that could suggest another physiological function exercised by mutant protein (Figure 6 D).

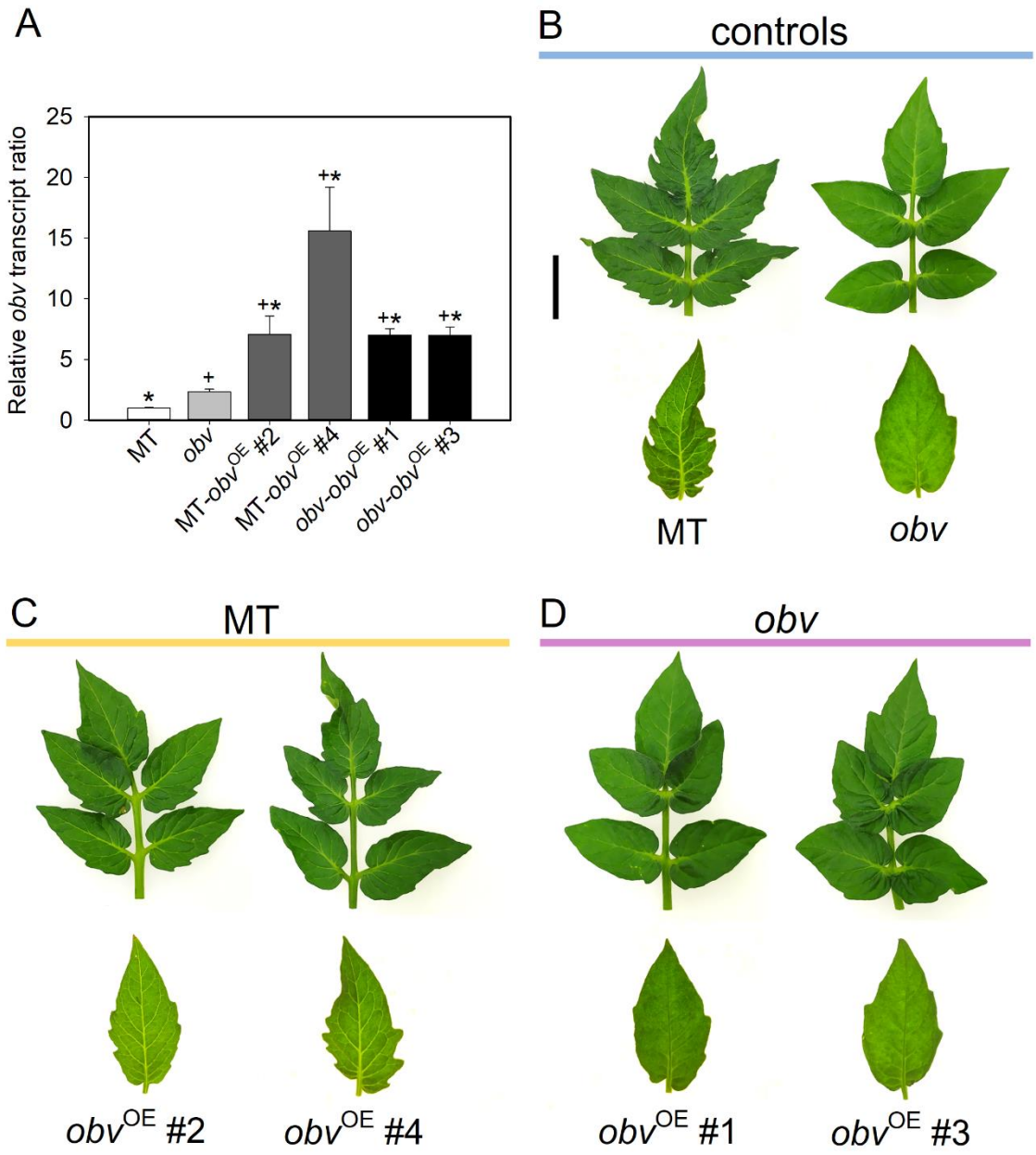

Figure 6. Characterization of transgenic lines overexpressing *obv* mutant allele. (A) Relative *obv* mRNA levels in leaves of MT, *obv* mutant and four overexpression lines, generation T1. Values were normalized against the MT (wild-type) sample. Asterisk indicates statistical difference in relation to the *obv* and sum sign shows statistical difference in relation to the MT. (B) Controls: Representative leaves and terminal leaflets of MT and *obv*. (C) Leaves and leaflets of MT (MT-*obv*^{OE} #2 and MT-*obv*^{OE} #4) and *obv* mutant (*obv*-*obv*^{OE} #1 and *obv*-*obv*^{OE} #3) transformed with overexpression construction. Lines #1 and #3 show that mutant allele high levels did not reverse *obv* phenotype. Bar = 2 cm.

In addition, we generated MT silenced lines using post-transcriptional gene silencing mechanism by an interference RNA (RNAi) construct (Supplementary Figure 3). First, we confirmed the reduction in transcript accumulation of the silenced lines (Figure 7 A). Of three lines silenced in MT, lines MT-*OBV*^{RNAi} #1 and #2 showed an intermediate phenotype and line MT-*OBV*^{RNAi} #3 had complete elimination of BSEs resulting in dark veins phenotype, as observed in *obv* mutant (Figure 7 C). We also silenced *obv* mutant allele in mutant plants to confirm that changes in gene expression level, as we see between MT and *obv*, are not responsible for the mutant phenotype (Figure 7 D and Supplementary Figure 9).

Taken together, these results show that a single amino acid change in *OBV* gene is responsible by switch between homobaric and heterobaric leaves in tomato, regardless of gene expression levels.

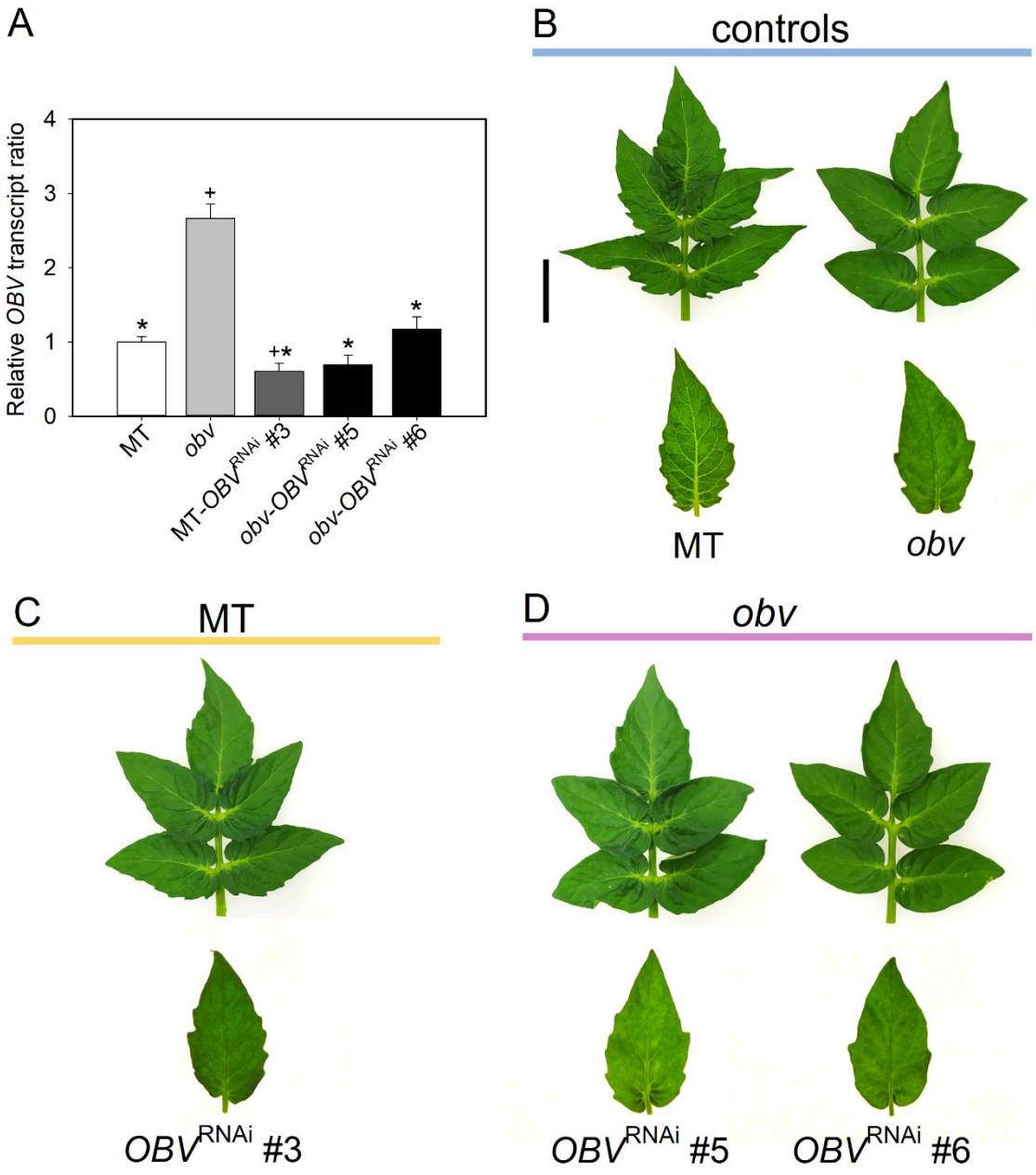

Figure 7. Characterization of transgenic lines silenced by interference RNA (RNAi). (A) Relative *obv* mRNA levels in leaves of MT, *obv* mutant and RNAi lines, generation T1. Values were normalized against the MT (wild-type) sample. Asterisk indicates statistical difference in relation to the *obv* and sum sign shows statistical difference in relation to the MT. (B) Controls: representative leaves and leaflets of MT and *obv*. (C) Phenotype of MT-*OBV*^{RNAi} #3 line, highlighting that the reduction in *OBV* expression generated a total loss of BSEs. (D) Mutant lines silenced (*obv*-*OBV*^{RNAi} #5 and *obv*-*OBV*^{RNAi} #6) without any visible phenotypic alteration, proving that changes in *OBV* expression are not associated with BSEs development. Bar = 2cm.

4. CONCLUSIONS

Using *in silico* tools, we identified a candidate tomato gene for the *obv* mutation, Solyc05g054030, which has a conserved SNP with skewed distribution between homobaric and heterobaric tomato cultivars. The *OBV* target gene belongs to the class of TFs zinc finger C2H2- type, with DNA-binding capability. Modelling of the OBV protein showed that the histidine at position 135 is a key amino acid for binding of zinc ion in the domain structure. When this residue is replaced by arginine, it is predicted that the resulting protein will lose one of its DNA-binding zinc finger domains, which could have strong functional consequences. We thus hypothesized that *OBSCURAVENOSA* gene is Solyc05g054030. We validated the gene function *in vivo* by complementation of *obv* mutant, showing that the insertion of functional *OBV* recovers clear veins phenotype in mutant. We report the discovery of a key regulator for the formation of BSEs in tomato and further elaborate on this finding in next chapters.

5. REFERENCES

Altschul SF, Gish W, Miller W, Myers EW, Lipman DJ (1990) "Basic local alignment search tool." Journal of Molecular Biology **215**:403-410

An L, Zhou Z, Sun L, Yan A, Xi W, Yu N, Cai W, Chen X, Yu H, Schiefelbein J, Gan Y (2012) A zinc finger protein gene ZFP5 integrates phytohormone signaling to control root hair development in *Arabidopsis*. Plant Journal **72**:474-490

Baresch A, Crifò C, Boyce CK (2019) Competition for epidermal space in the evolution of leaves with high physiological rates. New Phytologist **221**: 628-639

Bateman A, Coin L, Durbin R, Finn RD, Hollich V, Griffiths-Jones S, Studholme D J (2004) The Pfam protein families database. Nucleic Acids Research **32**:138-141

Capella-Gutiérrez S, Silla-Martínez JM, Gabaldón T (2009) TrimAl: a tool for automated alignment trimming in large-scale phylogenetic analyses. Bioinformatics **15**:1972-1973

Chitwood DH, Kumar R, Headland LR, Ranjan A, Covington MF, Ichihashi Y, Fulop D, Jiménez-Gómez JM, Peng J, Maloof JN, et al (2013) A quantitative genetic basis for leaf morphology in a set of precisely defined tomato introgression lines. Plant Cell **25**: 2465-81

Clemens KR, Wolf V, McBryant SJ, Zhang P, Liao X, Wright PE, Gottesfeld JM (1993) Molecular basis for specific recognition of both RNA and DNA by a zinc finger protein. Science **260**: 530-533

Cui D, Zhao J, Jing Y, Fan M, Liu J, Wang Z, Hu Y (2013) The *Arabidopsis* IDD14, IDD15, and IDD16 cooperatively regulate lateral organ morphogenesis and gravitropism by promoting auxin biosynthesis and transport. PLoS Genetics **9**: 1003759

Dellaporta SL, Wood J, Hicks JB (1983) A plant minipreparation: version II. Plant Molecular Biology Reporter **1**: 19-20

Edgar RC (2004) MUSCLE: multiple sequence alignment with high accuracy and high throughput. Nucleic Acids Research **5**:1792-7

Englbrecht CC, Schoof H, Böhm S (2004) Conservation, diversification and expansion of C2H2 zinc finger proteins in the *Arabidopsis thaliana* genome. BMC Genomics **5**: 39

Eshed Y, Zamir D (1995) An introgression line population of *Lycopersicon pennellii* in the cultivated tomato enables the identification and fine mapping of yield-associated QTL. Genetics **141**: 1147-1162

Expósito-Rodríguez M, Borges AA, Borges-Pérez A, Pérez JA (2008) Selection of internal control genes for quantitative real-time RT-PCR studies during tomato development process. BMC Plant Biology **8**: 131

Guindon S, Dufayard JF, Lefort V, Anisimova M, Hordijk W, Gascuel O (2010) "New algorithms and methods to estimate maximum-likelihood phylogenies: assessing the performance of PhyML 3.0." Systematic Biology **3**: 307-321

Haberlandt G (1882) Vergleichende anatomie des assimilatorischen gewebesystems des pflanzens. Jahrbücher für Wissenschaftliche Botanie **13**: 74-188

Hahne F, Ivanek R (2016) "Statistical Genomics: Methods and Protocols." In Mathé E, Davis S (eds.), chapter Visualizing Genomic Data Using Gviz and Bioconductor, 335-351

Hosmani PS, Gonzalez MF, Geest HV, Maumus F, Bakker LV, Schijlen E, Haarst JV, Cordewener J, Perez GS, Peters S, Fei Z, Giovannoni JJ, Mueller LA, Saha S (2019) "An improved de novo assembly and annotation of the tomato reference genome using single-molecule sequencing, Hi-C proximity ligation and optical maps" bioRxiv 767764; doi: https://doi.org/10.1101/767764

Inoue Y, Kenzo T, Tanaka-Oda A, Yoneyama A, Ichie T (2015) Leaf water use in heterobaric and homobaric leafed canopy tree species in a Malaysian tropical rain forest. Photosynthetica **53**: 177-186

Jones CM, Rick CM, Adams D, Jernstedt J, Chetelat RT (2007) Genealogy and fine mapping of *obscuravenosa*, a gene affecting the distribution of chloroplasts in leaf veins, and evidence of selection during breeding of tomatoes (*Lycopersicon esculentum*; Solanaceae). American Journal of Botany **94**: 935-47

Karimi M, Inzé D, Depicker A (2002). GATEWAY™ vectors for *Agrobacterium*-mediated plant transformation. Trends in plant science **7**: 193-195

Kenzo T, Ichie T, Watanabe Y, Hiromi T (2007) Ecological distribution of homobaric and heterobaric leaves in tree species of Malaysian lowland tropical rainforest. American Journal of Botany **94**: 764-775

Kim S, Choi K, Park C, Hwang HJ, Lee I (2006) SUPPRESSOR OF FRIGIDA4, encoding a C2H2-Type zinc finger protein, represses flowering by transcriptional activation of *Arabidopsis* FLOWERING LOCUS C. Plant Cell **18**: 2985-2998

Kraus JE, Arduin M (1997) Manual básico de métodos em morfologia vegetal. Rio de Janeiro: EDUR, 198

Kumar M, Le DT, Hwang S, Seo PJ, Kim HU (2019) Role of the INDETERMINATE DOMAIN Genes in Plants. International Journal of Molecular Sciences **20**: 2286

Lefort V, Longueville EJ, Gascuel O (2017) "SMS: Smart Model Selection in PhyML." Molecular Biology and Evolution, msx149

Liao X, Wang L, Zhu S, Zheng F, Yang C (2020) Identification, genomic organization, and expression profiles of single C2H2 zinc finger transcription factors in tomato (*Solanum lycopersicum*). Journal of Applied Genetics 1-15

Lin T, Zhu G, Zhang J, Xu X, Yu Q, Zheng Z, Huang Z (2014) Genomic analyses provide insights into the history of tomato breeding. Nature Genetics **46**: 1220-1226

Lu XD, Li Y, Su YP, Liang QJ, Meng HY, Li S, Shen SD, Fan YL, Zhang CY (2012) An *Arabidopsis* gene encoding a C2H2-domain protein with alternatively spliced transcripts is essential for endosperm development. Journal of Experimental Botany **63**: 5935-5944

Luchi S (2001) Three classes of C2H2 zinc finger proteins. Cellular and Molecular Life Sciences **58**: 625-635

Mcclendon JH (1992) Photographic survey of the occurrence of bundle-sheath extensions in deciduous dicots. Plant Physiology **99**: 1677-1679

Morita MT, Sakaguchi K, Kiyose S, Taira K, Kato T, Nakamura M, Tasaka M (2006) A C2H2-type zinc finger protein, *SGR5*, is involved in early events of gravitropism in *Arabidopsis* inflorescence stems. Plant Journal **47**: 619-628

Neger F (1918) Wegsamkeit der Laubblatter fur gase. Flora **111**: 152-161

Pabo CO, Peisach E, Grant RA (2001) Design and selection of novel Cys2His2 zinc finger proteins. Annual Review of Biochemistry **70**: 313-340

Pieruschka R, Chavarría-Krauser A, Schurr U, Jahnke S (2010) Photosynthesis in lightfleck areas of homobaric and heterobaric leaves. Journal of Experimental Botany **61**: 1031-1039

Pieruschka R, Schurr U, Jensen, M, Wolff WF, Jahnke S (2006). Lateral diffusion of CO_2 from shaded to illuminated leaf parts affects photosynthesis inside homobaric leaves. New Phytologist **169**: 779-788

Pino LE, Lombardi-Crestana S, Azevedo MS, Scotton DC, Borgo L, Quecini V, Figueira A, Peres LE (2010) The Rg1 allele as a valuable tool for genetic transformation of the tomato 'Micro-Tom' model system. Plant Methods **6**: 23

Price MN, Dehal PS, Arkin AP (2010) FastTree 2-approximately maximum-likelihood trees for large alignments. PLoS One **3**: 9490

Purcell S, Neale B, Todd-Brown K, Thomas L, Ferreira MAR, Bender D, Maller J, Sklar P, de Bakker PIW, Daly MJ, Sham PC (2007) PLINK: a toolset for whole-genome association and population-based linkage analysis. American Journal of Human Genetics, 81.

Rambaut A (2012) FigTree v1.4.4. Available at: http://tree.bio.ed.ac.uk/software/figtree/.

Razin SV, Borunova VV, Maksimenko OG, Kantidze OL (2012) Cys2His2 zinc finger protein family: classification, functions, and major members. Biochemistry **77**: 217-226

Ruijter JM, Ramakers C, Hoogaars WMH, Karlen Y, Bakker O, Van DEN, Hoff MJB, Moorman AFM (2009) Amplification efficiency: linking baseline and bias in the analysis of quantitative PCR data. Nucleic Acids Research **37**: 45

Scoffoni C, Pou A, Aasamaa K, Sack L (2008) The rapid light response of leaf hydraulic conductance: new evidence from two experimental methods. Plant, Cell and Environment **31**: 1803-1812

Terashima I (1992) Anatomy of non-uniform leaf photosynthesis. Photosynthesis Research **31**: 195-212

The UniProt Consortium, UniProt: a worldwide hub of protein knowledge (2019) Nucleic Acids Research **47**:506-515

Turner SD (2014) qqman: An R package for visualizing GWAS results using Q-Q and manhattan plots. biorXiv DOI: 10.1101/005165

Wylie RB (1943) The role of the epidermis in foliar organization and its relations to the minor venation. American Journal of Botany **30**: 273-280

Wylie RB (1952) The bundle sheath extension in leaves of dicotyledons. American Journal of Botany **39**: 645-651

Zhao T, Wu T, Zhang J, Wang Z, Pei T, Yang H, Xu X (2020) Genome-Wide Analyses of the Genetic Screening of C2H2-type Zinc Finger Transcription Factors and Abiotic and Biotic Stress Responses in Tomato (*Solanum lycopersicum*) based on RNA-Seq Data. Frontiers in Genetics **11**: 540

Zsögön A, Alves Negrini AC, Peres LEP, Nguyen HT, Ball MC (2015) A mutation that eliminates bundle sheath extensions reduces leaf hydraulic conductance, stomatal conductance and assimilation rates in tomato (*Solanum lycopersicum*). New Phytologist **205**: 618-626

6. SUPPLEMENTARY MATERIAL

Supplementary Table 1. Tomato accessions used for Genome-Wide Association Study (GWAS)

	Database (Sol Genomics) code	TGRC Accession	Cultivars	Phenotype	Amino acid
150 genomes	RF_000	LA3435	Heinz 1706	Mutant (*obv*)	Arginine 135
360 genomes	TS-49_SNPs	LA3238	Earliana	Mutant (*obv*)	Arginine 135
	TS-8_SNPs	LA4024	E-6203	Mutant (*obv*)	Arginine 135
	TS-3_SNPs	LA3475	M82	Mutant (*obv*)	Arginine 135
	TS-121_SNPs	LA3846	NC EBR-6	Mutant (*obv*)	Arginine 135
	TS-60_SNPs	LA2009	New Yorker	Mutant (*obv*)	Arginine 135
	TS-128_SNPs	LA0012	Pearson	Mutant (*obv*)	Arginine 135
	TS-133_SNPs	LA3528	Peto 95-43	Mutant (*obv*)	Arginine 135
	TS-186_SNPs	LA3214	Rowpac	Mutant (*obv*)	Arginine 135
	TS-151_SNPs	LA2399	T-5	Mutant (*obv*)	Arginine 135
	TS-171_SNPs	LA1706	UC-82	Mutant (*obv*)	Arginine 135
	TS-1_SNPs	LA0490	VF36	Mutant (*obv*)	Arginine 135
150 genomes	RF_003	EA06086	Gardener's Delight	Wild-type (*OBV*)	Histidine 135
	RF_001	LA2706	Moneymaker	Wild-type (*OBV*)	Histidine 135
	RF_077	TR00018	Red Cherry	Wild-type (*OBV*)	Histidine 135
	RF_055	LA1401	*S. galapagense*	Wild-type (*OBV*)	Histidine 135
	RF_074	LA0716	*S. pennellii*	Wild-type (*OBV*)	Histidine 135
	RF_047	LA1578	*S. pimpinellifolium*	Wild-type (*OBV*)	Histidine 135
360 genomes	TS-195_SNPs	LA0516	Ace	Wild-type (*OBV*)	Histidine 135
	TS-9_SNPs	LA2838A	Ailsa Craig	Wild-type (*OBV*)	Histidine 135
	TS-155_SNPs	LA0533	Condine Red	Wild-type (*OBV*)	Histidine 135
	TS-278_SNPs	LA0517	Early Santa Clara	Wild-type (*OBV*)	Histidine 135
	TS-5_SNPs	LA2711	Edkawi	Wild-type (*OBV*)	Histidine 135
	TS-212_SNPs	LA3242	Flora-Dade	Wild-type (*OBV*)	Histidine 135
	TS-4_SNPs	LA3856	Hawaii 7998	Wild-type (*OBV*)	Histidine 135
	TS-200_SNPs	LA3320	Hotset	Wild-type (*OBV*)	Histidine 135
	TS-264_SNPs	LA0025	King Humbert 1	Wild-type (*OBV*)	Histidine 135
	TS-10_SNPs	LA0502	Marglobe	Wild-type (*OBV*)	Histidine 135
	TS-163_SNPs	LA1504	Marmande	Wild-type (*OBV*)	Histidine 135
	TS-239_SNPs	LA3845	NC EBR-5	Wild-type (*OBV*)	Histidine 135
	TS-237_SNPs	LA3243	Platense	Wild-type (*OBV*)	Histidine 135
	TS-206_SNPs	LA0089	Prince Borghese	Wild-type (*OBV*)	Histidine 135
	TS-122_SNPs	LA1090	Rutgers	Wild-type (*OBV*)	Histidine 135
	TS-6_SNPs	LA3008	San Marzano	Wild-type (*OBV*)	Histidine 135
	TS-152_SNPs	LA1021	Santa Cruz B	Wild-type (*OBV*)	Histidine 135
	TS-188_SNPs	LA1506	Stone	Wild-type (*OBV*)	Histidine 135
	TS-97_SNPs	LA0154	Tiny Tim	Wild-type (*OBV*)	Histidine 135
	-	LA3911	MT- (Micro-Tom)	Wild-type (*OBV*)	Histidine 135

Supplementary Table 2. SNPs in coding and non-coding regions, consistently different between phenotypes dark x clear veins.

Locus	Region	SNPs (*OBV* → *obv*)
Solyc05g053680	Intron 2	A→T
Solyc05g053770	Exon 1 Promoter	T→A G→T
Solyc05g053780	Promoter	A→G
Solyc05g053790	Promoter Exon 1 Exon 2	G→A G→T A→G
Solyc05g053800	Promoter	A→C
Solyc05g053860	Downstream	C→T
Solyc05g053920	Promoter Exon 1	G→A A→G
Solyc05g054010	Exon 2	G→A
Solyc05g054030	Exon 3	A→G

* *OBV* = wild-type (clear veins); *obv* = mutant (dark veins)

Supplementary Table 3. *OBV* sequence accessions used for alignment analysis

Species	ID	Source
Arabidopsis thaliana	At2G01940	Phytozome
Capsicum annuum	Ca05g17800	Solgenomics
Glycine max	Glyma05G137000	Phytozome
Nicotiana benthamiana	Niben101Scf02911g03012	Solgenomics
Nicotiana tabacum	mRNA_117485	Solgenomics
Oryza sativa	Os09g27650	Phytozome
Solanum lycopersicum cv Heinz	Solyc05g054030	Solgenomics
Solanum lycopersicum cv MT	360 Tomato Genomes (TS-7)	Solgenomics
Solanum melongena	Sme2.502707.1g00006	Solgenomics
Solanum pennellii	Sopen05g032520	Solgenomics
Solanum tuberosum	Sotub05g026960	Solgenomics

Source: https://solgenomics.net/tools/blast/;
https://phytozome.jgi.doe.gov/pz/portal.html#!search?show=BLAST

Supplementary Table 4. Primers used for PCR and quantitative RT-PCR

Target Gene	Forward primer (5'-3')	Reverse primer (5'-3')
OBV	CACCCAATATTTCATCATATTGAATATATCTC	GATTTTTTATATGAGTGAACAATG
M13	GTAAAACGACGGCCAG	CAGGAAACAGCTATGAC
35S P	CCTCGGATTCCATTGCCCA	---
NPTII	GAGGCTATTCGGCTATGACTGG	ATCGGGAGCGGCGATACCGTA
TIP4	ATGGAGTTTTTGAGTCTTCTGC	GCTGCGTTTCTGGCTTAGG
EXP	GCTAAGAACGCTGGACCTAATG	TGGGTGTGCCTTTCTGAATG

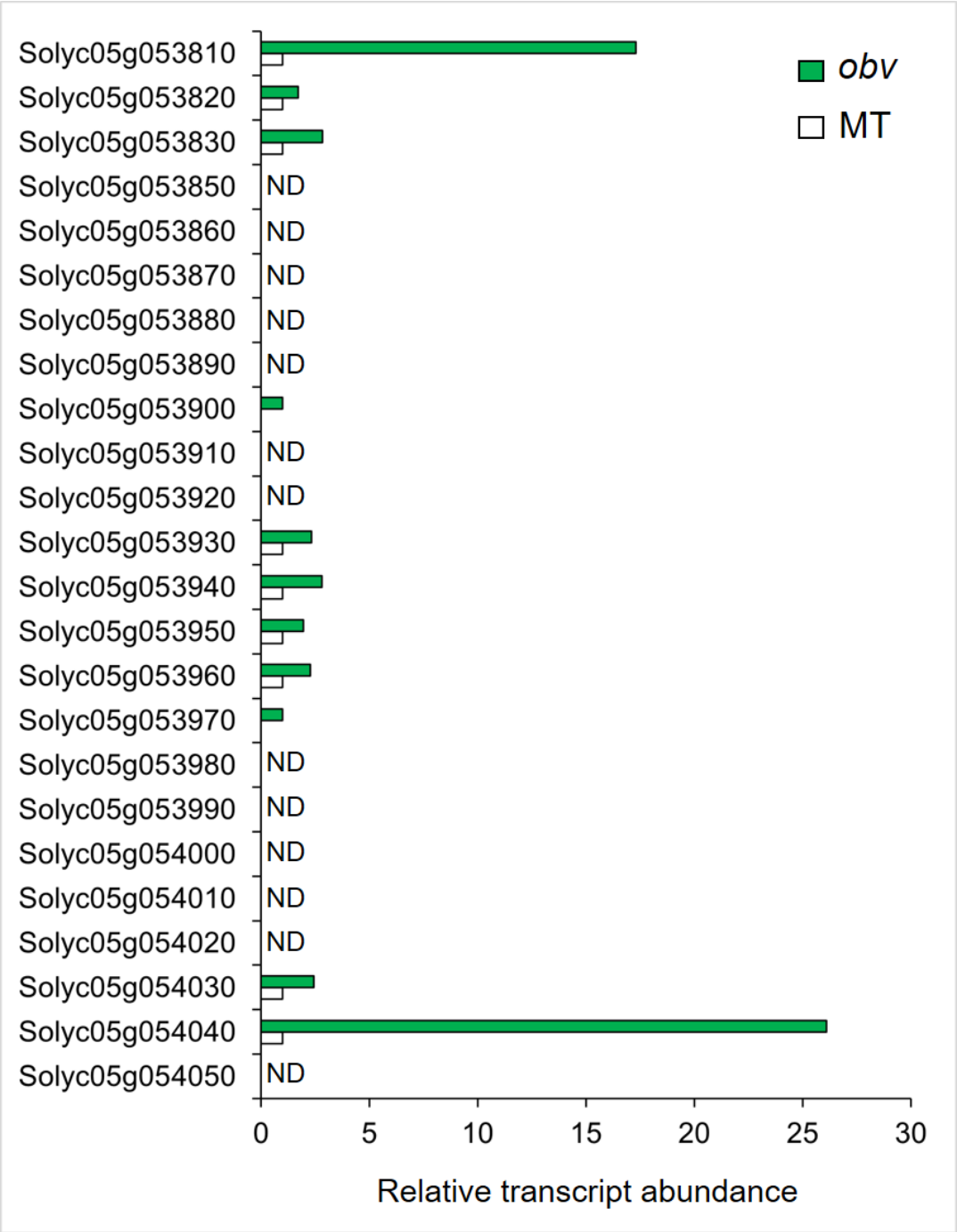

Supplementary Figure 1. Relative transcript abundance in young leaves of MT (wild-type) and *obv* mutant. ND = not detected.

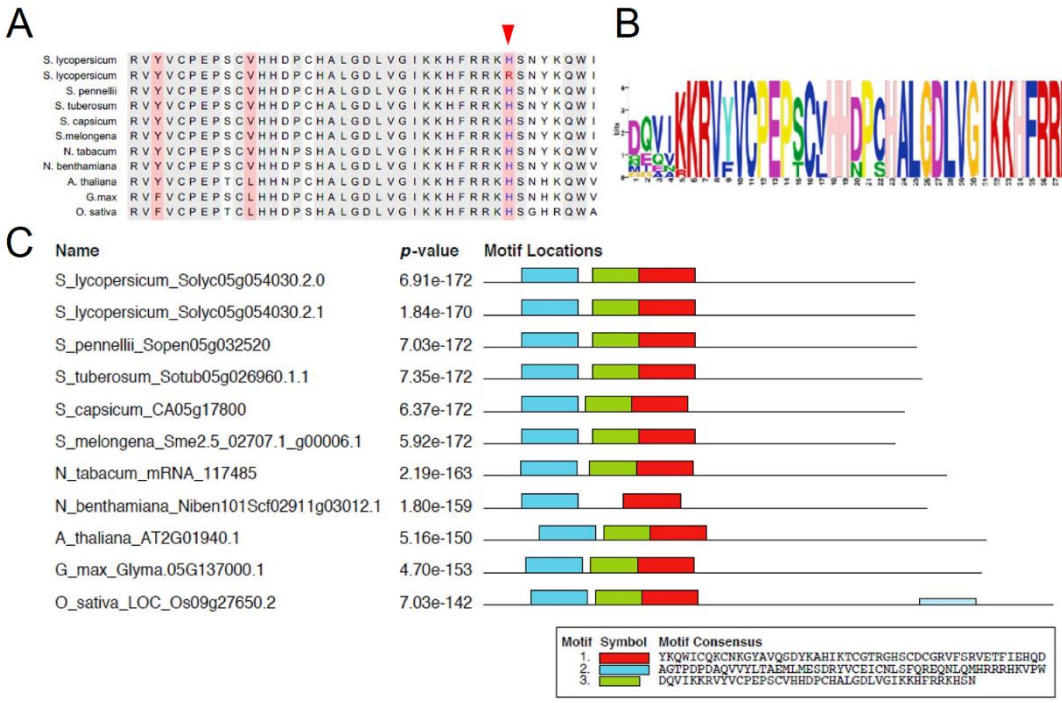

Supplementary Figure 2. Comparative amino acid sequence alignment of *OBV* gene. (A) Sequence comparison of the third zinc finger motif in some members from Solanaceae family and others species. Histidine residue is marked by arrow indicating the exchange for an arginine in *obv* cultivar (*Solanum lycopersicum* cv Heinz). (B) Sequence logo of the conserved amino acids in third zinc finger motif. The height of each amino acid indicates conservation ratio. (C) Three conserved Zinc finger motifs I, II, and III are shown by blue, green and red boxes respectively. Sequences used for alignment are listed in Supplementary Table 3.

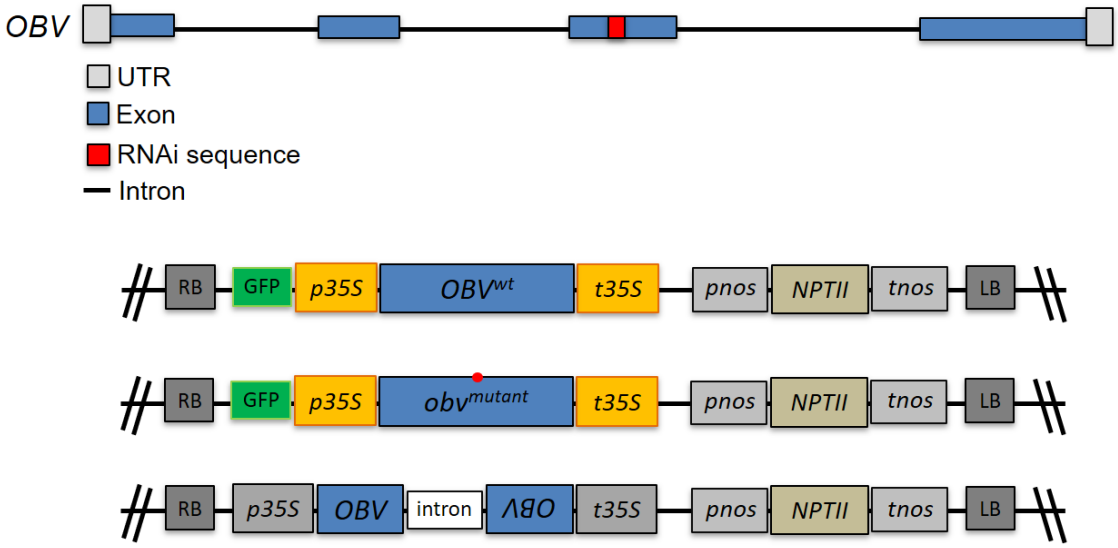

Supplementary Figure 3. Maps of the constructs designed for generation of overexpression and knockdown lines used in this work.

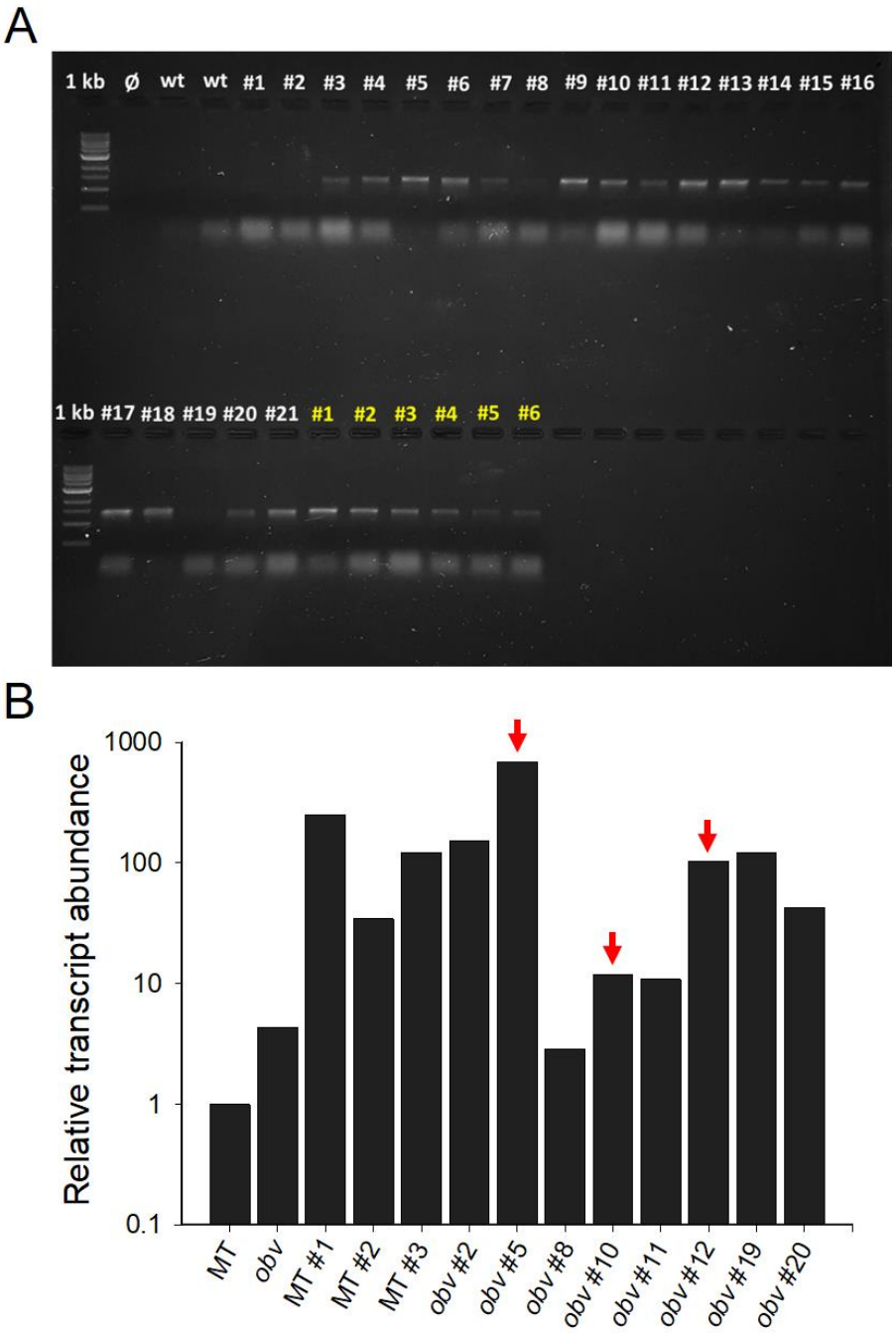

Supplementary Figure 4. Screening of transgenic lines (T0) overexpressing *OBV* functional. (A) Amplification of *OBV* gene. Ø corresponds to the negative control and wt to Micro-Tom (wild-type). The events in white correspond to *obv* plants transformed with *35S*::*OBV* construction and yellow events to the MT plants transformed with same construction. PCR product has ~ 1700 bp. The primers were used to amplify *OBV* gene and a part of *35S* promoter. (B) Relative *OBV* mRNA levels in leaves of MT, *obv* and some transgenic lines (MT-*OBV*^{OE} #1, #2 and #3; *obv*-*OBV*^{OE} #2, #5, #8, #10, #11, #12, #19 and #20). Values were normalized against MT sample. The three *obv* events selected for functional characterization are marked with red arrows.

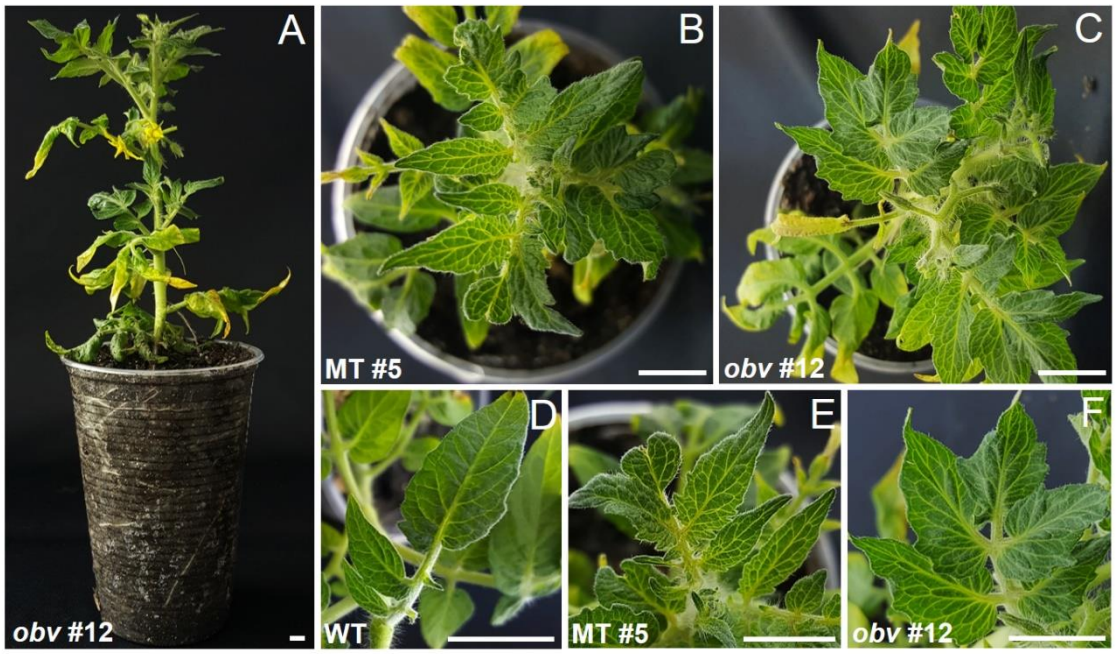

Supplementary Figure 5. Vegetative growth phenotypes of transgenic plants (T0) overexpressing *OBV* functional allele. (A) Representative transgenic plant (*obv-OBV*^{OE} #12) regenerated *in vitro*. (B - F) Details of the leaflets of MT (MT-*OBV*^{OE} #5) and *obv* mutant *(obv-OBV*^{OE} #12) highlighting the recovery of clear veins in mutant (C and F). Bars = 1 cm.

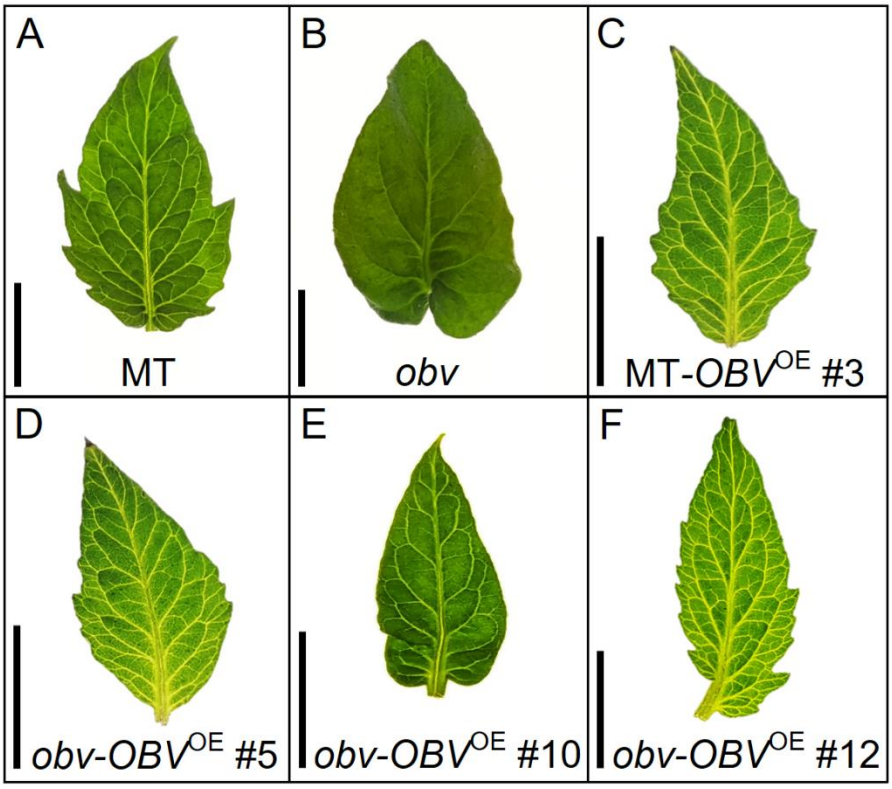

Supplementary Figure 6. Phenotyping of transgenic lines (T0) overexpressing *OBV* functional allele. (A and B) Details of MT (clear veins) and *obv* (dark veins) terminal leaflets *in vitro* regenerated. (C) Representative leaflet of MT transformed with *35S*::*OBV* construction. (D, E and F) Representative leaflets of *obv* mutant transformed with same construction, showing recovery of clear veins. Bars = 1 cm.

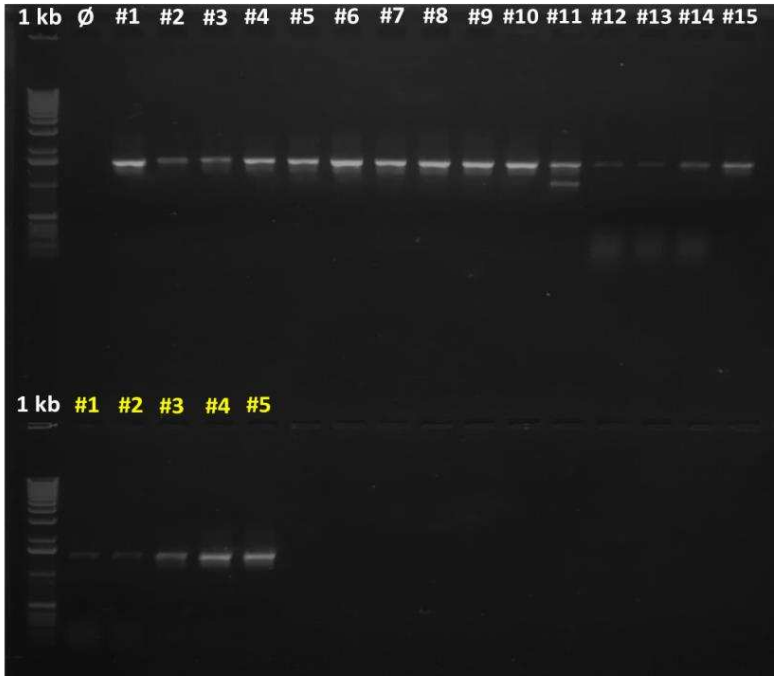

Supplementary Figure 7. Screening of transgenic lines (T0) overexpressing *obv* mutant allele. Amplification of the *obv* mutant gene. Ø corresponds to the negative control. The events in white correspond to *obv* plants transformed with *35S*::*obv* construction and events in yellow to the MT plants transformed with same construction. PCR product has ~ 1700 bp. The primers were used to amplify *obv* gene and part of *35S* promoter.

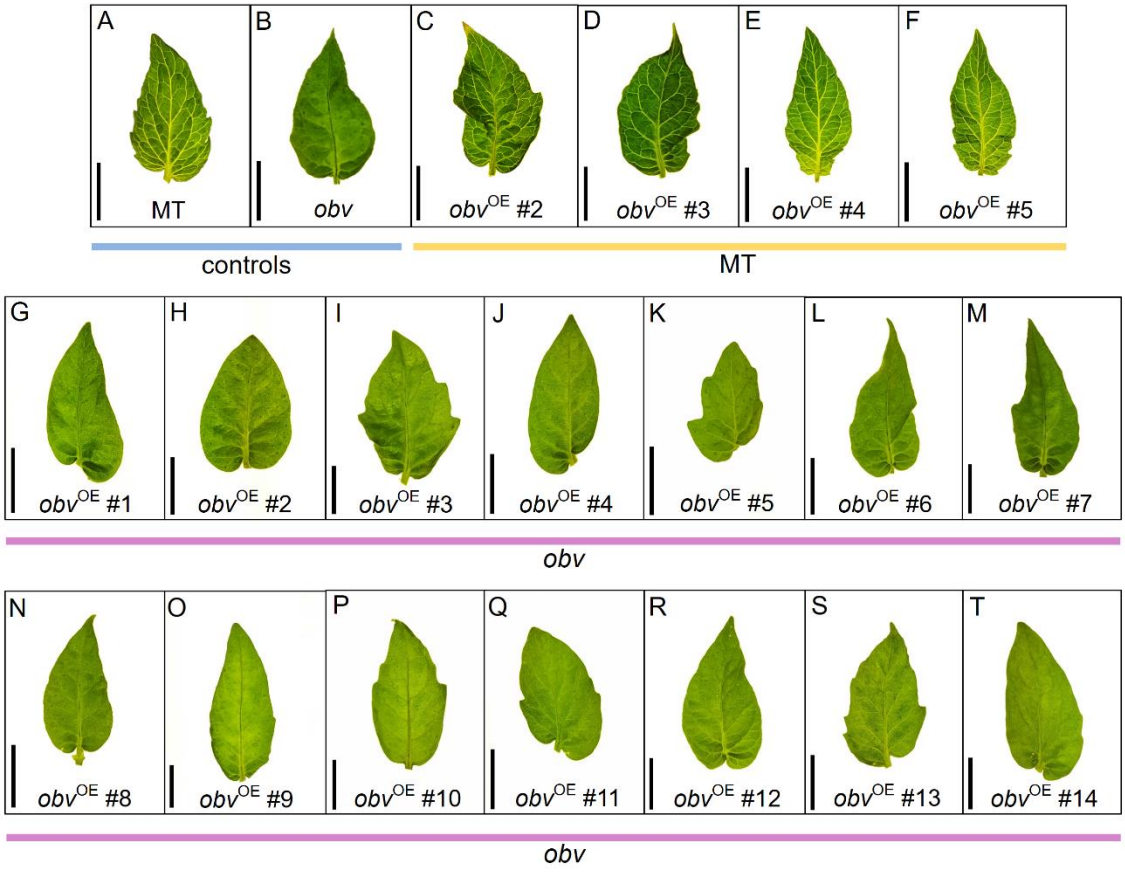

Supplementary Figure 8. Phenotyping of transgenic lines (T0) overexpressing *obv* mutant allele. (A and B) Terminal leaflets of MT (clear veins) and *obv* (dark veins) regenerated *in vitro*. (C-F) Representative leaflets of MT transformed with *35S*::*obv* construction. (G-T) Representative leaflets of *obv* transformed with the same construction. All lines overexpressing *obv* in the mutant background showed that the increase in mutant allele expression did not recover BSEs. Bars = 1cm.

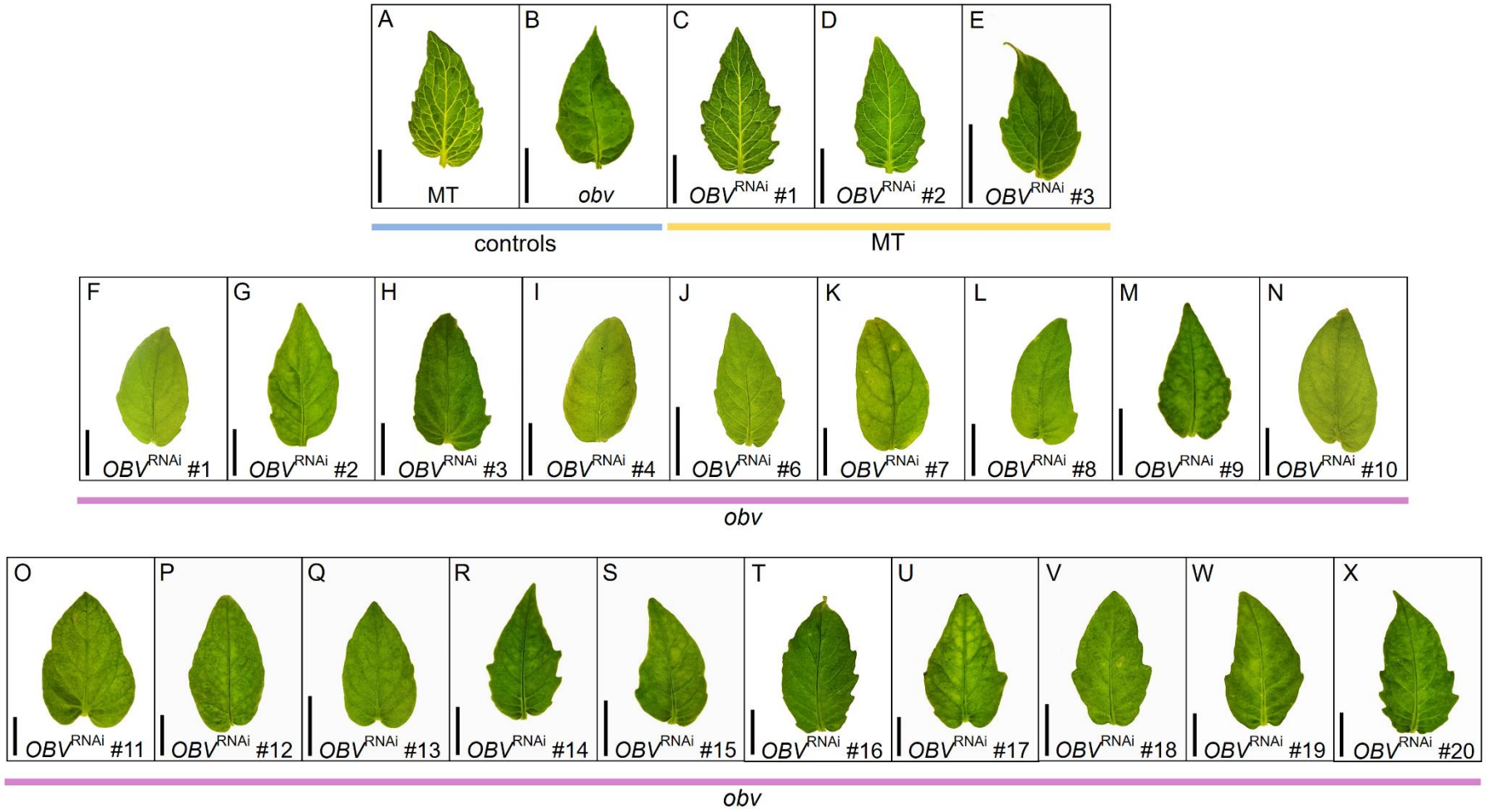

Supplementary Figure 9. Phenotyping of transgenic lines (T0) with *OBV* functional allele silenced by interference RNA (RNAi) (A e B) Terminal leaflets of the MT and *obv* regenerated *in vitro*. (C-E) Representative leaflets of MT transformed with *OBV*-RNAi construction. (F-X) Representative leaflets of *obv* transformed with the same construction. In MT-*OBV* ^{RNAi} line #3 the reduction in *OBV* expression generated total loss of BSEs. Bars = 1cm.

CHAPTER 2: Functional characterization of the *OBV* gene

1. INTRODUCTION

Transcription factors (TFs) containing zinc fingers domains represent a group of most abundant regulatory proteins among eukaryotes. The large family of zinc fingers proteins is divided into subfamilies based in the number and order of Cysteines and Histidines residues in their functional domains (*e.g.* C2H2, C3H, C3HC4, C2HC5, C4HC3, C2HC, C4, C6, and C8). The classic C2H2-type is composed of two Cys and two His, with sequence of 25 to 30 amino acids, following the conserved pattern: C-X2~4-C-X3-P-X5-L-X2-H-X3-H. According to the number of zinc fingers, C2H2-type proteins are grouped into four classes: (I) proteins containing only one C2H2; (II) proteins containing three C2H2 (as in the *OBV* gene); (III) proteins containing more than three and (IV) proteins containing multiple C2H2 (Laity et al., 2001; Fedotova et al., 2017; Wang et al., 2019).

The extensive duplication of C2H2 genes in plants has led to a great diversification in the structure of domains and biological functions. C2H2 proteins can perform their functions through direct binding with DNA or RNA, protein-protein interactions or even by membrane association (Laity et al., 2001; Razin et al., 2012). These proteins are involved in numerous processes of plant development, from germination to control of roots formation, flowers and changes in plant architecture (Li et al., 2013). The zinc finger C2H2 (*INDETERMINATE DOMAIN1/ENHYDROUS*) promotes seed maturation in *Arabidopsis*, through the regulation of gibberellin signaling genes and physical interaction with DELLA proteins (Feurtado et al., 2011). Some members of a zinc finger subfamily (*AtIDD3, AtIDD6, AtIDD10*) form a complex interaction network with SHORT-ROOT/SCARECROW (SHR/SCR) proteins to regulate division, differentiation and cell destiny during root development (Ogasawara et al., 2011; Risueno et al., 2015). The zinc finger of maize (*ZmID1*) and its ortholog in rice (*OsEhd2*) regulate the transition to flowering by inducing florigen expression (Kozaki et al., 2004; Wu et al., 2008).

In tomato, a comprehensive study identified 112 zinc fingers C2H2-type across the genome and 24 were constitutively expressed in all tissues, showing the importance of these regulators to the entire plant development (Ming et al., 2019) Analysis of the expression pattern of several zinc fingers under conditions of abiotic stress, such as temperature, light, drought and osmotic stress, revealed potential roles in the mediation

of stress responses (Khatun et al., 2017). Despite the extensive diversification, it is necessary to better understand the functions and mechanisms of these regulatory proteins, especially in crops of agronomic interest such as tomato. Some important questions remain unclear, such as which genes are regulated by zinc fingers TFs and what other transcription factors they interact with.

Auxin is a key hormone, essential for the regulation of almost all plant development processes including division, expansion and cell differentiation, gametogenesis, embryogenesis, root development, branching, fruit formation and shoot morphogenesis (Vanneste and Friml., 2009). Auxin performs its functions in two main ways: establishing auxin gradients in organs and tissues or through changes in a complex signaling network. The former is achieved by modifications in biosynthesis or polar auxin transport and the latter by alterations in signaling members, such as receptors *AUXIN RESPONSE FACTOR* (ARFs), *AUXIN/INDOLE-3-ACETIC ACID* (Aux/IAAs) and other regulatory proteins (Swarup and Péret., 2012; Li et al., 2016).

Recently, the relationship between auxin and zinc finger proteins in the shoot morphogenesis has been explored. The regulatory proteins *AtIDD*14, *AtIDD*15 and *AtIDD*16 are responsible for maintaining the shoot gravitropism and leaf morphogenesis. These TFs activate the transcription of the *TRYPTOPHAN AMINOTRANSFERASE* (*TAA1*), *YUCCA* (*YUC5*) and *PIN-FORMED* (*PIN1*) genes directly regulating auxin biosynthesis and transport (Cui et al., 2013). The zinc finger *AtIDD4* is involved in specifying the adaxial/abaxial leaf polarity, a function shared with members of the auxin signaling, *AtARF3* and *AtARF4* (Reinhart et al., 2013; Machida et al., 2015). The physical interaction between zinc finger proteins and auxin signaling members was confirmed *in vivo*, showing that *AtZAT6* and *AtIAA17* can interact with each other to control auxin responses by changes in signaling (Shi et al., 2018).

As occurs for ARFs and Aux/IAAs, zinc finger C2H2 proteins have multiple functions on plants development, some functions are more specific to each zinc finger, whereas others are redundant. Zinc fingers modulate the expression by binding to the promoter region of target genes to suppress or activate transcription. In addition, exhibit the ability to interact with each other and with tissue-specific TFs forming complex protein networks, with various combinations. This versatility is responsible for the great functional diversity of C2H2 family (Kumar et al., 2019). However, many members of

the family still remain unexplored, as is the case of Zinc finger C2H2-type tomato protein, here identified as OBV.

For this, we performed the functional characterization of a Zinc finger C2H2-type protein (OVB) in tomato. We showed its role in regulating of BSEs development, through an auxin-mediated pathway, and unveiled its main pleiotropic effects on plant development.

2. MATERIAL AND METHODS

Plant material and growth conditions

Tomato seeds (*S. lycopersicum* cv Micro-Tom and *obv* mutant) were sown on polyethylene trays containing Tropostrato® commercial substrate and kept under greenhouse conditions, ~800 µmol m^{-2} s^{-1}, photoperiod 12/12-h and air temperature 26/18°C day/night. Upon appearance of the first true leaf, seedlings of each genotype were transplanted to pots with capacity of 350 ml. The basic fertilizing was done with NPK 2 g L^{-1} (10-10-10) and limestone 4 g L^{-1}.

The *in vitro* seedling cultivation was conducted under controlled conditions (photoperiod of 16-h/8-h day/night, light intensity of 45 ± 3 µmol m^{-2} s^{-1} and temperature of 25 ± 1 °C) in flasks with 30 mL of half-strength MS medium (Murashige and Skoog, 1962) jellified with agar 4 g L^{-1}, pH 5.7 ± 0,05. Seeds were surface sterilized by agitation in 30% (v/v) commercial bleach (2.7% [w/v] sodium hypochlorite) for 15 min followed by three rinses with sterile distilled water.

Phenotypic characterization

The morphological measurements and leaf characterization were made in MT, *obv* mutant and overexpression lines (in background MT and *obv*), after opening of the first flower. The plant height was measured from the ground level to first inflorescence. The length and diameter of the internodes were obtained by measuring the 4th, 5th and 6th internodes counted from the ground level. Stem diameter was measured using a mechanical pachymeter (Mitutoyo® Vernie Caliper model, Japan) measuring from the level of the cotyledons. The leaves number until first inflorescence was obtained by counting of the leaves on main stem, from the bottom up. The leaf angle was determined using a protractor, based on the insertion of the 5th, 6th and 7th leaf. Leaf complexity was

assessed by counting of leaflets on the 5th, 6th and 7th leaf. All these growth measurements were evaluated in 12 plants per genotype, in control and homozygous transgenic plants, T3 and T4 generation.

For leaf characterization, three terminal leaflets were selected per plant, in eight plants per genotype. The leaflets were digitized using an HP Scanjet G2410 scanner (Hewlett-Packard, Palo Alto, California, USA) and measurements of perimeter, leaflet area, circularity and serration number were obtained using the software Image Pro-Plus® (version 4.5, Media Cybernetics, Silver Spring, USA). Leaflet shape was analyzed as described in Barbosa et al. (2019) using SHAPE (Iwata & Ukai 2002).

Total leaf area and specific leaf area (SLA) were evaluated in eight plants per genotype. The total leaf area was calculated digitizing all leaves in a scanner and calculating the area using Image-Pro Plus. The determination of SLA was calculated through the relationship between leaf area (LA) and dry mass (LDW), as described by the equation:

$$SLA\ (cm^2\ g^{-1}) = LA/LDW$$

Branching pattern analysis was carried out in 12 replicates and assessed through visual observation and scoring three types of ramification stages in the leaf axils: no primordium, visible primordium and fully-developed branch. The accumulation of biomass was determined from root, stem and leaves dry mass by destructive analysis at 60 days after germination, in eight plants per genotype. Root, stem and leaf were collected separately and dried at 70°C for 72 hours.

Vein density measurements

Vein density was measured in five terminal leaflets per genotype. The leaflets were collected and fixed in methanol for 48 hours, then the solution was changed to 100% lactic acid and leaflets were incubated at 100°C until the material was completely translucent (5-6 hours). The diaphanized leaflets were analyzed in the photomicroscope (Zeiss AxioScope A1) and minor vein density was measured as length of minor veins (<0.05-µm diameter) per unit leaf area using the software Image Pro-Plus®.

Gas exchange

Gas exchange analyses were performed in MT, *obv* mutant and overexpression lines (MT-*OBV*^{OE} #3/#5 and *obv*-*OBV*^{OE} #10/#12) at 50 days after germination, using terminal

leaflets of fully expanded fifth leaf. Gas exchange measurements were made in the interval from 8:00 am to 12:00 am, using an open-flow gas exchange system infrared gas analyzer (IRGA) model LI-6400XT coupled with a fluorescence chamber (LI-Cor, Lincoln, NE, USA). The analyses were performed under common conditions for photon flux density (1000 μmol m^{-2} s^{-1}, from an LED source), leaf temperature (25 ± 0.5°C), leaf-to-air vapor pressure difference (16.0 ± 3.0 mbar), air flow rate into the chamber (500 μmol s^{-1}) and reference CO_2 concentration of 400 ppm (injected from a cartridge), using an area of 2 cm^2 in the leaf chamber. Intrinsic transpiration efficiency (TE_i) was obtained as the ratio between photosynthesis (A) and stomatal conductance (g_s). Instantaneous carboxylation efficiency was calculated through ratio between A and intercellular carbon (C_i). The parameters were carried out in six plants per genotype.

Hydraulic conductance (K_{leaf})

Leaf water potential (Ψ_w) was measured in the terminal leaflet of the fifth fully expanded leaf in MT, *obv* mutant and overexpression lines, at 50 days after germination, using a Scholander-type pressure chamber (model 1000, PMS Instruments, Albany, NY, USA). The hydraulic conductance (K_{leaf}) was estimated using the transpiration rates and the water potential difference between the transpiring and non-transpiring leaflet. The non-transpiring leaflet consisted of the lateral leaflet of the same leaf, which was covered with plastic film in the night before the measurements. K_{leaf} was calculated according to:

$$K_{leaf} = E / (\Psi_L - \Psi_X)$$

Where, E is the transpiration rate (mmol m^{-2} s^{-1}) determined during gas exchange measurements, and ($\Psi_L - \Psi_X$) corresponds to the pressure gradient between the transpiring and non-transpiring leaflet (MPa). The parameters were carried out in six plants per genotype.

Real-time quantitative PCR (qRT)

The leaf primordia (≤ 0.5 cm) were collected from Micro-Tom (wild type), *obv* mutant and overexpression lines for extraction of total RNA using Trizol® (Ambion, Life Technology), according to the manufacturer recommendations. The cDNA synthesis was performed with SuperScript™ III First-Strand Synthesis System (Invitrogen). Real-Time quantitative PCR reactions (qRT) were performed in a thermocycler Real-Time StepOnePlus PCR (Applied Biosystems) with a final volume of 14μl using reagent SYBR

Green Master Mix (Thermo Fisher Scientific). The melting curves were analyzed for nonspecific amplifications and dimerization of primers. Absolute fluorescence data were analyzed using the software LinRegPCR (Ruijter et al., 2009) to obtain the values of quantification cycle (Cq) and calculate the primer efficiency. The abundance of transcripts was normalized against the geometric mean of two reference genes, *TIP4* and *EXPRESSED* (Expósito-Rodriguez et al., 2008). All the primers used are listed in Supplementary Table 1.

For *OBV* expression profile, germinated seeds, root tips (≤ 2 cm), hypocotyls, leaf primordia (≤ 0.5 cm), expanding leaf 1 (≤ 2 cm), expanding leaf 2 (≤ 3 cm), mature leaf, flowers (petals + anthers), immature green fruits (IG3) and red ripe fruits (RR) were collected from MT plants.

In situ hybridization

The *OBV* expression analyzed by *in situ* hybridization assay was performed according to Oliveira et al. (2017). Terminal leaflets of Micro-Tom plants harboring *OBV* wild-type allele were collected and processed. The stages of the leaflets used were leaf primordia with approximately 0.5 cm and expanded leaves (4 -5 cm).

Histochemical GUS analysis

Seedlings of MT, *obv* mutant and overexpression lines (20-days-old grown *in vitro*) carrying the auxin-responsive synthetic promoter (*DR5*) (Ulmasov et al., 1995) fused to the reporter gene *uid* (encoding a GUS) were used in this assay. For each genotype, four seedlings were kept in water and four maintained with exogenous auxin (20 µM), during 3 h. The seedlings were incubated at 37 °C for 12 hours, in GUS staining solution (100 mM sodium phosphate buffer, pH 7.2, 10 mM EDTA, 0.1% Triton and 1 mM 5-bromo-4-chloro-3-indolyl-D-glucuronic acid) to reveal GUS activity (described in Wang et al., 2005). After staining, the seedlings were washed in ethanolic series (70%, 80%, 95% e 100%, one hour for each series at 37 °C) to remove chlorophyll.

Auxin sensitivity assays

For hypocotyl elongation assays, MT and *obv* seeds were grown on half-strength MS medium under photoperiod of 16-h/8-h day/night, 45 ± 3 µmol m^{-2} s^{-1} light intensity and 25 ± 1 °C. Hypocotyls were excised from 8-days-old seedlings, cut into 1 cm sections and preincubated on buffer (10 mM KCl; 1 mM MES-KOH [pH 6] and 1% [w/v] Suc) for 2

hours at 25°C in the dark to deplete endogenous auxin. Then, segments were incubated in the same buffer supplemented with α-naphthalene acetic acid (NAA) at increasing concentrations (0, 0.1, 1, 10, 100 e 1000 µM) for 24 hours under agitation, 45 ± 3 µmol m^{-2} s^{-1} light intensity and 25 ± 1 °C (Silva et al., 2018 with modifications). For each genotype, three biological replicates were conducted and each replicate was composed of 20 segments. Hypocotyls were photographed and the relative growth rate evaluated using the software Image Pro-Plus®.

For root regeneration from cotyledon explants, seeds of MT, *obv* and overexpression lines were germinated *in vitro* in half-strength MS medium under the same conditions described above. Cotyledons from 12-days-old seedlings were excised and incubated on petri dishes containing MS medium with or without IAA supplementation (0; 0.04; 0.4; 4 and 40 µm). The explants were kept in 25 ± 1 °C under photoperiod of 16-h/8-h and light intensity of 10-20 µmol m^{-2} s^{-1} for 15 days (Wang et al., 2005 with modifications). After this period, the number of explants with visible roots was determined. Four replicates were conducted by genotype and each replica was composed by a petri dish with 12 explants.

Polar auxin transport assays (PAT)

Hypocotyl sections with 10-mm were excised from MT and *obv* seedlings 2-week-old and incubated in 5 mM phosphate buffer (pH 5.8) containing 1 µM IAA for 2 hours at 25°C ± 2°C on a rotary shaker (200 rpm). These segments were placed between receiver blocks (1% [w/v] agar in water) and donor blocks (1% [w/v] agar in 5 mM phosphate buffer [pH 5.8] containing 1 µM IAA and 100 nM [^{3}H] IAA) oriented with their apical ends toward the donor blocks. After 4 hours of incubation inside a humid chamber at 25°C ± 2°C, the receiver blocks were removed and stored in a 3 mL scintillation cocktail (Ultima Gold; PerkinElmer). Receiver blocks plus scintillation cocktail were shaken overnight at 100 rpm and 28°C ± 2°C before analysis in a scintillation counter. As negative control, some hypocotyl segments were sandwiched for 30 min between NPA-containing blocks (1% [w/v] agar in water containing 20 µM NPA) an auxin transport inhibitor. ^{3}H dpm was converted to fmol of auxin transported as described by Lewis and Muday (2009).

Auxin quantification

Endogenous IAA levels were determined by gas chromatography-tandem mass spectrometry-selecting ion monitoring (Shimadzu model GCMS-QP2010 SE). Samples (50–100 mg fresh weight) were extracted and methylated as described (Rigui et al., 2015). About 0.25 µg of the labeled standard [$^{13}C_6$]IAA (Cambridge Isotopes) was added to each sample as an internal standard. The chromatograph was equipped with a fused-silica capillary column (30 m i.d., 0.25 mm, 0.5-µm-thick internal film) DB-5 MS stationary phase using helium as the carrier gas at a flow rate of 4.5 mL min^{-1} in the following program: 2 min at 100°C, followed by a ramp of 10°C min^{-1} to 140°C, 25°C min^{-1} to 160°C, 35°C min^{-1} to 250°C, 20°C min^{-1} to 270°C and 30°C min^{-1} to 300°C. The injector temperature was 250°C, and the following mass spectrometer operating parameters were used: ionization voltage, 70 eV (electron impact ionization); ion source temperature, 230°C; and interface temperature, 260°C. Ions with mass-to-charge ratios of 130 and 189 (corresponding to endogenous IAA) and 136 and 195 (corresponding to [$^{13}C_6$]IAA) were monitored, and endogenous IAA concentrations were calculated based on extracted chromatograms at mass-to-charge ratios of 130 and 136.

Promoter analysis

The promoter sequence of the *OBV* gene (5000 bp upstream of the start codon) from *S. lycopersicum* cv Heinz was extracted from database for Solanaceae Sol Genomics (https://solgenomics.net/locus/37560/view). The nucleotide sequence was used as entry in the Database of Plant *Cis*-acting Regulatory DNA Elements (PLACE) (https://www.dna.affrc.go.jp/PLACE/?action=newplace). The most relevant *cis*-elements were selected and their locations in the promoter region were noted.

Statistical analysis

The experimental design was completely randomized. The data were submitted to analysis of variance (ANOVA) using Sisvar® version 5.6 and the means were compared by Tukey test at 5% level of significance ($P \leq 0.05$).

3. RESULTS AND DISCUSSION

3.1 *OBV* effects on plant development

Having produced evidence that *OBV* is responsible for the formation of BSEs in tomato leaves, we next decided to explore its mechanism of action and potential pleiotropic effects. We first characterized the expression profile of *OBV* in seeds, roots, hypocotyl, leaves in different stages, flowers and fruits (immature green and red ripe). The *OBV* gene is highly expressed in flowers and leaves especially young leaves (Figure 1A), corroborating publicly available expression data (Sato et al., 2012). We show that accumulation of *OBV* transcripts is accentuated in specific regions in the primordial leaf and apical meristem. We further narrowed down our characterization and we show that *OBV* transcripts are concentrated in leaves to a region around the vascular bundle, as indicated by the probe signal using *in situ* hybridization in leaf cross-sections (Figure 1B-E).

To obtain a robust understanding of phenotypic effects promoted by the *OBV* gene, we used *obv* mutants complemented with overexpression construction and included plants in MT background transformed with the same construction. We selected two lines for each background: MT-*OBV*^{OE} #3; MT-*OBV*^{OE} #5 and *obv*-*OBV*^{OE} #10; *obv*-*OBV*^{OE} #12 to be used in the functional characterization. All overexpression lines used were homozygous, in T3 or subsequent generations and had the *OBV* expression level confirmed by qPCR (Supplementary Figure 1). We conducted a comprehensive analysis to investigate possible actions of the *OBV* gene in the phenology, growth and morphology of MT and *obv* plants.

We observed that all lines overexpressing *OBV* gene in MT (MT-*OBV*^{OE} #3; MT-*OBV*^{OE} #5) and *obv* (*obv*-*OBV*^{OE} #10; *obv*-*OBV*^{OE} #12) had a delay in flowering and a discreet reduction in lateral branching (Supplementary Figures 2, 3). In general, the ox-lines showed a reduction in height, caused by shortening of the internodes (Supplementary Table 2). Other characteristics, such as the accumulation of biomass in roots and stems, were also negatively impacted in the ox-lines. Despite this reduction, the leaf dry mass and ratio root/shoot remained similar to MT (wild-type) in almost all lines (Supplementary Figure 4).

Previous works reported that the gas exchanges are different between heterobaric and homobaric leaves (karabourniotis et al., 2000; Nikolopoulos et al., 2002). In tomato,

under control conditions, the photosynthetic assimilation rate is the same in leaves with or without BSEs. However, stomatal conductance is lower in homobaric leaves (Zsogon et al., 2015; Barbosa et al., 2019). We explored some gas exchange parameters in the plants with different levels of *OBV* expression and saw that in most of them, the photosynthesis (*A*), stomatal conductance (g_s), intrinsic transpiration efficiency (TE_i) and instantaneous carboxylation efficiency (*A*/*Ci*) were similar to wild-type MT (Supplementary Figure 5). We show that leaf structure and function were recovered in the complemented mutants.

Curiously, the increase in *OBV* expression in MT and *obv* mutant generated a steeper leaf insertion angle (Figure 1F, G). Steeper leaf angle is a trait of agricultural value, as it improves photosynthetic performance and allows high density cultivation (Sakamoto et al., 2006). The more erect leaves position enhances the capture of light in periods of low light intensity (*e.g.* winter or morning). On the other hand, in periods of intense light (*e.g.* summer or midday), steep angles decrease the interception of light, minimizing the risks of photoinhibition and leaf overheating, thus improving water-use efficiency (Falster and Westoby, 2003). The leaf insertion angle is a characteristic regulated by auxin and brassinosteroids (Sakamoto et al., 2006). In rice, it was shown that a zinc finger transcription factor (*Loose Plant Architecture1*; *LPA1*) changes plant architecture, through control of leaf insertion angle (Wu et al., 2013). Therefore, the combinatorial effect of *OBV* and hormonal signalling may have caused a reduction in the leaf angle of tomato plants.

Finally, in the reproductive phase we observed that fruit morphology in all ox-lines was also altered, resulting in rounder fruit shape (Figure 1H, Supplementary Figure 6). Some fruits shape has a greater demand by the consumer market and therefore are required in breeding programs. The molecular bases that control this trait are still being elucidated to facilitate manipulation by new breeding techniques, such as genetic editing. In tomato, fruit shape is governed by mutations in four main genes: *SUN*, *OVATE*, *SOV1* and *FS8.1*, which promote changes in the number and cellular expansion mediated by signalling and auxin polar transport (Wang et al., 2019). We showed that additional regulators, such as *OBV* transcription factor, can control fruit shape directly or, potentially through links with auxin.

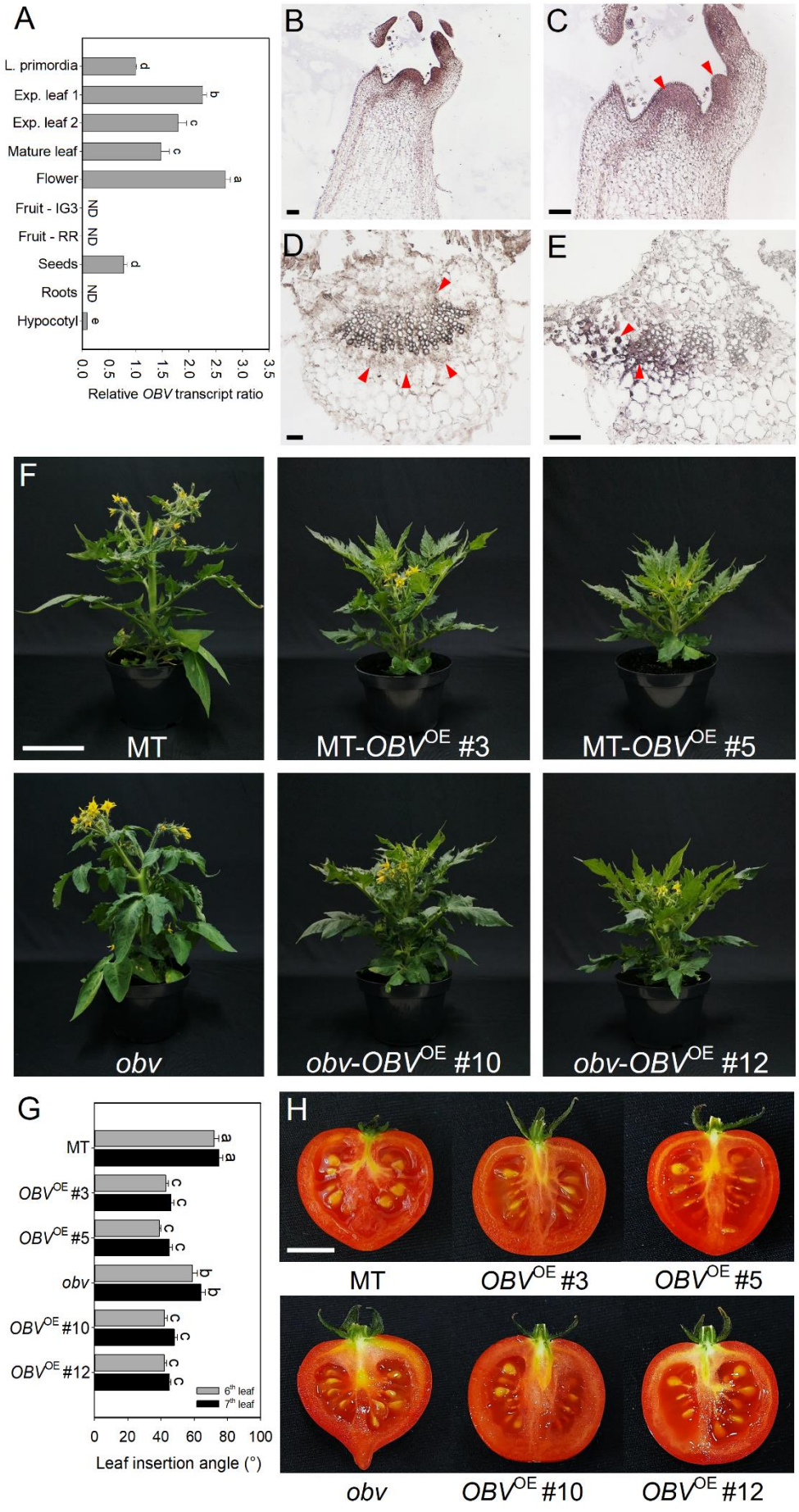
A
L. primordia
Exp. leaf 1
Exp. leaf 2
Mature leaf
Flower
Fruit - IG3
Fruit - RR
Seeds
Roots
Hypocotyl
ND
0.0 0.5 1.0 1.5 2.0 2.5 3.0 3.5
Relative OBV transcript ratio
B
C
D
E
F
MT
MT-OBV^OE #3
MT-OBV^OE #5
obv
obv-OBV^OE #10
obv-OBV^OE #12
G
MT
OBV^OE #3
OBV^OE #5
obv
OBV^OE #10
OBV^OE #12
6th leaf
7th leaf
0 20 40 60 80 100
Leaf insertion angle (°)
H
MT
OBV^OE #3
OBV^OE #5
obv
OBV^OE #10
OBV^OE #12

Figure 1. Characterization of the *OBV* gene in tomato (*Solanum lycopersicum* cv Micro-Tom). (A) Relative *OBV* mRNA levels in leaves, flowers, fruits, seeds, roots and hypocotyl of MT. In roots and fruits (immature green and red ripe) *OBV* expression was not detected. ND = not detected. (B-E) *In situ* hybridization showing *OBV* expression patterns in MT leaves. (B) Longitudinal section of apical meristem and leaf primordium. (C) Close view of the apical meristem showing the probe signal accumulated in a large part of the meristem and at the primordial initiation points (arrows). (D and E) Cross-section of terminal leaflet expanded. The arrows show the specific regions around the vascular bundles where *OBV* transcripts accumulate. Scale bars: 100 µm. (F) Representative plants of MT (harboring *OBV* functional allele), *obv* (harboring *obv* mutant allele) and overexpression lines generation T3, homozygous (harboring high levels of *OBV* functional allele) at 60 days after germination (dag). Bars = 5 cm. (G) Leaf insertion angle in two representative leaves (6^{th} and 7^{th}) measured at 50 dag in MT, *obv* and ox-lines. Data are means ± se (n = 12 plants). Different letters indicate statistically significant differences (Tukey's test, $P < 0.05$). (H) Effect of the *OBV* in the fruit shape of MT, *obv* mutant and ox-lines. Bars = 1 cm.

Besides the absence of BSEs, the *obv* mutant has subtle phenotypic characteristics that distinguish it from wild-type MT plants. Whereas MT leaflets have a wrinkled texture and highly serrated leaf margin, in *obv* mutant the leaflets have a relatively slick texture and the margins rounder. We thus decided to conduct a leaf characterization to relate the differences found in leaf morphology to the different levels of *OBV* expression using MT, *obv* and the four selected ox-lines. We first compared the leaflet shape using the SHAPE software. The *obv* leaf differs from the other genotypes, showing an oval shape and margins smooth. While the leaves of all ox-lines, including those in the mutant background, had a format similar to wild-type MT, with elliptical shape and acuminated tip (Supplementary Figure 8).

Next, we evaluated characteristics related to the degree of leaf serration. We found that *obv* mutant has a smaller perimeter and perimeter^2, followed by MT and lastly the four ox-lines. The perimeter relates with leaf cutout, therefore we can see that all ox-lines with a very pronounced serration the perimeter is larger (Figure 2A, B). The extreme leaflets serration explains the significant loss of leaflets area in these four ox-lines (Figure 2C). Despite the drastic reduction in the leaflets area, total leaf area has not been compromised (Figure 2D). We also measured leaflet circularity and serration number and confirmed that *obv* had increased roundness and decreased leaf margin serrations. The ox-lines, either in the MT or the *obv* background showed a reduction in circularity and increase in serration number (Figure 2E, F).

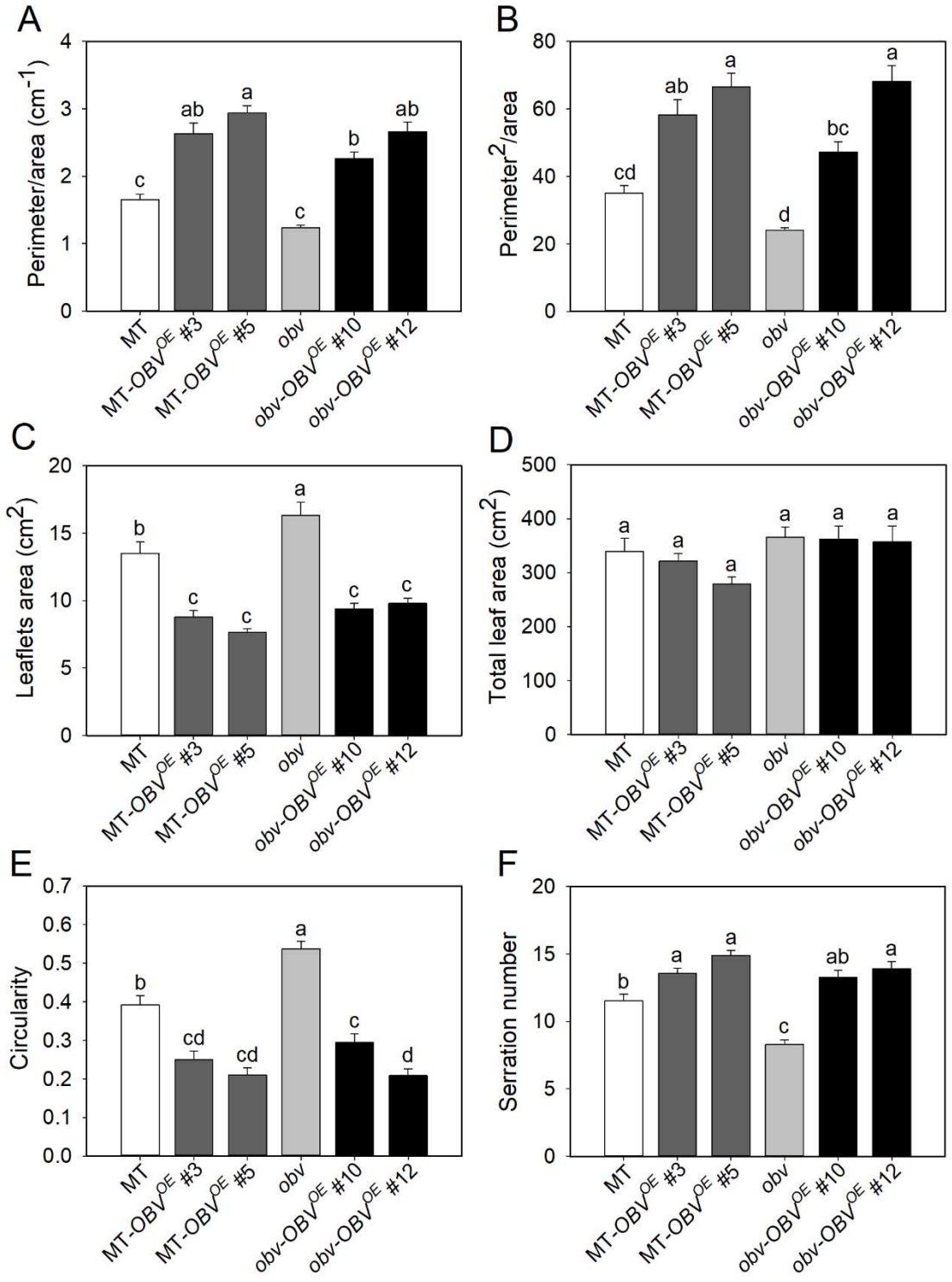

Figure 2. *OBV* alters leaf morphology in tomato (*Solanum lycopersicum* cv Micro-Tom). Morphological parameters evaluated in MT, *obv* mutant and overexpression lines generation T3, homozygous: (A) relationship between perimeter/area; (B) perimeter^2/area; (C) terminal leaflets area; (D) total leaf area; (E) Circularity and (F) serration number. Bars are mean values ± s.e.m. (n = 20 terminal leaflets per genotype). Different letters indicate significant differences by Tukey's test at 5% probability.

The role of auxin in the regulation of leaf morphogenesis and development of vascular tissue is well described (Vanneste and Friml, 2009). During the formation of serrations, the leaf margin is interspersed with regions auxin maxima and minima. The points of auxin accumulation promotes intense cell division and expansion, while in places where auxin is not accumulated, growth is repressed. This pattern of differential growth then gives rise to margin serration. In the repression sites, transcription factors *GOBLET* (*GOB*) and ENTIRE (*Aux/IAA9*) act in a redundant way to restrain the auxin responses and thus inhibit cell proliferation (Koenig et al., 2009). Cell growth sites are formed by the activity of PIN and AUX1/LAX transporters that redirect the flow of auxin to target regions. The expression of specific ARFs, such as *ARF19*, also is required for divisions and cell differentiation (Ben-Gera et al., 2012; Xiong and Jiao, 2019).

Given the intimate association between BSEs and leaf veins, we also interrogated if our various OBV^{OE} genotypes could have alterations in vein density, a key ecophysiological trait influencing plant water relations (Sack and Scoffoni, 2013). Our results revealed a reduction in vein density in the *obv* mutant compared to MT plants. All ox-lines had similar vein density to the wild-type MT calling attention to the *obv* lines, where the expression of *OBV* functional besides recovering BSEs has also restored the vein density (Figure 3B, C). We observed a similar behavior in leaf hydraulic conductance (K_{leaf}). K_{leaf} was higher in heterobaric (MT) than in homobaric (*obv*) leaves and all ox-lines, especially in the mutant background, presented high K_{leaf} as in MT (Figure 3D). The relationship between veins and K_{leaf} showed that veins density positively influences the hydraulic conductance in the tomato leaves (Figure 3E, F).

Architecture and veins density are crucial traits for increases in the hydraulic and photosynthetic capacity of the leaf (Sack and Scoffoni, 2013). The presence of BSEs affects conductance hydraulic and vein architecture, as noticed in MT and *obv*, allowing to change the leaves functionality through the manipulation of BSEs. As well as the other traits observed in OBV^{OE} lines, the vein development is regulated by biosynthesis, transport and auxin signalling (Cheng et al., 2006; Verna et al., 2015; Wang et al. 2005). This set of evidence indicates that all pleiotropic effects generated by *OBV* have a connection with auxin and may involve genes for biosynthesis, transport or hormonal signalling.

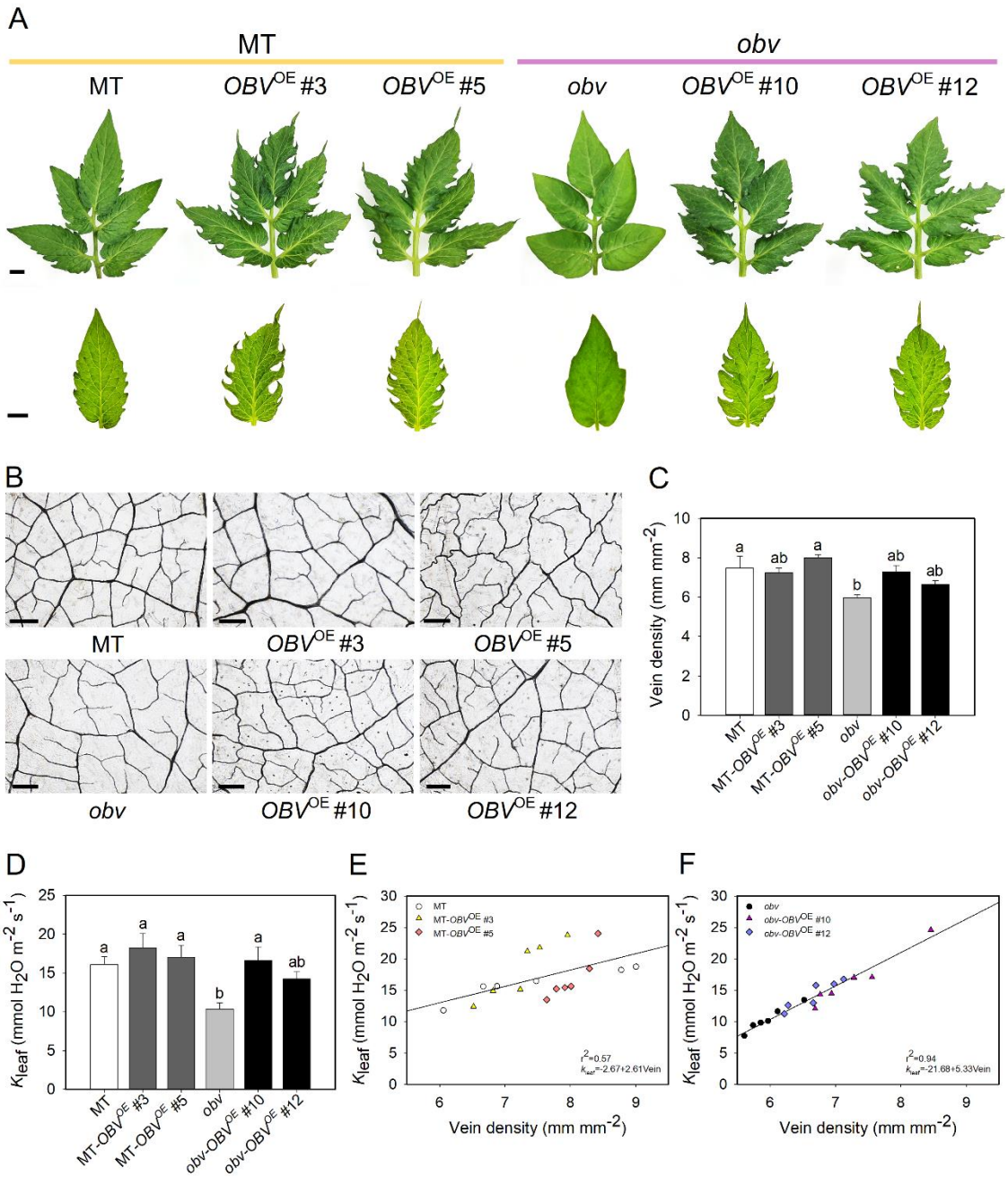

Figure 3. Impacts of the *OBV* gene on leaf morphology, vein density and hydraulic conductance. (A) Leaf and leaflets phenotype of MT (*Solanum lycopersicum* cv Micro-Tom), *obv* mutant and overexpression lines, generation T3 homozygous. Bars = 1cm. (B) Relationship between *OBV* functional expression and veins density. Representative sections of MT, *obv* and ox-lines. Scale bar =100 µm. (C) Histogram show density of veins (secondary and higher order) measured in sections (7,8 mm^2) of the diaphanized terminal leaflet. (D) Leaf hydraulic conductance in MT (heterobaric), *obv* mutant (homobaric) and ox-lines (heterobaric). Bars are mean values ± s.e.m. (n=6 leaflets per genotype). Different letters indicate significant differences by Tukey's test at 5% probability. (E-F) Relationship between K_{leaf} and vein density for MT (white), MT-*OBV*^{OE} #3 (yellow), MT-*OBV*^{OE} #5 (pink), *obv* (black), *obv*-*OBV*^{OE} #10 (purple) and *obv*-*OBV*^{OE} #12 (blue). Each point corresponds to an individual measurement.

3.2 Assessment of the relation between *OBV* and auxin

The *OBV* effects on auxin-regulated traits, together with functional annotations of the gene (Supplementary Table 4) and the characterization of *OBV* orthologs in *Arabidopsis* (*IDD14*, *IDD15* and *IDD16*) (Morita et al., 2006; Cui et al., 2013) suggested a potential role for auxin as a mediator of BSE development. To investigate a probable relationship between *OBV* and auxin, we examined the expression of a *β-glucuronidase* reporter gene (*GUS*) under control of the auxin-responsive synthetic *DR5* promoter in wild-type MT and *obv* mutant plants. In MT, *GUS* expression was observed mainly in leaves, in the regions of veins, but was poorly detectable in the hypocotyl and root system (Figure 4A). In *obv* mutant, the *GUS* signal was greatly intensified in the veins regions (Figure 4B). After treatment with exogenous auxin (20 μM IAA), the *GUS* expression increased similarly in MT and *obv* (Figure 4C, D).

Auxins, like other plant hormones, can exert their effect through alterations in metabolism (biosynthesis/degradation), transport and signaling. Therefore, we first determined IAA concentrations in leaf tissues, more precisely in leaf primordia, where *OBV* expression is intense, and no clear differences were found between MT, *obv* and overexpression lines (Figure 4E). To investigate polar auxin transport (PAT) in MT and the *obv* mutant, a radioactive auxin (^{3H}IAA) transport assay was conducted in detached hypocotyls. This is an indirect method to infer how much auxin is transported through the organ. No differences were found between genotypes either (Figure 4F). Lastly, we examined auxin sensitivity in MT and *obv* through a dose-response assay in hypocotyl elongation. After 24 hours of treatment with synthetic auxin (α-naphthalene acetic acid, NAA) hypocotyl elongation occurred in MT even in concentrations of 0.1 mM, while in the *obv* mutant, hypocotyl elongation was inhibited in a 10-fold lower concentration (0.01 mM) (Figure 4G). These results indicate that *obv* is more sensitive to the inhibitory effect of high auxin concentrations.

To investigate better this greater auxin sensitivity, we decided to conduct a second auxin sensitivity assay, known as *in vitro* root regeneration, this time including the OBV^{OE} lines. All genotypes emitted adventitious roots starting with the dose of 0.4 μM IAA, at which point MT and *obv* showed similar sensitivity, whereas in OBV^{OE} lines the formation of roots was reduced (Figure 5A). At higher doses (4 and 40 μM IAA), the *obv* mutant had an increased emission of roots, confirming its greater auxin sensitivity in

relation to MT (Figure 5B). All *OBV*^{OE} lines showed a significant reduction in root formation. The high levels of *OBV* expression resulted in a dramatic reduction in sensitivity to auxin (Figure 5D).

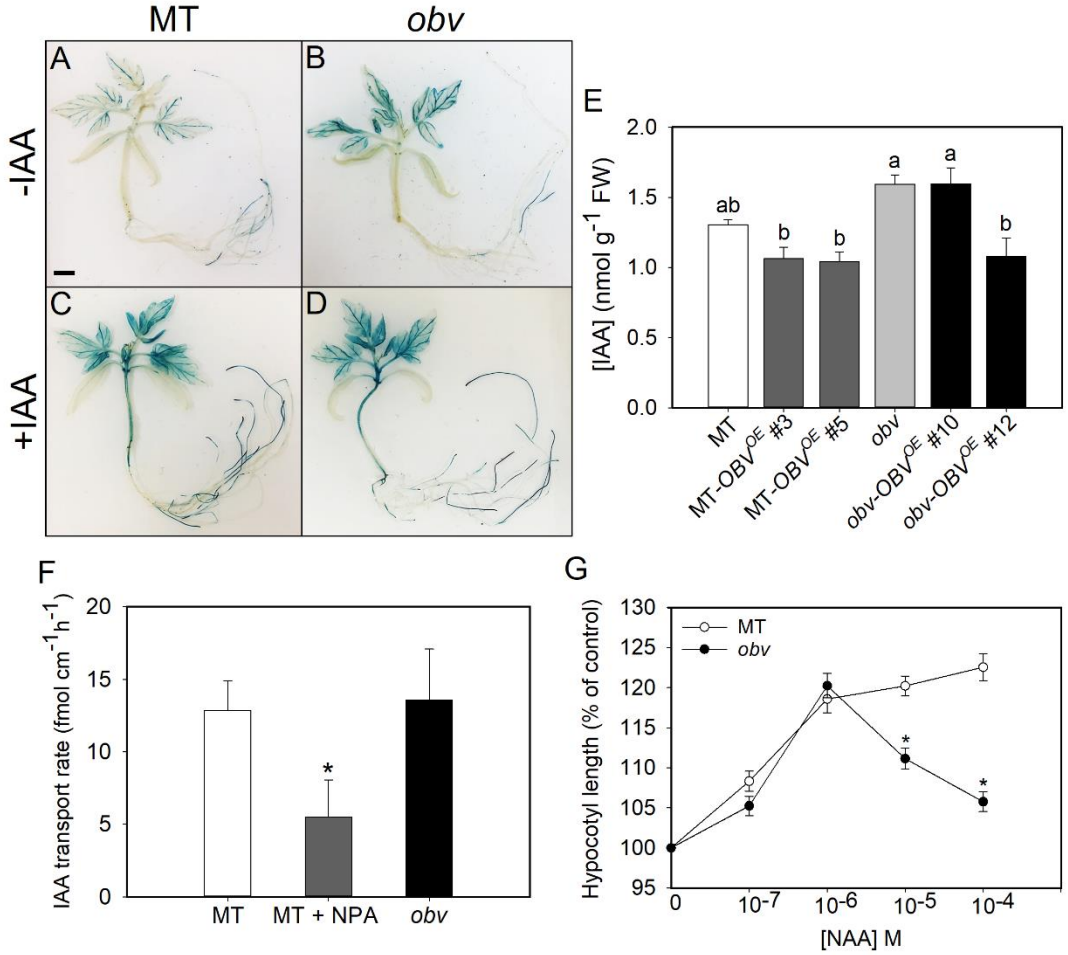

Figure 4. Relationship between *OBV* and auxin. (A-D) Histochemical GUS analysis in homozygous lines of MT and *obv* mutant containing *DR5*::*GUS* construct. (A) Expression pattern of *GUS* reporter gene in MT seedlings (B) and *obv* mutant, that shows the most pronounced signal in the regions of vein. (C and D) Expression pattern of *GUS* in MT and *obv* after treatment with exogenous auxin (20 µM IAA) Bars = 1 cm. (E) Auxin levels in leaf primordia (≤ 0.5 cm) of MT, *obv* and four *OBV*^{OE} lines, generation T3. Data represent means of four biological replicates. Each biological replica was composed by a pool of three plants. Different letters indicate significant differences by Tukey's test at 5% probability. FW = Fresh weight. (F) [^{3}H]IAA transport in detached hypocotyls of MT and *obv*. The NPA is an auxin polar transport inhibitor and was used as negative control. Data are means (±SE) of at least ten biological replicates. (G) Auxin dose response in hypocotyl segments. Elongation is given as increase in percentage at final length over the initial length after 24 h incubation in a solution containing the NAA under increasing concentrations. Data are means (±SE) of three biological replicates with ≥ 20 segments for each replicate. Statistically significant differences compared with the MT were determined using Tukey test: *P<0.05.

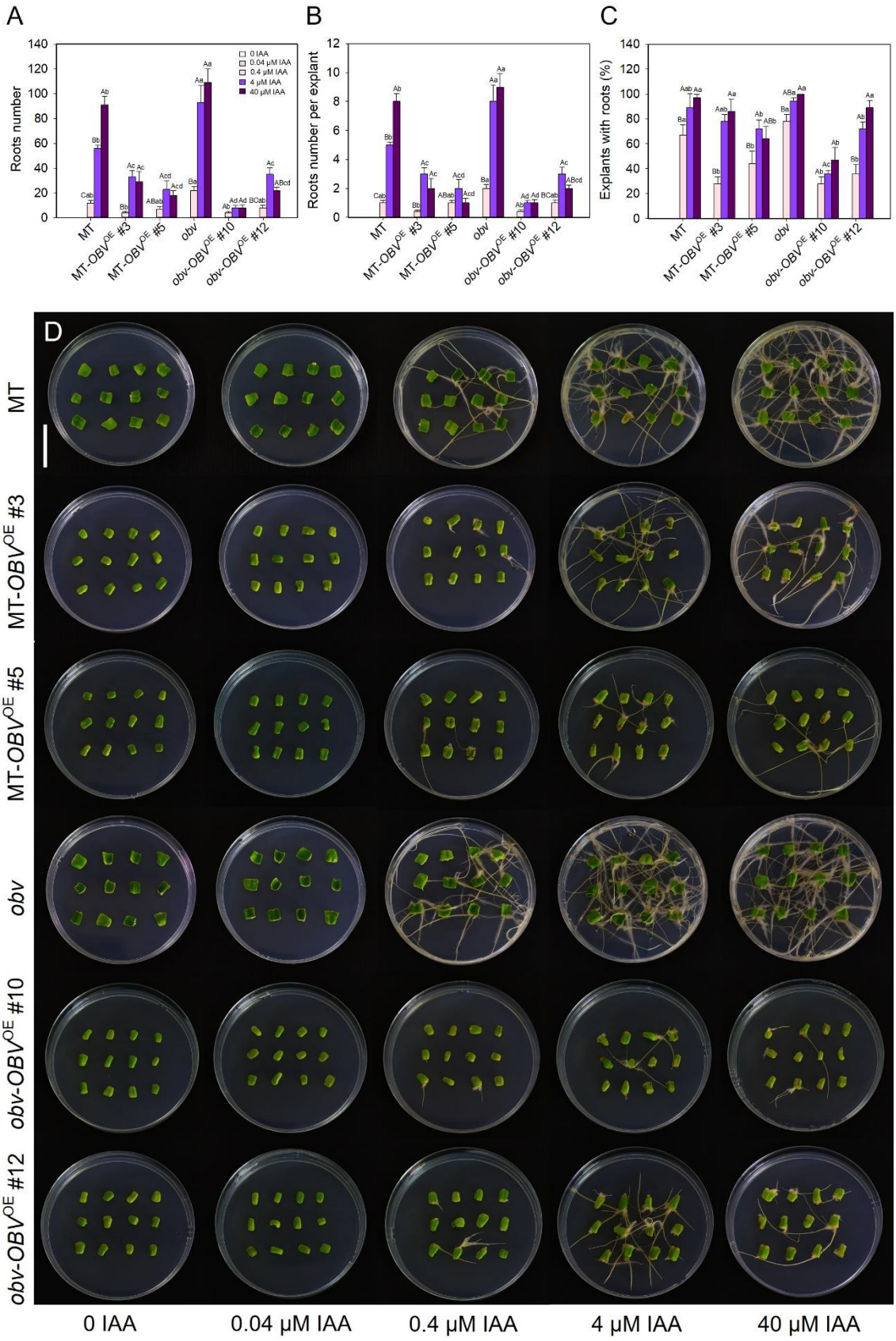
A
B
C
D
Roots number
Roots number per explant
Explants with roots (%)
0 IAA
0.04 μM IAA
0.4 μM IAA
4 μM IAA
40 μM IAA
MT
MT-OBV^OE #3
MT-OBV^OE #5
obv
obv-OBV^OE #10
obv-OBV^OE #12
0 IAA
0.04 μM IAA
0.4 μM IAA
4 μM IAA
40 μM IAA

Figure 5. Reduction of auxin sensitivity in *OBV* overexpression lines. Auxin dose-response assay in 12-day-old cotyledon explants. (A) Total number of emitted roots induced from the concentration of 0.4, 4 and 40 µm IAA, after 15 days of cultivation. (B) Number of roots per explant. (C) Percentage of explants with emitted roots. n = 4 plates with 12 explants per plate. (D) Illustration of the dose-response assay showing a significant reduction in the emission of roots in OBV^{OE} lines. Different letters indicate statistically significant differences by Tukey's test, $P < 0.05$. Uppercase letters compare doses within the same genotype, lowercase letters compare dose effect between different genotypes. Bar = 1cm.

The repression in the auxin response was reinforced with a second GUS assay, this time on *OBV*^{OE} lines. Independent of the background, all the *OBV*^{OE} lines had a visible reduction in the GUS signal. Only a few points on the seedling were detected (Figure 6C, E, G, I -arrows). After exogenous auxin treatment the signal was intensified, however, the intensity remained lower than in MT (Figure 6D, F, H, J). These assays show that increase in *OBV* expression in the plant generates a repression in response to auxin.

The results described above suggested that *OBV* could cause alterations in auxin signaling. Thus, we next analyzed the expression profiles of *AUXIN RESPONSE FACTOR* (*ARF*) and *AUXIN/INDOLE-3-ACETIC* (*Aux/IAA*) transcriptional regulators. We analyzed leaf primordia (≤ 0.5 cm) of MT, *obv* mutant and three *obv-OBV*^{OE} complemented lines to detect expression changes of the signaling components at a developmental stage corresponding to the formation of BSEs in leaves. The results showed multiple changes in expression patterns, including consistent upregulation (*ARF*3, 9B, 10A, 10B, 19 and *Aux/IAA*4 and 14) and downregulation (*Aux/IAA*1A, 1B, 2, 3, 7B, 11, 13, 26 and 35) (Figure 6K).

Analyzing the expression profile of MT and *obv* we found two transcriptional regulators (*ARF4* and *IAA15*) with strong upregulation in the mutant. Consistently, both TFs were downregulated in the mutants complemented with *OBV* functional allele. In tomato, the transcriptional repressor *IAA15* is involved in the development of axillary branches and formation of trichomes on leaves and stems (Deng et al., 2012). The transcriptional repressor *ARF4* control traits related to tomato fruit quality, such as increased sugar content, greater firmness and prolonged shelf life (Sagar et al., 2013a; Sagar et al., 2013b). *ARF4* also been shown to be involved in abiotic stress responses, the loss of gene function improved tolerance of tomato plants to salinity and water deficit (Bouzroud et al., 2020; Chen et al., 2021). In leaves, *arf4* regulates the stomatal conductance and leaf winding caused by disproportionate growth of cells in the abaxial face. Despite of reported effects until now, other likely roles of *ARF4* in leaf development remains unclear. We showed a differentiated expression of *ARF4* in leaves of *obv* mutant and *OBV*^{OE} lines. A recent work reported that *ARF4*, as seen in *OBV*, is expressed in the vascular bundles (Chen et al., 2021), supporting the hypothesis of a possible involvement of *ARF4* in BSEs development.

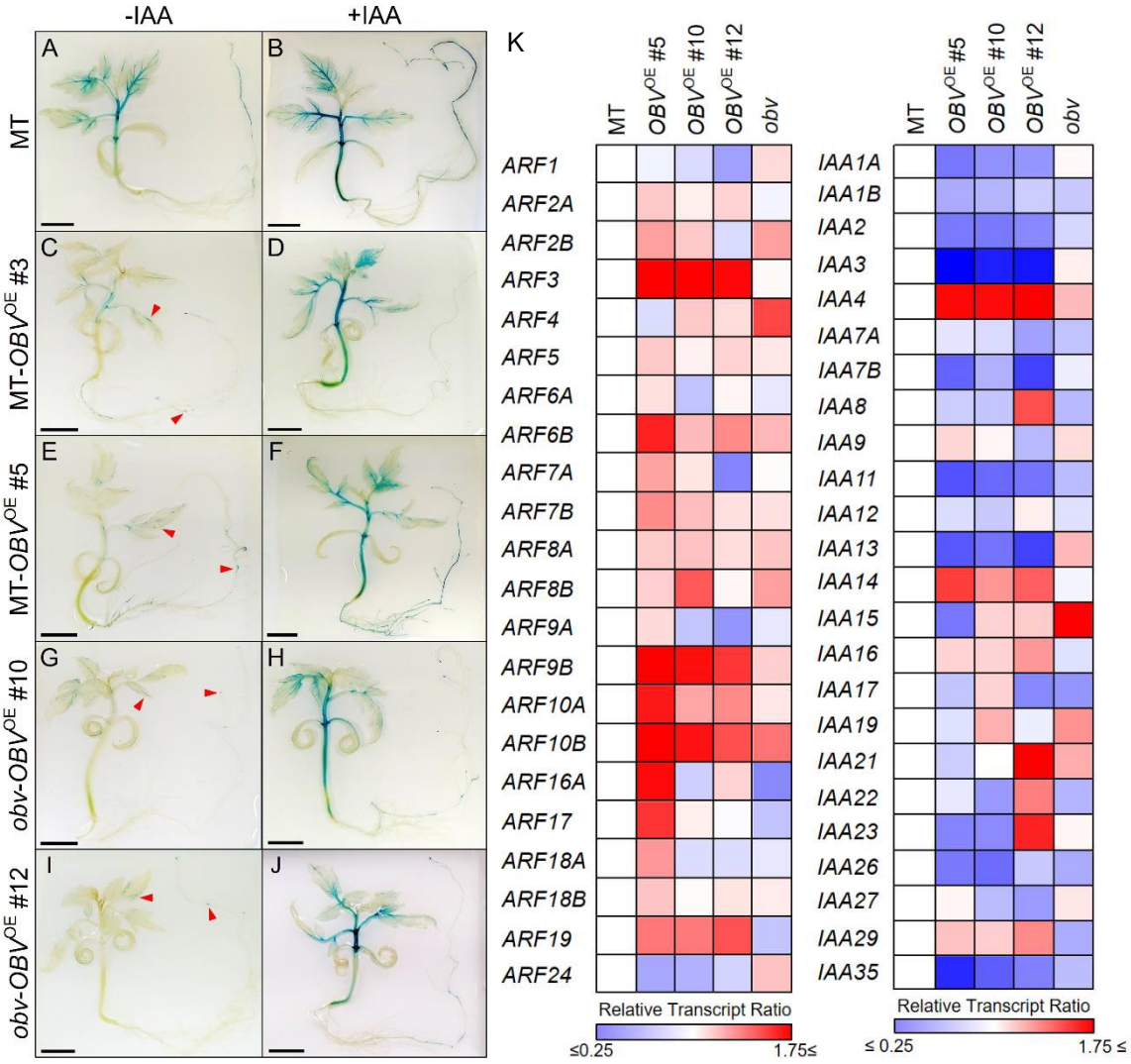

Figure 6. *OBV* alters auxin response and signaling. Histochemical GUS analysis in MT (MT x *DR5*::*GUS* F_1) and overexpression lines (*OBV*^{OE} x *DR5*::*GUS* F_1) seedlings at 30 days after germination. Expression pattern of *GUS* reporter gene fused to the auxin-inducible *DR5* promoter in wild-type seedlings and *OBV*^{OE} lines (A, C, E, G, I), that show a minor sign throughout the seedling. (B, D, F, H, J) Expression pattern of GUS in MT and *OBV*^{OE} lines treated with exogenous auxin (20 µM IAA). Bars = 1 cm. (K) Transcriptional profile of *AUXIN RESPONSE FACTOR* (*ARF*) and *AUXIN/INDOLE-3-ACETIC* (*Aux/IAA*) genes from leaf primordia. Heat map represents the transcript profiles in MT, *obv* and three complemented lines (*obv*-*OBV*^{OE} #5, *obv*-*OBV*^{OE} #10 and *obv*-*OBV*^{OE} #12). Values represent means of four biological replicates normalized against the wild-type sample. Statistically significant differences in comparison with the wild-type are represented by colored squares ($P < 0.05$).

We had noticed in previous work, that tomato lines with loss of *ARF4* function lacked translucent veins in the leaves. We assessed the potential role of *ARF4* in BSEs development using a CRISPR/Cas9-generated knockout mutant (*arf4*) and a transcriptionally silenced line harboring an *ARF4*-antisense transgene (*ARF4*-as). First, we confirmed the lack of BSEs in leaves of both *arf4* and *ARF4*-as plants through water infiltration assay (Figure 7A), visually analyzing the leaflets against light (Figure 7B, C) and in cross-sectional images (Figure 7D). Next, we conducted qPCR analyses and found that *OBV* expression is increased in *arf4* and *ARF4*-as leaves (Figure 7E). We further found that *ARF4* expression was increased in the *obv* mutant but not in the *obv*-*OBV*^{OE} #5, #10 and #12 complemented lines (Figure 7F). Taken together, these results suggest an involvement of *ARF4* and auxin signaling machinery with *OBV* in the control of BSE development.

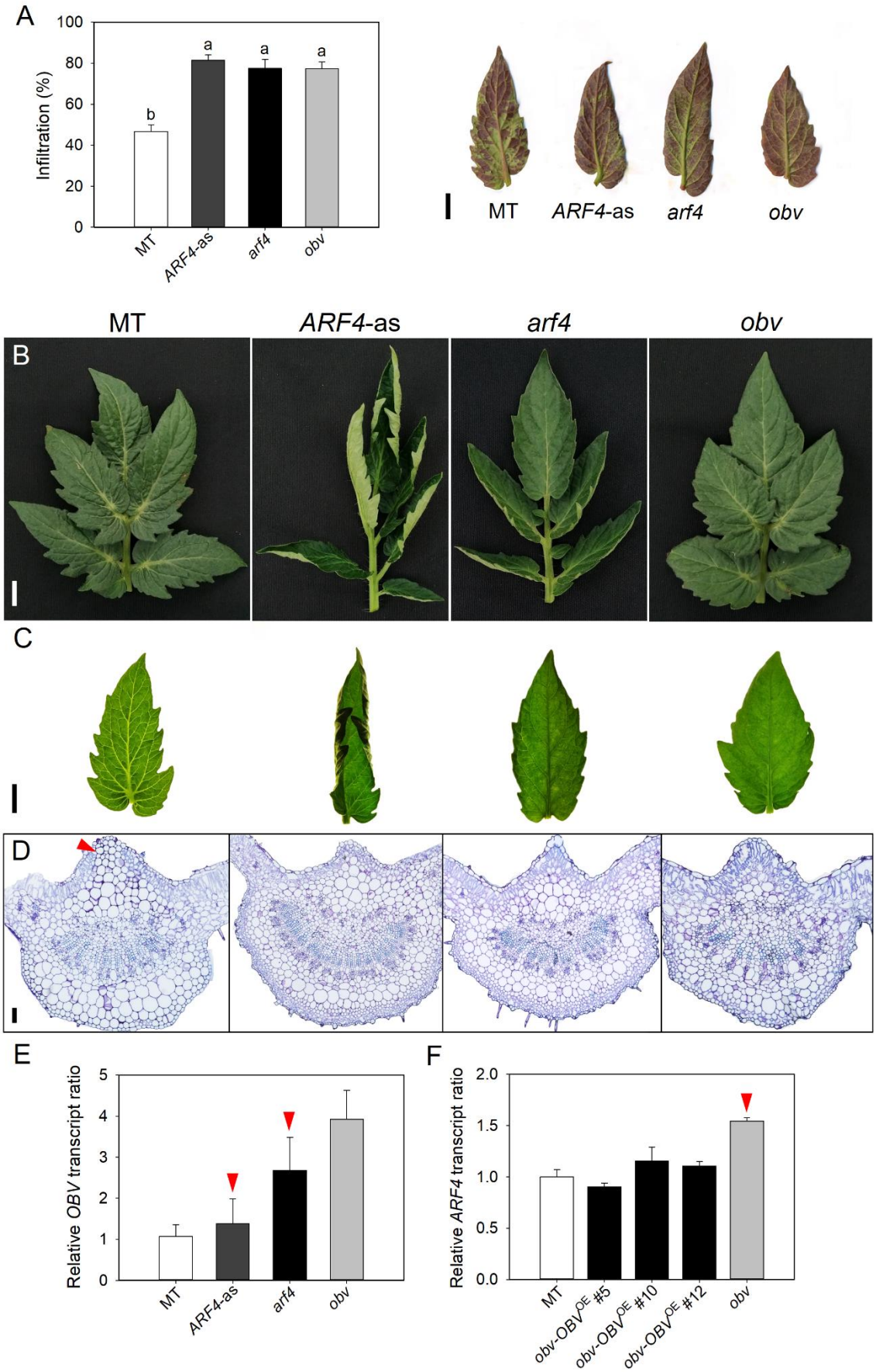
A
Infiltration (%)
100
80
60
40
20
0
a
a
a
b
MT
ARF4-as
arf4
obv
MT
ARF4-as
arf4
obv
B
MT
ARF4-as
arf4
obv
C
D
E
Relative OBV transcript ratio
5
4
3
2
1
0
MT
ARF4-as
arf4
obv
F
Relative ARF4 transcript ratio
2.0
1.5
1.0
0.5
0.0
MT
obv-OBV^OE #5
obv-OBV^OE #10
obv-OBV^OE #12
obv

Figure 7. Control of BSEs development by *ARF4* and *OBV* (A) The infiltration rate shows the percentage of leaf area filled with 1% acid fuchsin dye. The dispersion of the liquid in heterobaric leaves (MT) is hampered by compartmentalization of the mesophyll. In homobaric leaves (*ARF4*-as, *arf4* and *obv*), the liquid is dispersed more easily due to absence of BSEs. The dye infiltration was made with same pressure in detached leaflets. Bars are mean values ± s.e.m. (n=7 leaflets). Different letters indicate significant differences by Tukey's test at 5% probability. (B) Representative leaf of MT, *ARF4*-as, *arf4* e *obv* respectively. (C) Details of terminal leaflet under transmitted light evidencing clear or dark vein phenotypes. (D) Leaf lamina cross-sections at the midrib showing the presence (MT) and absence (*ARF4*-as, *arf4* and *obv*) of BSEs. Bars = 1 cm and 100 µm for cross-sections. (E) Relative *OBV* mRNA levels in young leaves of MT, *ARF4*-as, *arf4* and *obv*. (F) Relative *ARF4* mRNA levels in young leaves of MT, complemented lines and *obv*. Red arrow indicates transcripts upregulated. Values were normalized against the MT (wild-type) sample.

To better investigate the interaction of *ARF4* with *OBV* in BSEs development we next carried out a complementation test with *obv* and *arf4* mutants (Supplementary Figure 9). In the F_1 hybrid progeny generated by crossing *obv* × *arf4* 100% of the plants showed wild type leaves (with clear veins). In the F_2 generation we screened a population of 96 plants and classified them into four phenotypic classes: plants with wild-type (MT) leaves; plants with *obv* leaves; plants with *arf4* leaves and plants with leaves of both phenotypes (*obv*/*arf4*). Leaves with clear veins were classified as wild-type (MT) and leaves with dark veins were classified as *obv*. The leaves grouped as *arf4* had the majority of dark veins, with exception of a few light regions, and leaf blade curl. Finally, the leaves classified as double mutant had totally dark veins and leaf blade curl. We validate the observed phenotypic frequencies with a Chi-square test, to verify through observed phenotypic proportions a possible epistasis between the *ARF4* and *OBV* genes. Then, we quantified the degree of leaf rolling in two groups of plants (*arf4* leaves and *obv*/*arf4* leaves) and compared them with the *arf4* mutant parental. This quantitative assessment in an F_2 population makes it possible to clarify whether the trait has an additive effect or not, and thus to hypothesize if both genes act in different genetic pathways or in the same pathway.

The results showed a distortion in the proportion of phenotypic segregation (9:3:3:1), the frequencies found indicated a semi-dominant effect for the *arf4* mutation but not epistasis between the *ARF4* and *OBV* genes (Supplementary Figure 10). The quantification of leaf rolling degree demonstrated a non-additive effect in segregating

plants. This result suggests that both genes, *ARF4* and *OBV*, may be acting in the same genetic pathway to control formation of BSEs in tomato.

The analysis of *OBV* promoter region (5000 bp upstream from the ATG start codon) provided more insights about its relationship to components of auxin signaling machinery. Besides finding *cis*-elements involved with various types of stress and hormones, we identified two elements typically involved in the response to auxin (Supplementary Table 5). The first is a SAUR motif involved in auxin responsiveness, located 3559 bp upstream and contains CATATG signal sequence. The second is an Auxin Responsive Factor binding element (ARFAT), located 4598 bp upstream and contains TGTCTC recognition sequence (Supplementary Figure 11) (Ulmasov et al., 1995). The presence of these *cis*-elements in *OBV* promoter indicates a probable regulation mediated by auxin, and this regulation could be directly by *ARF4* transcript factor or some intermediate protein responsive to auxin.

Based on the results obtained in this work, we propose a hypothetical model to explain the control of BSEs development in tomato leaves. In this model, we suggest three distinct situations that occur in the wild-type (MT), *obv* mutant and *arf4* mutant. In MT leaves, the transcription of *ARF4* and *OBV* genes is activated by mechanisms involving auxin-dependent signaling. Both genes, *ARF4* and *OBV*, are transcript factors and expression of the two coincides in region of the vascular bundles. In a first situation, functional ARF4 and OBV proteins physically interact to form a heterodimer that will downregulate levels of *ARF4* and *OBV* in tissues, resulting in the formation of BSEs in leaves. In the second situation, a predicted protein intermediate (Serine/Threonine phosphathese, Solyc05g018300) can mediate the interaction between *ARF4* and *OBV* (Figure 8A). In *obv* leaves, the mutated protein, with deletion of one of the zinc-finger domains, cannot interact with ARF4 and/or other components, causing the loss of BSEs (Figure 8B). In *arf4* leaves, the mutated protein again fails to conduct physical interaction with OBV, resulting in the loss of BSEs (Figure 8C). We used the STRING platform (https://string-db.org/) to conduct an *in silico* protein interaction analysis and find putative proteins that participate in the same genetic network of OBV. The potential physical interaction between ARF4, OBV and Serine/Threonine proteins will be validated in future stages, through BiFC interaction assays.

A negative feedback loop between *ARF4* and *OBV* transcription factors is required to regulate the levels of these transcripts in vascular tissues and lead to the formation of sheath extensions. Regulatory feedback loops between zinc fingers proteins and other TFs have already been reported in *Arabidopsis*. The zinc finger proteins of the *INDETERMINATE DOMAIN* (*IDD*) family *JACKDAW* and *MAGPIE* physically interact with *SHORT-ROOT* (*SHR*) and *SCARECROW* (*SCR*) to modulate their transcriptional activity, and regulate cell division and differentiation in the root apex (Ogasawara et al., 2011). A negative feedback loop also occurs with the transcription factors *SHR*, *SCR* and *SCARECROW-LIKE 23*, that form a heterotrimeric complex to regulate the expression of each other and direct the formation of starch sheath in hypocotyls (Yoon et al., 2016).

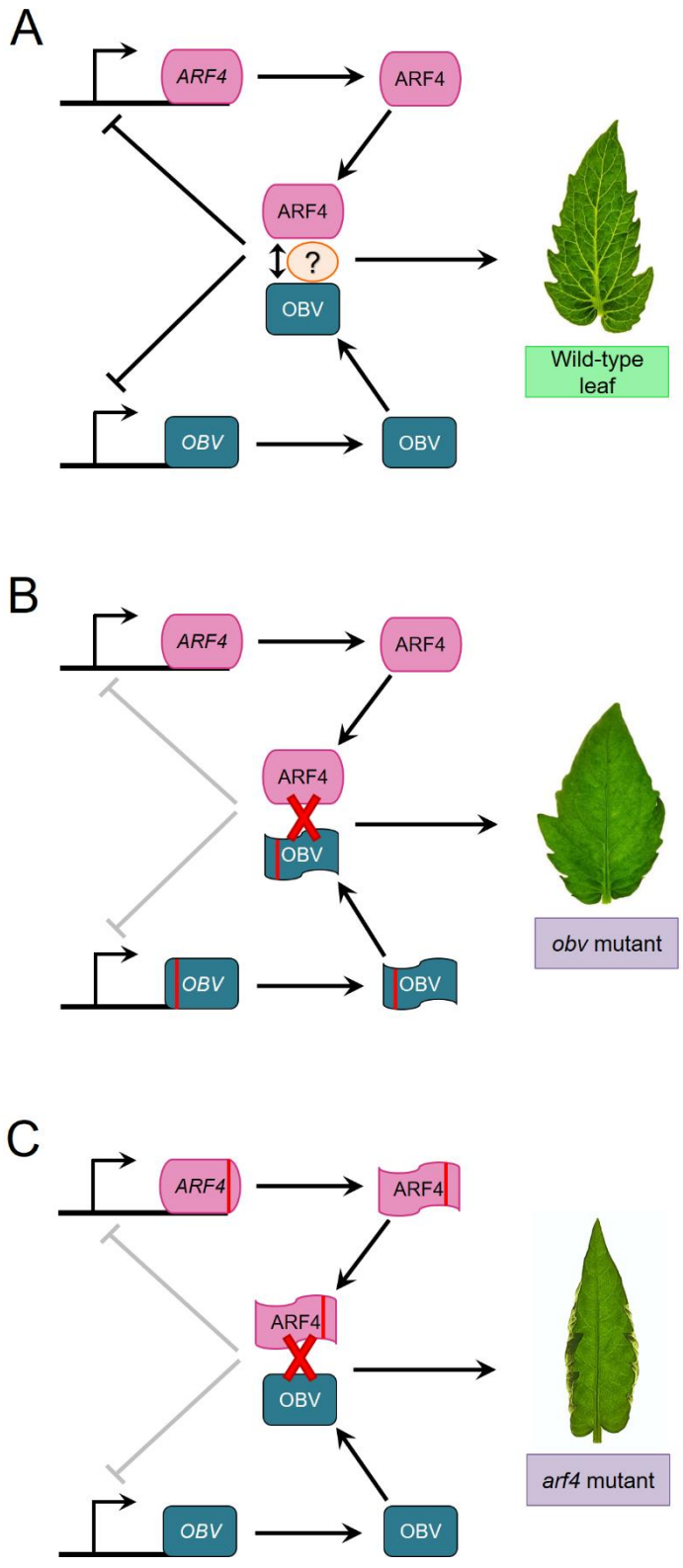

Figure 8. Hypothetical model for control of BSEs development in tomato. (A) In the wild-type, both transcription factors *ARF4* and *OBV* are transcripts. The proteins from these genes interact directly or through some intermediate protein to form a heterodimer that will downregulate levels of *ARF4* and *OBV* in tissues. This regulatory feedback is necessary for the formation of BSEs in leaves. (B) In the case of *obv* mutant, the gene is

transcript but the mutated protein cannot interact with ARF4 to maintain regulation of the two TFs, resulting in loss of BSEs. (C) In the *arf4* mutant, the two proteins cannot interact to form the heterodimer, resulting again in the absence of BSEs.

4. CONCLUSIONS

The *OBV* gene has a very specific expression pattern that is restricted to flowers and leaves, mainly young leaves. At the tissue level, *OBV* expression is concentrated around the vascular bundles. Besides involvement in the formation of BSEs in tomato, *OBV* mediates agronomically relevant effects such as controlling the leaf insertion angle, fruit shape, leaves serration and vein density.

Several results obtained so far support our hypothesis that formation of BSEs is controlled by *OBV* and requires the involvement of auxin. The *obv* mutant is more sensitive to auxin and all overexpression lines of the *OBV* have repression in the auxin response. Several components of the auxin signaling are changed in the *obv* and in the ox-lines, some members are upregulated (*ARF3*, *ARF9B*, *ARF10A*, *ARF10B*, 19 and *Aux/IAA4* and 14) and others downregulated (*Aux/IAA1A*, *IAA1B*, *IAA2*, *IAA3*, *IAA7B*, *IAA11*, *IAA13*, *IAA26* and *IAA35*). Especially for the *ARF4* factor, we observed a strong upregulation of *ARF4* in the *obv* mutant and the opposite also occurs, *OBV* is upregulated in the *arf4* mutant, resulting in loss of BSEs in both mutants. This regulation loop suggests the involvement of *ARF4* and *OBV*, possibly in the same molecular pathway, to control the BSEs development through auxin-mediated mechanism.

For next steps of this work, we intend to clarify how *OBV* and *ARF4* interact, if both TFs could physically interact or through intermediate proteins to regulate each other expression. Other molecular components that may participate in this genetics pathway also will be investigated to provide insight about development control of BSEs in tomato. In the last chapter, we explore the agronomic impact of some traits influenced by *OBV* in tomato.

5. REFERENCES

Barbosa MAM, Chitwood DH, Azevedo AA, Araújo WL, Ribeiro DM, Peres LEP, Martins SVC, Zsögön A (2019) Bundle sheath extensions affect leaf phenotypic plasticity in response to irradiance. Plant Cell and Environment **42**: 1575-1589

Ben-Gera H, Shwartz I, Shao MR, Shani E, Estelle M, Ori N (2012) ENTIRE and GOBLET promote leaflet development in tomato by modulating auxin response. Plant Journal **70**: 903-915

Bouzroud S, Gasparini K, Hu G, Barbosa MAM, Rosa BL, Fahr M, Zouine M (2020) Down regulation and loss of auxin response factor 4 function using CRISPR/Cas9 alters plant growth, stomatal function and improves tomato tolerance to salinity and osmotic stress. Genes **11**: 272

Chen M, Zhu X, Liu X, Wu C, Yu C, Hu G, Hao Y (2021) Knockout of Auxin Response Factor *SlARF4* Improves Tomato Resistance to Water Deficit. International journal of molecular sciences **22**: 3347

Cheng Y, Dai X, Zhao Y (2006) Auxin biosynthesis by the YUCCA flavin monooxygenases controls the formation of floral organs and vascular tissues in *Arabidopsis*. Genes and Development **20**:1790-1799

Cui D, Zhao J, Jing Y, Fan M, Liu J, Wang Z, Hu Y (2013) The *Arabidopsis* IDD14, IDD15, and IDD16 cooperatively regulate lateral organ morphogenesis and gravitropism by promoting auxin biosynthesis and transport. PLoS Genetics **9**: 1003759

Deng W, Yang Y, Ren Z, Audran-Delalande C, Mila I, Wang X, Li Z (2012) The tomato *SlIAA15* is involved in trichome formation and axillary shoot development. New Phytologist **194**: 379-390

Expósito-Rodríguez M, Borges AA, Borges-Pérez A, Pérez JA (2008) Selection of internal control genes for quantitative real-time RT-PCR studies during tomato development process. BMC Plant Biology **8**: 131

Falster DS, Westoby, M (2003) Leaf size and angle vary widely across species: what consequences for light interception? New Phytologist **158**: 509-525

Fedotova AA, Bonchuk AN, Mogila VA, Georgiev PG (2017) C2H2 zinc finger proteins: the largest but poorly explored family of higher eukaryotic transcription factors. Acta Naturae **9**: 33

Feurtado JA, Huang D, Wicki-Stordeur L, Hemstock LE, Potentier MS, Tsang E W, Cutler AJ (2011) The *Arabidopsis* C2H2 zinc finger INDETERMINATE DOMAIN1/ENHYDROUS promotes the transition to germination by regulating light and hormonal signaling during seed maturation. Plant Cell **23**: 1772-1794

Han G, Lu C, Guo J, Qiao Z, Sui N, Qiu N, Wang B (2020). C2H2 zinc finger proteins: Master regulators of abiotic stress responses in plants. Frontiers in Plant Science **11**: 115

Khatun K, Nath UK, Robin AHK, Park JI, Lee DJ, Kim MB, Chung MY (2017) Genome-wide analysis and expression profiling of zinc finger homeodomain (ZHD)

family genes reveal likely roles in organ development and stress responses in tomato. BMC genomics **18**: 1-16

Koenig D, Bayer E, Kang J, Kuhlemeier C, Sinha N (2009) Auxin patterns *Solanum lycopersicum* leaf morphogenesis. Development **136**: 2997-3006

Kozaki A, Hake S, Colasanti J (2004) The maize *ID1* flowering time regulator is a zinc finger protein with novel DNA binding properties. Nucleic Acids Research **32**: 1710-1720

Kumar M, Le DT, Hwang S, Seo PJ, Kim HU (2019). Role of the INDETERMINATE DOMAIN Genes in Plants. International Journal of Molecular Sciences **20**: 2286

Laity JH, Lee BM, Wright PE (2001) Zinc finger proteins: new insights into structural and functional diversity. Current opinion in structural biology **11**: 39-46

Lewis DR, Muday GK (2009) Measurement of auxin transport in *Arabidopsis thaliana*. Nature Protocols **4**: 437-451

Li SB, Xie ZZ, Hu CG, Zhang JZ (2016) A review of auxin response factors (ARFs) in plants. Frontiers in Plant Science **7**: 47

Li WT, He M, Wang J, Wang YP (2013) Zinc finger protein (ZFP) in plants-A review. Plant Omics **6**: 6

Machida C, Nakagawa A, Kojima S, Takahashi H, Machida Y (2015) The complex of ASYMMETRIC LEAVES (AS) proteins plays a central role in antagonistic interactions of genes for leaf polarity specification in *Arabidopsis*. Wiley Interdisciplinary Reviews: Developmental Biology **4**: 655-671

Ming N, Ma N, Jiao B, Lv W, Meng Q (2020) Genome wide identification of C2H2-type zinc finger proteins of tomato and expression analysis under different abiotic stresses. Plant Molecular Biology Reporter **38**: 75-94

Moreno-Risueno MA, Sozzani R, Yardımcı GG, Petricka JJ, Vernoux T, Blilou I, Benfey PN (2015) Transcriptional control of tissue formation throughout root development. Science **350**: 426-430

Morita MT, Sakaguchi K, Kiyose S, Taira K, Kato T, Nakamura M, Tasaka M (2006) A C2H2-type zinc finger protein, *SGR5*, is involved in early events of gravitropism in *Arabidopsis* inflorescence stems. Plant Journal **47**: 619-628

Murashige, T, Skoog F (1962) A Revised Medium for Rapid Growth and Bio Assays with Tobacco Tissue Cultures. Physiologia Plantarum **15**: 473-497

Ogasawara H, Kaimi R, Colasanti J, Kozaki A (2011) Activity of transcription factor JACKDAW is essential for SHR/SCR-dependent activation of SCARECROW and MAGPIE and is modulated by reciprocal interactions with MAGPIE, SCARECROW and SHORT ROOT. Plant Molecular Biology **77**: 489

Oliveira EJ, Koehler AD, Rocha DI, Vieira LM, Pinheiro MVM, De Matos EM, Da Cruz ACF, Da Silva TCR, Tanaka FAO, Nogueira FTS, Otoni WC (2017) Morpho-histological, histochemical, and molecular evidences related to cellular reprogramming

during somatic embryogenesis of the model grass *Brachypodium distachyon*. Protoplasma **254**: 2017-2034

Razin SV, Borunova VV, Maksimenko OG, Kantidze OL (2012) Cys2His2 zinc finger protein family: classification, functions, and major members. Biochemistry **77**: 217-226

Reinhart BJ, Liu T, Newell NR, Magnani E, Huang T, Kerstetter R, Barton MK (2013) Establishing a framework for the Ad/abaxial regulatory network of *Arabidopsis*: ascertaining targets of class III homeodomain leucine zipper and KANADI regulation. Plant Cell **25**: 3228-3249

Rigui AP, Gaspar M, Oliveira VF, Purgatto E, Carvalho MA (2015) Endogenous hormone concentrations correlate with fructan metabolism throughout the phenological cycle in *Chrysolaena obovata*. Annals of Botany **115**: 1163-1175

Ruijter JM, Ramakers C, Hoogaars WMH, Karlen Y, Bakker O, Van DEN, Hoff MJB, Moorman AFM (2009) Amplification efficiency: linking baseline and bias in the analysis of quantitative PCR data. Nucleic Acids Research **37**: 45

Sack L, Scoffoni C (2013) Leaf venation: structure, function, development, evolution, ecology and applications in the past, present and future. New Phytologist **198**: 983-1000

Sagar M, Chervin C, Mila I, Hao Y, Roustan JP, Benichou M, Gibon Y, Biais B, Maury P, Latché A, Pech JC, Bouzayen M, Zouine M (2013) *SlARF4*, an auxin response factor involved in the control of sugar metabolism during tomato fruit development. Plant Physiology **161**: 1362-1374

Sagar M, Chervin C, Roustan JP, Bouzayen M, Zouine M (2013). Under-expression of the Auxin Response Factor *Sl-ARF4* improves post-harvest behavior of tomato fruits. Plant signaling & behavior **8**: 25647

Sakamoto T, Morinaka Y, Ohnishi T, Sunohara H, Fujioka S, Ueguchi-Tanaka M, Tanaka H (2006) Erect leaves caused by brassinosteroid deficiency increase biomass production and grain yield in rice. Nature Biotechnology **24**: 105-109

Sato S, Tabata S, Hirakawa H. et al. (2012) The tomato genome sequence provides insights into fleshy fruit evolution. Nature **485**: 635-641

Shi H, Zhang S, Lin D, Wei Y, Yan Y, Liu G, Chan Z (2018) Zinc finger of *Arabidopsis thaliana* 6 is involved in melatonin-mediated auxin signaling through interacting INDETERMINATE DOMAIN 15 and INDOLE-3-ACETIC ACID 17. Journal of Pineal Research **65**: 12494

Silva WB, Vicente MH, Robledo JM, Reartes DS, Ferrari RC, Bianchetti R, Zsögön A (2018) *SELF-PRUNING* acts synergistically with *DIAGEOTROPICA* to guide auxin responses and proper growth form. Plant Physiology **176**: 2904-2916

Swarup R, Péret B (2012) AUX/LAX family of auxin influx carriers-an overview. Frontiers in Plant Science **3**: 225

Ulmasov T, Liu ZB, Hagen G, Guilfoyle TJ (1995) Composite structure of auxin response elements. Plant Cell **7**: 1611-1623

Vanneste S, Friml J (2009) Auxin: a trigger for change in plant development. Cell **136**: 1005-1016

Verna C, Sawchuk MG, Linh NM, Scarpella E (2015) Control of vein network topology by auxin transport. BMC Biology **13**: 1-16

Wang H, Jones B, Li Z, Frasse P, Delalande C, Regad F, Bouzayen M (2005) The tomato *Aux/IAA* transcription factor *IAA9* is involved in fruit development and leaf morphogenesis. Plant Cell **17**: 2676-2692

Wang K, Ding Y, Cai C, Chen Z, Zhu C (2019) The role of C2H2 zinc finger proteins in plant responses to abiotic stresses. Physiologia plantarum **165**: 690-700

Wang Y, Clevenger JP, Illa-Berenguer E, Meulia T, van der Knaap E, Sun L (2019) A comparison of sun, ovate, fs8. 1 and auxin application on tomato fruit shape and gene expression. Plant and Cell Physiology **60**: 1067-1081

Wu C, You C, Li C, Long T, Chen G, Byrne ME, Zhang Q (2008) *RID1*, encoding a Cys2/His2-type zinc finger transcription factor, acts as a master switch from vegetative to floral development in rice. Proceedings of the National Academy of Sciences of the USA **105**: 12915-12920

Wu X, Tang D, Li M, Wang K, Cheng Z (2013) Loose Plant Architecture1, an INDETERMINATE DOMAIN protein involved in shoot gravitropism, regulates plant architecture in rice. Plant Physiology **161**: 317-329

Xiong Y, Jiao Y (2019) The diverse roles of auxin in regulating leaf development. Plants **8**: 243

Yoon EK, Dhar S, Lee MH, Song JH, Lee SA, Kim G, Lim J (2016) Conservation and diversification of the SHR-SCR-SCL23 regulatory network in the development of the functional endodermis in *Arabidopsis* shoots. Molecular plant **9**: 1197-1209

6. SUPPLEMENTARY MATERIAL

Supplementary Table 1: Primers used for PCR and quantitative RT-PCR

Target Gene	Forward primer (5'-3')	Reverse primer (5'-3')
OBV	CACCCAATATTTCATCATATTGAATATATCTC	GATTTTTTATATGAGTGAACAATG
TIP4	ATGGAGTTTTTGAGTCTTCTGC	GCTGCGTTTCTGGCTTAGG
EXP	GCTAAGAACGCTGGACCTAATG	TGGGTGTGCCTTTCTGAATG
ARF1	TGCTTTAGGAATGTGGAAGTC	GGAACCATTCTCACCATAACC
ARF2A	GCAAGGTCAAGAGTTATCGA	CATTGGTTTCTCAGACAAGTC
ARF2B	CTGGGTTAAGCGACAAGCTC	CCCCGCATTTGATACAGAG
ARF3	GATTGTTTTGCTCCCTTGGA	GTGGCTGACCCCGATAGATA
ARF4	TGAAAGCCATCAACTCTCGG	ATCCCATCTGACCATCAAGCATC
ARF5	TTCCGAGCCAAGAAAAGAAA	CACTCGCATCAGTTGGAAGA
ARF6A	CCAACATATCCCTAGTACTTCAG	GTGCCTGAGATATTAGTTGGT
ARF6B	AGCCCATCAGAGTTTGTCATAC	ATTGTGCCCATATACCTACGAA
ARF7A	CGCCTCTGGATTACTCAATG	CACCCTGTCGTTAGCAAATG
ARF7B	TTCGCATGATGTTTGAGACT	CTTGGAACTGAAGAATGGACTA
ARF8A	AGCCCGTCCAATATGTTCAG	TTTGATGGTTGCTTCTGCTG
ARF8B	CATCTCCTTCCGACCACAGT	TGGTGGATCAATTTGTCCTGC
ARF9A	CAAAGAGTTCCATCATTCAATCTC	GACCTCATCATTGTCTTCTTCAG
ARF9B	AGGTCCATTAGTTGATGTTCCA	CTTGTTCAGCCAGAAGTTGAA
ARF10A	ATTCTCTGTGCCTAGATACTG	CTATAAATGTGCCTAAACTTCCA
ARF10B	GACATGGGATGAACCAGATTTG	GGAAACTCTTGTGGCAAACAC
ARF16A	CGGTATTGACAACTCGGAGAT	TTCGCGCTGTTTTCATGAAG
ARF16B	TACCATGATTCCCAAGCCAAGTA	GACCAAACAGTACGAATTGTGT
ARF17	GCATCCGATTAGTCAGAGTGAAG	CCTCCTCCATTATTCGCATCTG
ARF18	AAGCTTCCTATCTTATCATTGGA	AATCTACACTCGGCATTGTC
ARF19	CTGGTGGATGAATCTGTTGTC	TACTTAGACAGCTCTGAACCT
ARF24	CTGGTTCATTGTTGGATGTTTC	CCACATGAAGTCTTGGAAAGTAG
IAA1	TGTTGCCAAGGCACAAATTG	GGTTGGATGATGTTTTTCCTGTTAG
IAA2	ACAGTTCCATCATCCACAAG	ACCATCCATGCTCACTTTAAC
IAA3	GCCACCAGTTCGATCATACA	ATAAGGTGCTCCATCCATGC
IAA4	ACTCCACCTGTTGCCAAGAC	AGATAAGGGGCTCCATCCAT
IAA7	TGATTCATGCAAGCGTTTACG	TGGCTCTTGGTGCTAGTCCAA
IAA8	AAGGATCTATCTTCAGCACTAGA	TCCGCCAATTTGCTTTCTTTA
IAA9	CAGAGGGGAAGTTTCTGTCG	CAACCTGTGCCTTTGTAGCA
IAA11	GATGAAACTGGGCTTGAATTG	CACAACCTGACTGGCACTTG
IAA12	ACAAAGATGGAGACTGGATGCT	CGGTCTTCCACCATTTCTTCC
IAA13	AAGCGGTGAAAAGGAACAAG	TGCTTCTGAGGGATTCTTGGA
IAA14	CCACCAGTGAGATCATTTAGGA	AGGTGCACCATCCATGCAAA
IAA15	ATCGGAGACAGCCAAATCAG	TTTGCTGGAGGTTTGTTTCC
IAA16	GTGCCAAGCTCTAATGATCCT	GCACCGTCAACACTAACTT
IAA17	CAAGAATTATTTGATGCCTTAACCA	CTATTCAAAAGGTCCATCAGTTTCC
IAA19	TGTCGGCGATGTTCCATG	GTCTCTTGCTCCAAGCCCTAT
IAA21	TGTTCAAGCTCAACATAGGTGAAT	CCAACAAGCATCAAATCACCTT
IAA22	CTGAGCTGAGATTAGGGTTACC	AGGAGCTGTCCATCTCTGAT
IAA23	CACTCAACTCCTTAAAGCAATGGA	TCCTCAGTCTCTTGCATGATGAC
IAA26	CCTCCAATTCGTTCCTTTAGGA	GGAATACCATCCATGTTGATCTT
IAA27	GCAAGAGAAGCTCAGTGA	ACATCTCCCAAGGAACATCG
IAA29	GGTTTTGATGATAGCTTCTCCGAT	CGTCTTACGTTCAACTACTCCTT
IAA32	AGGAATGACCAATGGAGGATT	GGGAAGAATGCTTCATCTTTCC
IAA33	CCTTGTTGGTGATCTCAGTTG	CTTCCAGTGCGTGAATTTGG
IAA35	AAATGGAAGGAGTTGGAATTGC	ATGGTACATCACCAGCAAGAAG
IAA36	TGGAAGGAGTAGCCATTGGA	TGGTACATCTCCAGCAAGCA

Supplementary Table 2. Growth parameters measured in MT, *obv* mutant and overexpression lines.

Parameters are as follows: height of the primary shoot (cm); length of the three internodes (cm); diameter of the three internodes (cm); stem diameter (cm leaves number on primary shoot (leaves number up to first inflorescence); leaf insertion angle in three leaves (°) and leaflets number in three leaves. Measurements were performed at 50 days after germination. Data are means ± se (n = 12 plants). Different letters indicate statistically significant differences (Tukey's test, $P < 0.05$).

Parameters	**MT**	**MT-** ***OBV*^{OE} #3**	**MT-** ***OBV*^{OE} #5**	***obv***	***obv* -** ***OBV*^{OE} #10**	***obv* -** ***OBV*^{OE} #12**
Plant height (cm)	15.89 ± 0.43a	10.32 ± 0.20b	8.43 ± 0.19c	15.30 ± 0.30a	10.99 ± 0.27b	10.04 ± 0.20b
Length of the internodes (cm)						
Internode 4th	1.30 ± 0.07a	0.77 ± 0.05b	0.52 ± 0.02c	1.19 ± 0.05a	0.81 ± 0.05b	0.70 ± 0.03bc
Internode 5th	1.52 ± 0.05a	0.97 ± 0.04b	0.70 ± 0.03c	1.57 ± 0.09a	1.01 ± 0.05b	0.88 ± 0.03bc
Internode 6th	1.52 ± 0.09a	1.03 ± 0.04b	0.77 ± 0.03c	1.59 ± 0.08a	1.08 ± 0.04b	1.04 ± 0.04b
Diameter of the internodes (cm)						
Internode 4th	0.64 ± 0.02b	0.60 ± 0.01b	0.47 ± 0.01c	0.70 ± 0.01a	0.66 ± 0.02ab	0.63 ± 0.01b
Internode 5th	0.68 ± 0.02ab	0.62 ± 0.01b	0.48 ± 0.01c	0.74 ± 0.01a	0.66 ± 0.02b	0.64 ± 0.01b
Internode 6th	0.72 ± 0.02a	0.63 ± 0.01b	0.49 ± 0.01c	0.73 ± 0.01a	0.64 ± 0.02b	0.61 ± 0.01b
Stem diameter (cm)	0.57 ± 0.01ab	0.51 ± 0.01b	0.43 ± 0.01c	0.58 ± 0.02a	0.55 ± 0.02ab	0.54 ± 0.02ab
Leaves to 1st inflorescence	11 ± 0.18a	11 ± 0.13a	11 ± 0.12a	10 ± 0.15b	11 ± 0.23a	11 ± 0.19a
Leaf insertion angle (°)						
Leaf 5th	72 ± 2.24a	63 ± 1.26b	57 ± 1.04b	63 ± 2.47b	61 ± 1.38b	57 ± 1.72b
Leaf 6th	75 ± 2.22a	46 ± 1.82c	45 ± 1.87c	64 ± 2.62b	48 ± 1.98c	45 ± 1.09c
Leaf 7th	72 ± 2.78a	43 ± 1.37c	39 ± 0.97c	59 ± 2.94b	42 ± 1.72c	42 ± 1.25c
Leaflets number						
Leaf 5th	5 ± 0.0a	5 ± 0.18a	5 ± 0.19a	5 ± 0.11a	5 ± 0.0a	5 ± 0.0a
Leaf 6th	6 ± 0.22a	6 ± 0.19a	7 ± 0.29a	6 ± 0.23a	7 ± 0.26a	7 ± 0.34a
Leaf 7th	7 ± 0.40a	7 ± 0.29a	8 ± 0.25a	7 ± 0.41a	8 ± 0.24a	8 ± 0.30a

Supplementary Table 3. Agronomic parameters measured in MT, *obv* mutant and overexpression lines.

Parameters are as follows: average length of fruits (mm); average diameter of fruits (mm) and fruit shape obtained by the relationship between length and diameter. Measurements were performed at 10; 16; 22; 28; 34 and 40 days after anthesis (DAA). Data are means ± se (n = 15 fruits). Different letters indicate statistically significant differences (Tukey's test, $P < 0.05$).

Parameters	MT	MT-*OBV*^{OE} #3	MT-*OBV*^{OE} #5	*obv*	*obv* - *OBV*^{OE} #10	*obv* - *OBV*^{OE} #12
Fruit length (mm)						
10 DAA	9.86 ± 0.25ab	9.22 ± 0.35bc	9.63 ± 0.39ab	10.67 ± 0.43a	9.74 ± 0.20ab	8.18 ± 0.21c
16 DAA	16.09 ± 0.36b	14.82 ± 0.44bcd	14.13 ± 0.48cd	18.03 ± 0.41a	15.50 ± 0.28bc	13.75 ± 0.31d
22 DAA	19.57 ± 0.47b	18.78 ± 0.40bc	17.18 ± 0.56c	23.12 ± 0.50a	19.43 ± 0.25b	17.92 ± 0.41bc
28 DAA	20.78 ± 0.48bc	19.99 ± 0.45bcd	18.38 ± 0.59d	24.69 ± 0.52a	20.91 ± 0.24b	19.00 ± 0.31cd
34 DAA	22.36 ± 0.45bc	21.48 ± 0.41bcd	19.58 ± 0.61d	26.30 ± 0.61a	23.06 ± 0.26b	21.05 ± 0.38cd
40 DAA	22.87 ± 0.43bc	21.85 ± 0.45bcd	19.91 ± 0.63d	26.79 ± 0.60a	23.78 ± 0.29b	21.77 ± 0.36cd
Fruit diameter (mm)						
10 DAA	9.02 ± 0.30ab	8.23 ± 0.49bc	7.04 ± 0.35c	8.14 ± 0.38bc	9.67 ± 0.27a	7.54 ± 0.25c
16 DAA	16.04 ± 0.33ab	14.38 ± 0.43b	11.67 ± 0.34c	15.97 ± 0.64ab	16.68 ± 0.39a	14.38 ± 0.30b
22 DAA	20.58 ± 0.40a	18.45 ± 0.53b	14.60 ± 0.40c	20.30 ± 0.61a	20.71 ± 0.34a	18.11 ± 0.32b
28 DAA	22.28 ± 0.38a	20.23 ± 0.39b	16.38 ± 0.51c	22.27 ± 0.59a	22.95 ± 0.32a	20.40 ± 0.30b
34 DAA	24.44 ± 0.36a	21.91 ± 0.38b	17.64 ± 0.63c	24.20 ± 0.62a	24.93 ± 0.38a	21.81 ± 0.31b
40 DAA	25.31 ± 0.34a	22.37 ± 0.37b	18.10 ± 0.67c	25.06 ± 0.63a	25.94 ± 0.45a	22.35 ± 0.31b
Fruit shape						
10 DAA	1.10 ± 0.01bc	1.17 ± 0.04b	1.34 ± 0.03a	1.37 ± 0.04a	1.01 ± 0.02c	1.09 ± 0.02bc
16 DAA	1.00 ± 0.01bc	1.04 ± 0.03b	1.21 ± 0.02a	1.16 ± 0.02a	0.93 ± 0.01c	0.98 ± 0.02bc
22 DAA	0.95 ± 0.01bc	1.03 ± 0.03b	1.20 ± 0.02a	1.15 ± 0.02a	0.94 ± 0.01c	0.99 ± 0.01bc
28 DAA	0.93 ± 0.01bc	0.99 ± 0.02b	1.12 ± 0.02a	1.11 ± 0.02a	0.91 ± 0.01c	0.94 ± 0.01bc
34 DAA	0.91 ± 0.01c	0.98 ± 0.02b	1.11 ± 0.02a	1.09 ± 0.02a	0.93 ± 0.01bc	0.95 ± 0.01bc
40 DAA	0.90 ± 0.01c	0.98 ± 0.02b	1.11 ± 0.02a	1.07 ± 0.02a	0.92 ± 0.01bc	0.96 ± 0.01bc

Supplementary Table 4: GO Enrichment Analysis by Gene Ontology for the *OBV* gene (http://www.geneontology.org/page/go-enrichment-analysis)

GO-group	GO-ID	Term
Biological process	GO:0009965	**leaf morphogenesis**
	GO:0048573	**photoperiodism, flowering**
	GO:0010363	regulation of plant-type hypersensitive response
	GO:0009937	regulation of gibberellic acid mediated signaling pathway
	GO:0048765	**root hair cell differentiation**
	GO:0009959	**negative gravitropism**
	GO:0031348	negative regulation of defense response
	GO:0045604	**regulation of epidermal cell differentiation**
	GO:0010075	**regulation of meristem growth**
	GO:0010029	**regulation of seed germination**
	GO:0010260	**organ senescence**
	GO:0009867	jasmonic acid mediated signaling pathway
	GO:0048527	**lateral root development**
	GO:0009590	**detection of gravity**
	GO:0006612	protein targeting to membrane
	GO:0010167	response to nitrate
	GO:0016558	protein import into peroxisome matrix
	GO:0010310	regulation of hydrogen peroxide metabolic process
	GO:0010431	seed maturation
	GO:2000904	regulation of starch metabolic process
	GO:0048510	regulation of transition from vegetative to reproductive phase
	GO:0009862	salicylic acid mediated signaling pathway
	GO:0051302	**regulation of cell division**
	GO:0010031	circumnutation
	GO:0010106	cellular response to iron ion starvation
	GO:0045893	positive regulation of transcription, DNA-templated
	GO:0035304	regulation of protein dephosphorylation
	GO:0009958	**positive gravitropism**
	GO:0000165	MAPK cascade
	GO:0015706	nitrate transport
	GO:0006635	fatty acid beta-oxidation
	GO:0006826	iron ion transport
	GO:0009617	response to bacterium
	GO:0045449	regulation of transcription, DNA-templated
Cellular component	GO:0005634	nucleus
	GO:0005667	transcription factor complex
Molecular function	GO:0003700	sequence-specific DNA binding transcription factor activity
	GO:0042803	protein homodimerization activity
	GO:0044212	transcription regulatory region DNA binding
	GO:0043621	protein self-association
	GO:0008270	zinc ion binding
	GO:0046982	protein heterodimerization activity

* Some annotations related to auxin are marked.

Supplementary Table 5. Functional characterization of *OBV* promoter from *Solanum lycopersicum* cv Heinz. *In silico* identification of cis-acting regulatory DNA elements in *OBV* sequence. The 5000 bp upstream from promoter were found in Solgenomics (https://solgenomics.net/; Solyc05g054030) and sequence analysis depicts presence of putative cis-acting determined by New Place Database (https://www.dna.affrc.go.jp/PLACE/?action=newplace).

Motif name	Signal Sequence	Local	Description
ABRERATCAL	MACGYGB	-2846	ABA responsive element; ABRE-related sequence
ARFAT	TGTCTC	-4598	Auxin Responsive Factor binding element
ARR1AT	NGATT	-4928; -4817; -4257; -4180; -4009; -3878; 3636; -3528; -3274; -3120; -3090; -2730; -2653; -2618; -2562; -2487; -2109; -2018; -1891; -1849; -1834; -1748; -1710; -1265; -986; -838; -726; -676; -537; -481; -409; -299; -291	ARR1 binding element, cytokinin-responsive factor
CACGTGMOTIF	CACGTG	-2846	Regulation of Abscisic Acid-induced transcription; motif involved in the network of phytochrome A-regulated gene expression
CATATGGMSAUR	CATATG	-3559	Motif involved in auxin responsiveness
CPBCSPOR	TATTAG	-4380; -3427; -2657; -376; -258 -119	Sequence critical for Cytokinin-enhanced protein binding *in vitro*
ERELEE4	AWTTCAAA	-4629; -4461; -1816	Ethylene regulation of fruit ripening genes
GAREAT	TAACAAR	-4002; -3973	GA-responsive seed germination genes; Gibberellic acid response
MYBGAHV	TAACAAA	-4002	Central element of Gibberellin (GA) response complex. *GAmyb* binds specifically to the TAACAAA-box; *GAmyb* is the sole GA-regulated transcriptional factor required for transcriptional activation of the high-pI alpha-amylase
MYCCONSENSUSAT	CANNTG	-4286; -4245; -3696; -3559; -3462; -2846; -2432; -2154; -1827; -1671; -1243; -1225; -808; -451; -403; -285	ABA signalling pathway, dehydration-responsive genes
PYRIMIDINEBOXOSRAMY1A	CCTTTT	-3100; -1099	Gibberellin-responsive sugar repression
WBOXATNPR1	TTGAC	-4115; -3510; -1137	Disease resistance, Salicylic Acid (SA) induced

WRKY71OS	TGAC	-4114; -3807; -3509; -1136; -992	Repression of the gibberellin signalling pathway
BOXCPSAS1	CTCCCAC	-2513	"Box-C" in *Asparagine Synthetase* gene; *AS1*-negatively regulated by light (pea)
GATABOX	GATA	-4985; -4886; -4713; -4568; -4059; -3951; -3906; -3691; -3590; -3547; -3450; -3407; -3194; -3011; -2976; -2907; -2573; -2472; -2323; -2099; -1405; -1328; -1219; -1175; -1158; -1144; -876; -757; -689; -366; -248	Chlorophyll a/b binding protein, Conserved in the promoter of all *LHCII* type I
GT1CONSENSUS	GRWAAW	-3554; -3515; -3450; -3284; -3188; -2920; -2323; -2171; -1328; -1205; -757; -366; -248	Light regulated elements
IBOX	GATAAG	-3590; -2472	Conserved sequence upstream of light-regulated genes
IBOXCORE	GATAA	-3590; -3450; -2907; -2472; -2323; -1328; -1158; -757; -366; -248	Light-regulated elements
IBOXCORENT	GATAAGR	-2472	Associated with light-responsive promoter regions
INRNTPSADB	YTCANTYY	-4925; -3293; -2795; -1787; -1360	Light-responsive transcription
HDZIP2ATATHB2	TAATMATTA	-4338	Binding site of the homeobox gene *ATHB-2* - regulated by light signals
REALPHALGLHCB21	AACCAA	-2813; -1922	Required for phytochrome regulation
SORLIP1AT	GCCAC	-4045; -1245	Light-induced promoters
-10PEHVPSBD	TATTCT	-4477; -3884; -3342; -3250	Light-responsive chloroplast genes for PSII reactions
BOXIINTPATPB	ATAGAA	-3191	"Box-II" found in the plastid *atpB* gene promoter (tobacco)
CACTFTPPCA1	YACT	-4158; -4152; -4143; -4109; -3266; -3166; -2951; -2935; -2583; -2441; -2406; -2353; -2298; -2254; -1347; -1303; -1259; -1063; -1016; -980 -960; -916; -881; -828; -794; -774; -720; -700; -684; -662; -632; -531; -511; -467; -437; -425; -403; -348; -318; -306; -285; -265; -165; -148; -128	Key component of *MEM1* (mesophyll expression module 1), found in the cis-regulatory element in the distal region of the phosphoenolpyruvate carboxylase
TAAAGSTKST1	TAAAG	-4775; -4613; -3855; -3159; -3003 -2807; -1977; -1546; -1536; -1451; -1094	Guard cell-specific gene expression
CIACADIANLELHC	CAANNNNATC	-4434; -2774	Circadian expression of *Lhc* gene (tomato)

ABRELATERD1	ACGTG	-2845	ABRE-like sequence required for etiolation-induced expression of *ERD1* (early responsive to dehydration)
ACGTATERD1	ACGT	-4938; -3903; -2845; -2383; -1607; -1285	Etiolation-induced expression for dehydration stress related gene *ERD1*
CBFHV	RYCGAC	-3776	Binding site of *CBF1* and *CBF2*; CBFs are also known as dehydration-responsive element (*DRE*) binding proteins (barley)
CRTDREHVCBF2	GTCGAC	-3776	Motif *CBF2* involved in regulation of low-temperature responsive genes
MYB1AT	WAACCA	-4199; -2814; -1923	*MYB* recognition site found in the promoters of the dehydration-responsive gene
MYB2AT	TAACTG	-103	Water-stress response genes
MYB2CONSENSUSAT	YAACKG	-103	Dehydration-responsive genes
MYBCORE	CNGTTR	-3399; -887; -498; -451; -332	Binding site for *MYB* and *ATMYB2* involved in regulation of genes that are responsive to water stress (*Arabidopsis*)
MYCATERD1	CATGTG	-3696	Drought-responsive elements
MYCATRD22	CACATG	-1243	Drought-responsive elements
PREATPRODH	ACTCAT	-4108; -2796; -2405	Hypoosmolality-inducible genes, L-Pro responsive. Involved in drought/high salinity stress.
BIHD1OS	TGTCA	-3152; -2428; -1276	Binding site of *OsBIHD1*; transcriptional factor in disease resistance responses (rice)
GT1GMSCAM4	GAAAAA	-3554; -3188; -2920; -2171; -1876; -1205	"GT-1 motif" found in the promoter *SCaM-4* - plays a role in pathogen- and salt-induced
MARABOX1	AATAAAYAAA	-2712; -1477	"A-box" found in SAR (Systemic acquired resistance)
MARARS	WTTTATRTTTW	-3654; -2645	"ARS element"; motif found in SAR
MARTBOX	TTWTWTTWTT	-4747; -4386; -4361; -4353; -4317; -4306; -3037; -2559; -2556; -1057	Motif found in SAR, "T-Box"
MYB1LEPR	GTTAGTT	-970	Regulates defense-related gene expression via GCC-box and non-GCC box cis elements like *Myb1*
SEBFCONSSTPR10A	YTGTCWC	-4599	Binding site of *SEBF* = silencing element binding factor, found in promoter of pathogenesis-related gene (potato)

AGMOTIFNTMYB2	AGATCCAA	-4270	AG-motif found at promoter of *NtMyb2* gene, defense-related gene Phenylalanine ammonia lyas*e* (*PAL*) (tobacco)
BOXLCOREDCPAL	ACCWWCC	-578; -233	Box-L-like sequences *PAL1* promoter region (carrot)
MYBPLANT	MACCWAMC	-234	Plant *MYB* binding site; Consensus sequence related in promoters of phenylpropanoid biosynthetic genes such as *PAL*, *CHS*, *CHI*
TATABOXOSPAL	TATTTAA	-4217; -3608; -2640; -107	Motif found in the promoter of *PAL* gene (rice)
ANAERO1CONSENSUS	AAACAAA	-4809; -4289; -4170; -3534	Motif involved in the fermentative pathway
SITEIIATCYTC	TGGGCY	-4827	Motif found in the promoter regions of cytochrome genes and nuclear genes encoding components of the oxidative phosphorylation machinery
TATAPVTRNALEU	TTTATATA	-1615	"TATA-like motif"; binding site of TATA protein; found in *Glyceraldehyde-3-phospate dehydrogenase* gene promoter (maize)
TATABOX5	TTATTT	-4906; -4730; -4386; -4353; -4317; -4304; -4218; -4033; -3845; -3735 -3613; -3373; -3108; -3037; -2941; -2559; -2211; -1423; -1055; -108	"TATA-box" found in the 5'upstream region of *Glutamine Synthetase* gene
SREATMSD	TTATCC	-4590	Sugar-repressive element (SRE), down-regulated genes after main stem decapitation
EBOXBNNAPA	CANNTG	-4286; -4245; -3696; -3559; -3462; -2846; -2432; -2154; -1827; -1671; -1243; -1225; -808; -451; -403; -285	"E-box" of *NAPA* storage-protein gene (*Brassica napus*)
AMYBOX1	TAACARA	-4002	"Amylase-box", conserved sequence found in 5'-upstream region of *Alpha-amylase* gene
AMYBOX2	TATCCAT	-3316	Conserved sequence found in 5'upstream region of *Alpha-amylase* gene
CGACGOSAMY3	CGACG	-3774	"CGACG element" found in *Amy3D* and *Amy3E* amylase genes

TATCCAYMOTIFOSRAMY3D	TATCCAY	-3316	Motif found *RAmy3D Alpha-amylase* gene promoter; responsible for sugar repression (rice)
TATCCAOSAMY	TATCCA	-3316	Element found in *Alpha-amylase* promoters (rice)
NAPINMOTIFBN	TACACAT	-910; -560	Motif found in *Albumina 2S* gene; storage protein (*Brassica napus*)
P1BS	GNATATNC	-1291; -1220	PHR1-binding sequence found in the upstream regions of phosphate starvation responsive genes
EECCRCAH1	GANTTNC	-2729; -1069; -1005	Cis-acting elements and DNA-binding proteins involved in CO_2 responsive transcriptional activation
CURECORECR	GTAC	-4932; -4671; -4159; -4144; -2777; -2534; -2442; -2435; -2395; -2385; -2164; -1388; -1348; -911; -775; -685; -512; -384; -266; -216; -166; -129	Copper-response element
SURECOREATSULTR11	GAGAC	-4053	Sulfate uptake; sulfate transporter
ATHB5ATCORE	CAATNATTG	-3419	Consensus binding sequence for class *I HDzip* (Homeodomein-leucine zipper) protein
GMHDLGMVSPB	CATTAATTAG	-2035	Binding site of homeodomain leucine zipper proteins; found in the phosphate response domain (soybean)
LECPLEACS2	TAAAATAT	-3044; -1968	Binding cis-element of *LeCp* (tomato *Cys* protease)
ACGTABOX	TACGTA	-3904; -1286	RITA-1 binding site expressed during seed development; promoter elements required for sugar-repression
DOFCOREZM	AAAG	-4774; -4612; -3854; -3675; -3530; -3220; -3158; -3002; -2966; -2806; -2489; -2465; -2330; -1976; -1873; -1545; -1535; -1450; -1093; -1044; -678; -68	Core site is required for binding of Dof (proteins DNA binding proteins) and *PBF* (endosperm specific)
DPBFCOREDCDC3	ACACNNG	-3463; -404; -286	ABRE + embryo-specification elements
GCN4OSGLUB1	TGAGTCA	-1990	Motif required for endosperm-specific expression
SEF1MOTIF	ATATTTAWW	-2641	*SEF1*-binding site; *SEF* = soybean embryo factor

SEF3MOTIFGM	AACCCA	-2039	*SEF3* binding site; *SEF* = soybean embryo factor
SEF4MOTIFGM7S	RTTTTTR	-4356; -4178; -4134; -4014; -4007; -3978; -3876; -3656; -2891; -1953; -1774; -1597; -1421; -1281; -1025	*SEF4* binding site; *SEF* = soybean embryo factor
-300ELEMENT	TGHAAARK	-3555; -2172; -1047	Endosperm formation genes
L1BOXATPDF1	TAAATGYA	-4149	"L1-box" - L1 layer-specific genes; SAM growth
CARGCW8GAT	CWWWWWWWWG	-4167; -2495; -2451; -2035; -958; -772; -698	Binding site for *AGL15* (*AGAMOUS-like* 15)
GTGANTG10	GTGA	-3808; -3693; -3452; -2738; -2731; -2327; -2019; -1835; -410; -292	Motif found in the promoter of the late pollen gene (*N. tabacum*)
MYBPZM	CCWACC	-577; -232	Floral organ pigmentation (kernel pericarp and cob pigmentation in maize)
POLLEN1LELAT52	AGAAA	-3768; -3189; -2998; -2921; -2468 -2275	Anther and pollen development
NTBBF1ARROLB	ACTTTA	-3935; -3888	DNA binding site of the Dof protein; *NtBBF1* is essential for tissue-specific and auxin-regulated expression of the *rolB* oncogene
NODCON1GM	AAAGAT	-3854; -3530; -2489; -2465; -678	Putative nodulin consensus sequences
NODCON2GM	CTCTT	-4485; -1426; -1301; -1014	Putative nodulin consensus sequences
OSE1ROOTNODULE	AAAGAT	-3854; -3530; -2489; -2465; -678	Motif characteristic of the promoters activated in infected cells of root nodules
OSE2ROOTNODULE	CTCTT	-4485; -1426; -1301; -1014	Sequence motif of the promoters activated in infected cells of root nodules
RHERPATEXPA7	KCACGW	-4939	Root Hair-specific cis-Elements
ROOTMOTIFTAPOX1	ATATT	-4945; -4892; -4885; -4846; -4529; -4373; -4359; -4120; -4016; -3980; -3788; -3690; -3546; -3308; -3296; -3040; -3020; -2658; -2641; -2634; -2628; -2599; -2572; -2526; -2346; -2305; -2113; -2104; -1964; -1927; -1685; -1587; -1339; -1197; -1152; -954; -905; -786; -768; -658; -652; -604; -555; -505; -429; -395; -377; -338; -310; -277; -259; -210; -140; -120; -47; -37	Root motif (root expression)
E2FCONSENSUS	WTTSSCSS	-1107	E2FBNTRNR: Cell cycle regulation genes
ATHB1ATCONSENSUS	CAATWATTG	-3419	Motif found in Athb-1 protein. This protein has a HD-Zip domain binds to DNA as a dimer (*Arabidopsis*)

RAV1BAT	CACCTG	-4245	DNA-binding protein, specifically binds to DNA with bipartite
RAV1AAT	CAACA	-3465; -2878; -1897	DNA-binding protein, specifically binds to DNA with bipartite
GT1CORE	GGTTAA	-4978; -3147; -1628	Critical for GT-1 binding to box-II of *rbcS*
CCAATBOX1	CCAAT	-4399; -2811; -2785; -1226	Act cooperatively with HSEs (Heat shock element) to increase the HS promoter activity
S1FBOXSORPS1L21	ATGGTA	-4674; -1915	Downregulating *RPS1* and *RPL21* promoter activity
TATABOX2	TATAAAT	-4081; -3362; -2869; -1497; -1193	"TATA-box" elements are critical for accurate initiation
TATABOX3	TATTAAT	-3545; -3241; -3028; -1963	"TATA-box" elements are critical for accurate initiation
TATABOX4	TATATAA	-3900; -3007; -2097; -2088; -1940; -1613; -874; -856; -158	"TATA-box" elements are critical for accurate initiation
CTRMCAMV35S	TCTCTCTCT	-19; -17; -15; -13; -11; -9	CT-rich motif (inverted GAGA) found in a 60-nucleotide region downstream of the transcription start site of the *CaMV35S*; Can enhance gene expression
POLASIG1	AATAAA	-3765; -3389; -3301; -3054; -2858; -2809; -2712; -2703; -1959; -1477; -943; -593	Putative polyadenylation signal in nuclear genes
POLASIG2	AATTAAA	-2311; -2271	Poly A signal
POLASIG3	AATAAT	-4337; -3895; -3831; -3725; -3446; -3418; -3358; -3231; -2916; -2694; -2284; -2265; -2069; -1480	Consensus sequence for polyadenylation signal
CAATBOX1	CAAT	-4924; -4593; -4408; -3965; -3739; -3658; -3419; -3390; -3179; -2810; -2784; -2769; -2154; -1793; -1513; -1310; -1225; -1131; -808; -800; -324; -49	CAAT promoter consensus sequence
CCA1ATLHCB1	AAMAATCT	-4561	*MYB*-related transcription factor, CCA1 binding site
MYBST1	GGATA	-4060; -3408; -1329; -1220; -1145; -758; -367; -249	Core motif of *MYB* binding site
ACGTTBOX	AACGTT	-1608	"T-box"
TBOXATGAPB	ACTTTG	-2440	"T-box"

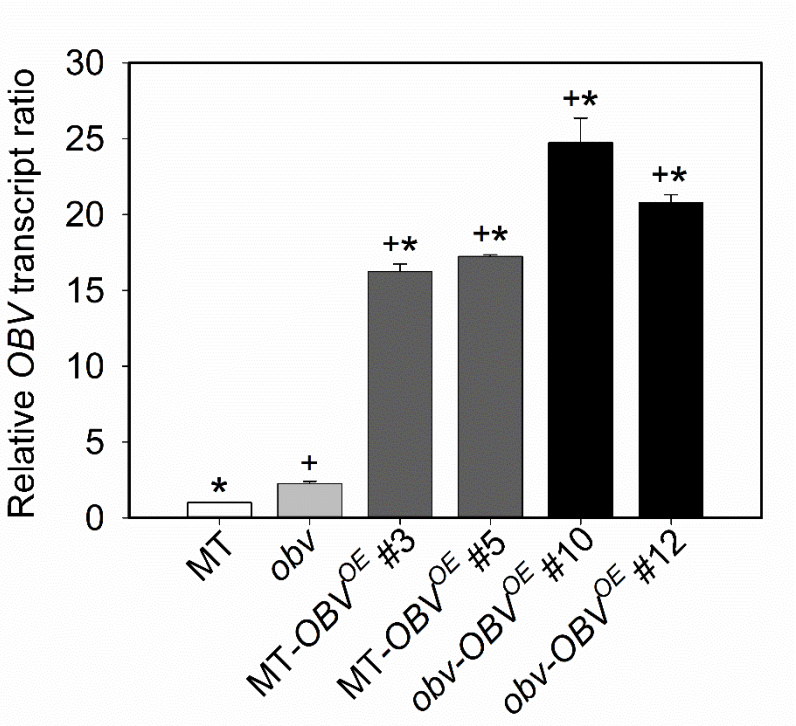

Supplementary Figure 1. Relative *OBV* mRNA levels in young leaves of Micro-Tom (MT), *obv* mutant and four overexpression lines. All homozygous OBV^{OE} lines are in the T4 generation. Values were normalized against the MT (wild-type) sample. Asterisk indicates statistical difference in relation to the *obv* and sum sign shows statistical difference in relation to the MT.

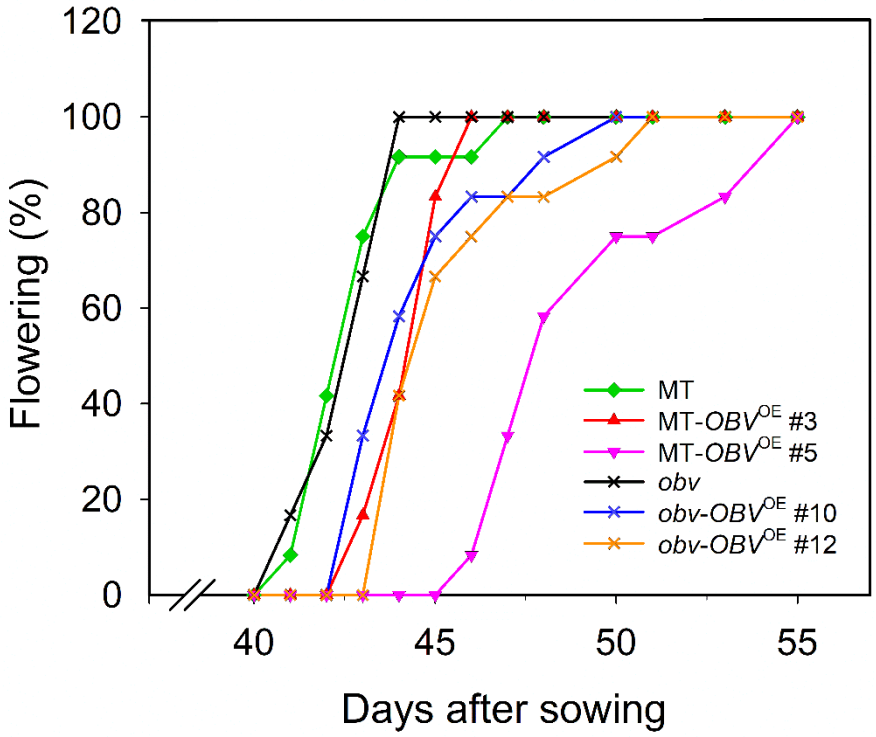

Supplementary Figure 2. Overexpression of the *OBV* functional allele promotes delay in flowering time. Chronological time to flowering in MT, *obv* mutant and OBV^{OE} lines. The percentage of plants with the first one open flower is show (n = 12). The lines overexpressing *OBV* in MT background (MT-OBV^{OE} #3; MT-OBV^{OE} #5) and *obv* background (*obv*-OBV^{OE} #12; *obv*-OBV^{OE} #12) flourish later than MT and *obv* mutant.

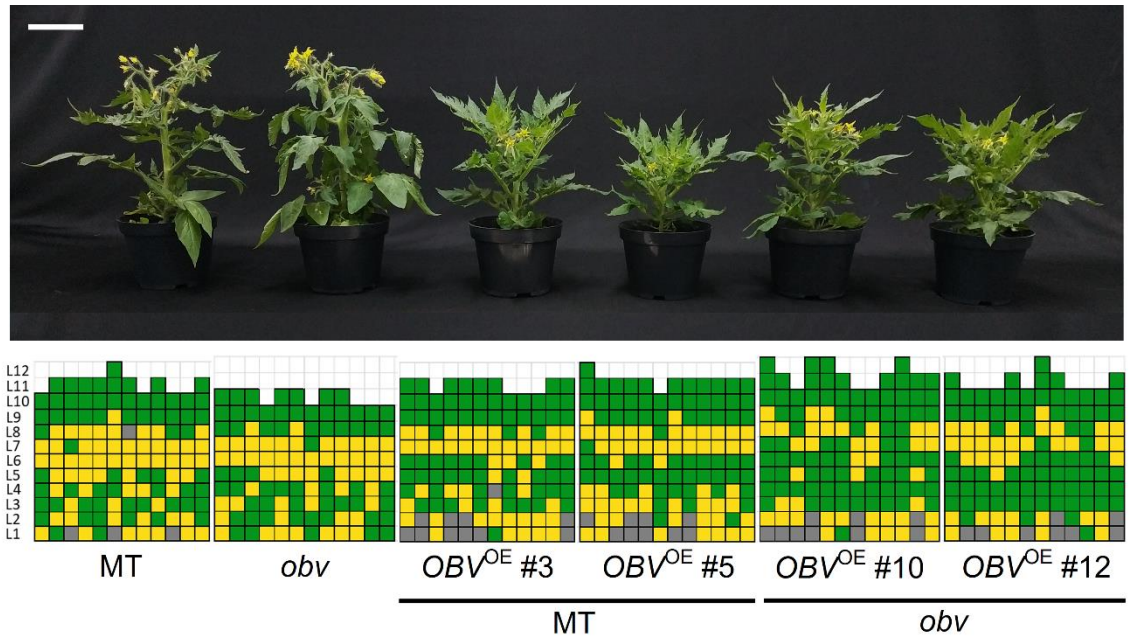

Supplementary Figure 3. Impacts of *OBV* on plant phenotype and side branching in tomato cv Micro-Tom (MT). Representative plants of MT (harboring *OBV* functional allele), *obv* (harboring *obv* mutant allele) and overexpression lines (harboring high levels of *OBV* functional allele) at 60 days after germination (dag). Bars = 5 cm. Diagram of colors depict the distribution of side branches in each genotype at 50 dag (n = 12 plants). The lines show leaf number (L1-L12) and the columns show the repetitions in each genotype. Gray denotes absence of an axillary bud, yellow denotes a visible bud (greater than 1 cm) and dark green a full branch (with one or multiple leaves).

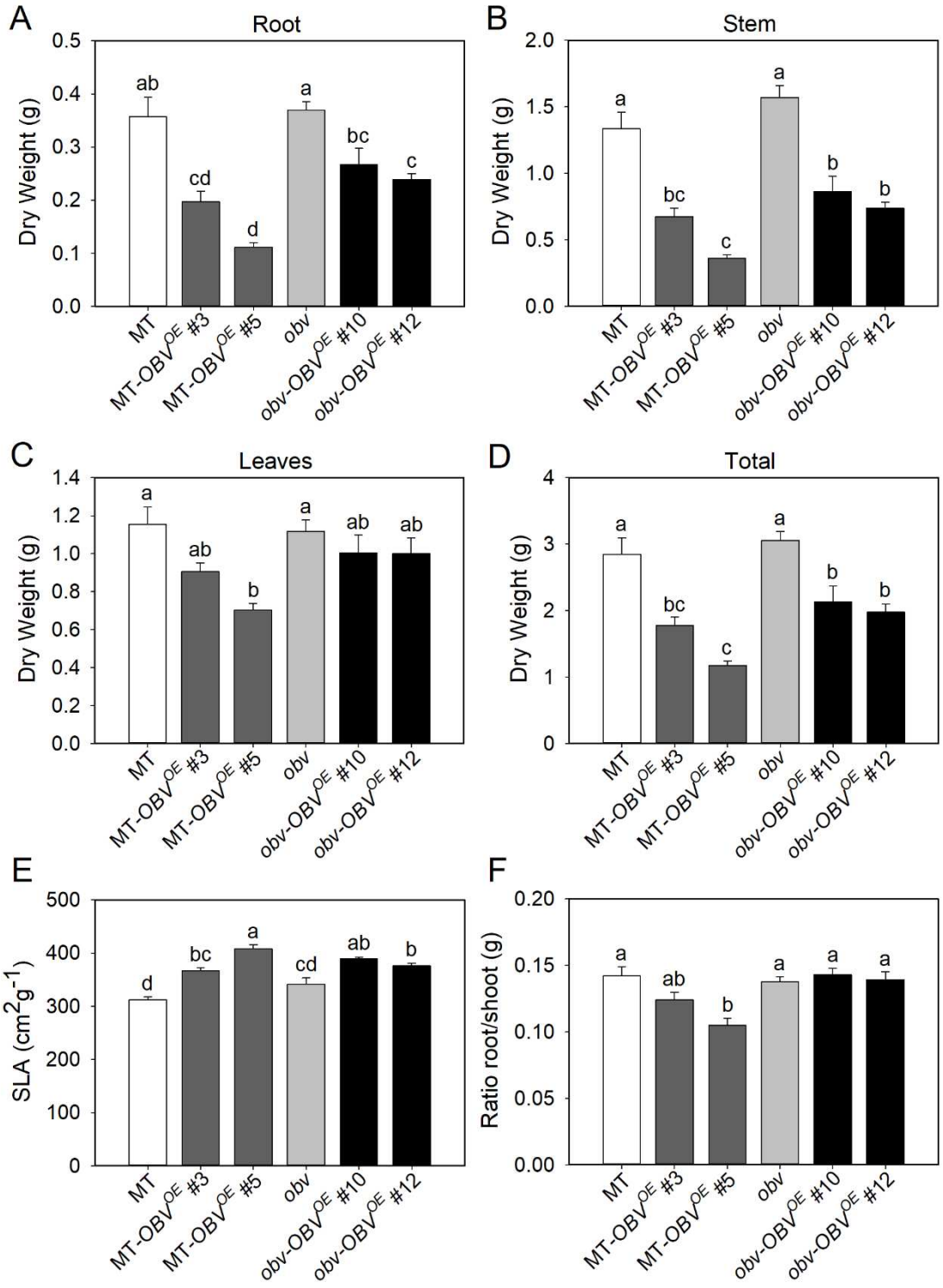

Supplementary Figure 4. **Overexpression of the *OBV* functional allele promotes reduction in the biomass accumulation.** (A) root dry weight, (B) stem dry weight, (C) leaves dry weight, (D) total dry weight, (E) specific leaf area (SLA) and (F) ratio root-shoot. Dry weight and SLA were determined through destructive analysis in MT, *obv* and *OBV*^{OE} lines with 60 dag. Bars are mean values ± s.e.m. (n=8 plants). Different letters indicate significant differences by Tukey's test at 5% probability.

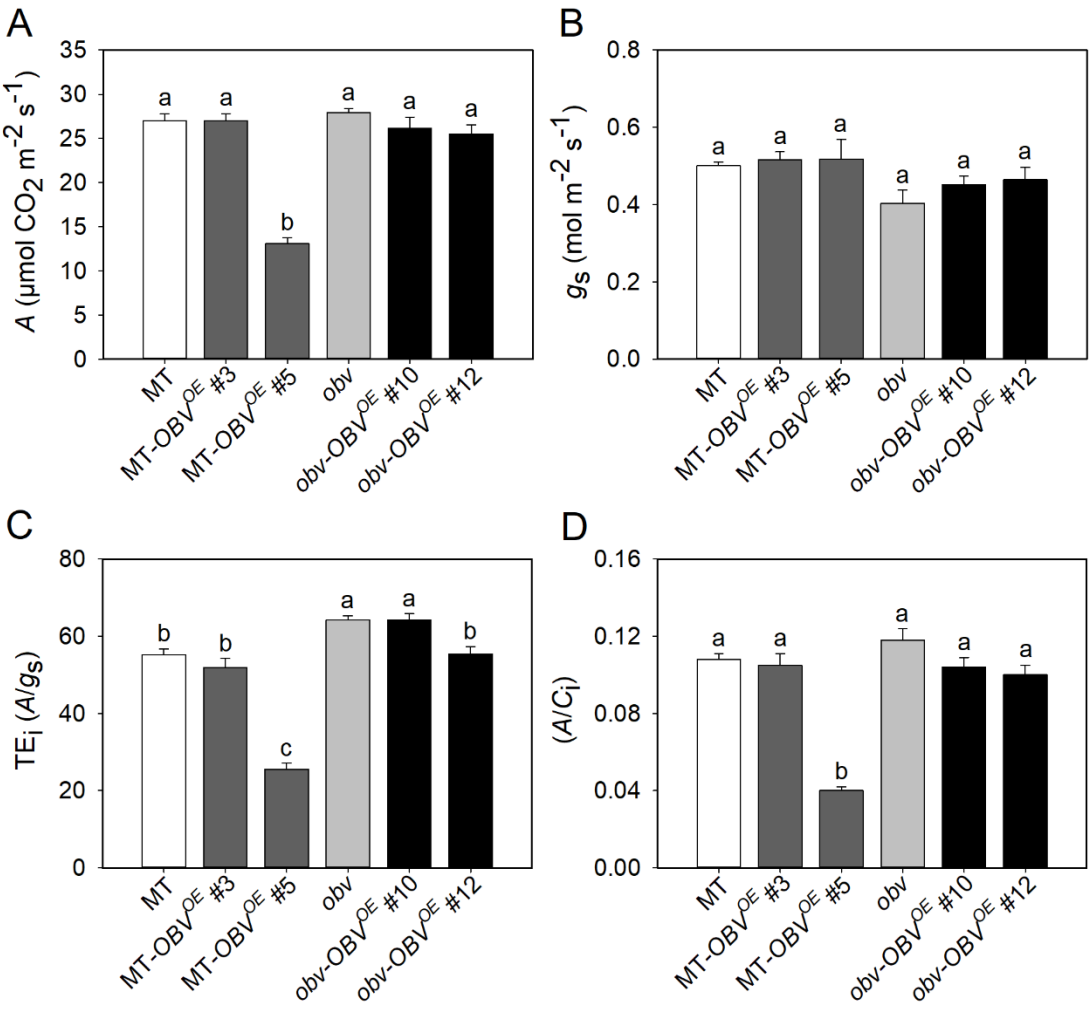

Supplementary Figure 5. **Gas exchange parameters determined in fully expanded leaves of Micro-Tom (MT), *obv* mutant and *OBV*^{OE} lines.** (A) photosynthetic CO_2 assimilation, (B) stomatal conductance, (C) A/g_s ratio or intrinsic transpiration efficiency (TE_i) and (D) A/C_i indicates instantaneous carboxylation efficiency. Bars are mean values ± s.e.m. (n=6 plants). Different letters indicate significant differences by Tukey's test at 5% probability.

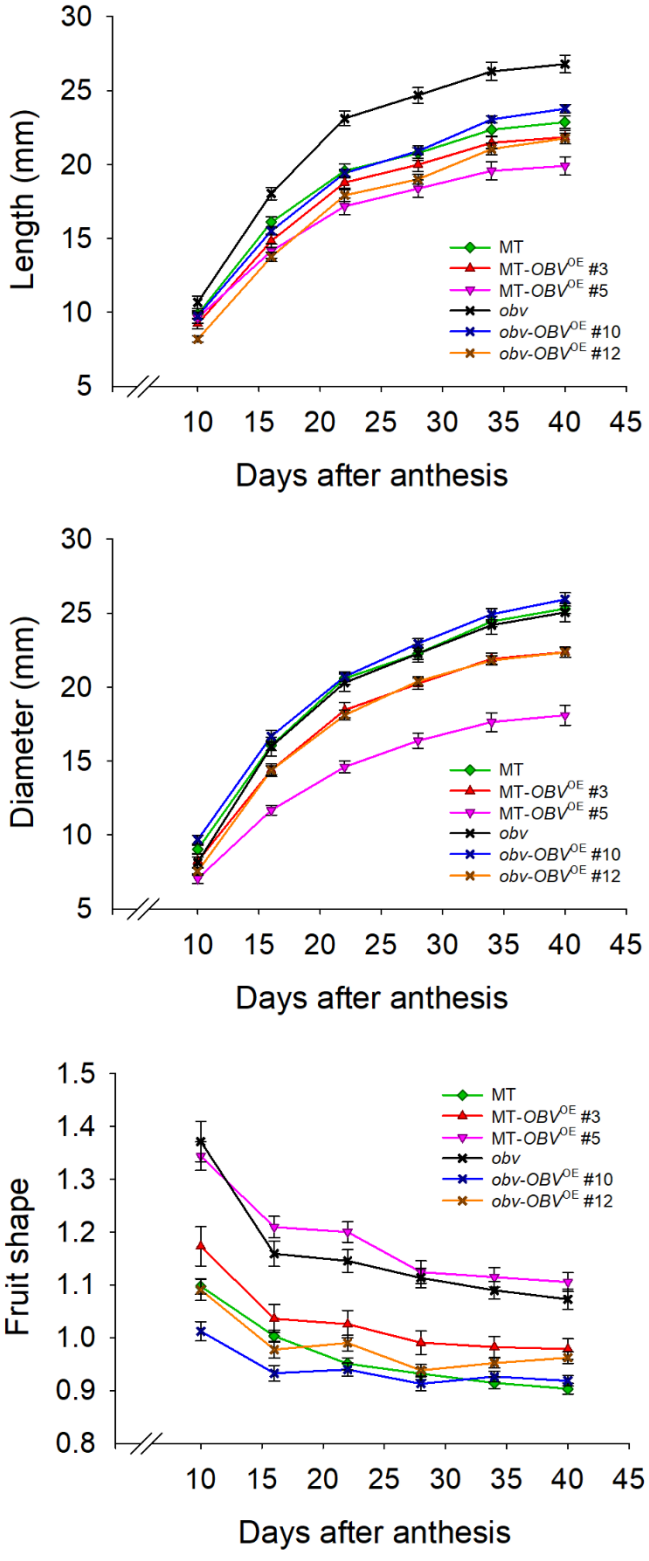

Supplementary Figure 6. Agronomic parameters evaluated in Micro-Tom (MT), *obv* mutant and overexpression lines. The histograms show length of fruits (mm); diameter of fruits (mm) and fruit shape (obtained by the relationship between length and diameter). Measurements were performed at 10; 16; 22; 28; 34 and 40 days after anthesis. Data are mean values ± s.e.m. (n=15 fruits).

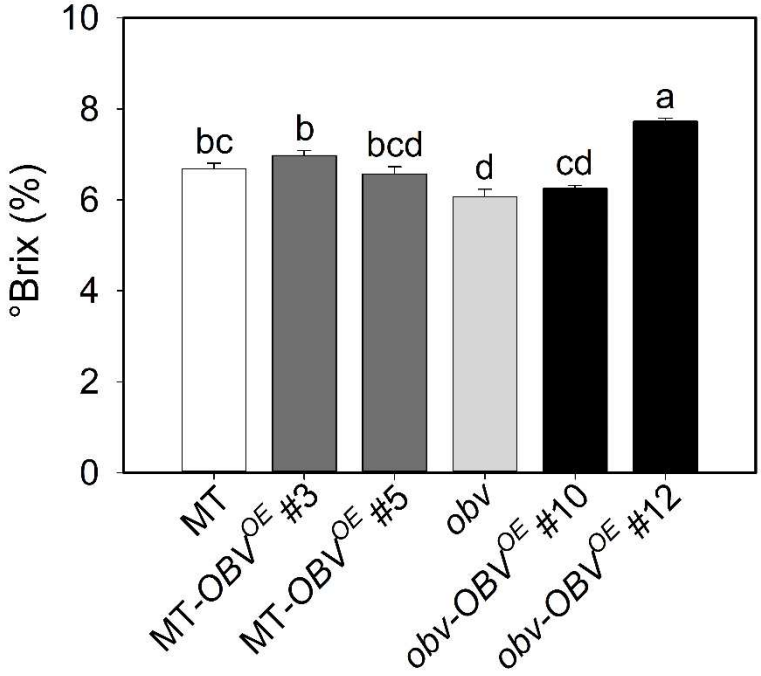

Supplementary Figure 7. Determination of the soluble solids content (°Brix) in ripe fruits of Micro-Tom (MT), *obv* mutant and overexpression lines. The Brix was measured in three mature fruits per plant (in six plants) at 55 days after anthesis. Bars are mean values ± s.e.m. (n=18 fruits). Different letters indicate significant differences by Tukey's test at 5% probability.

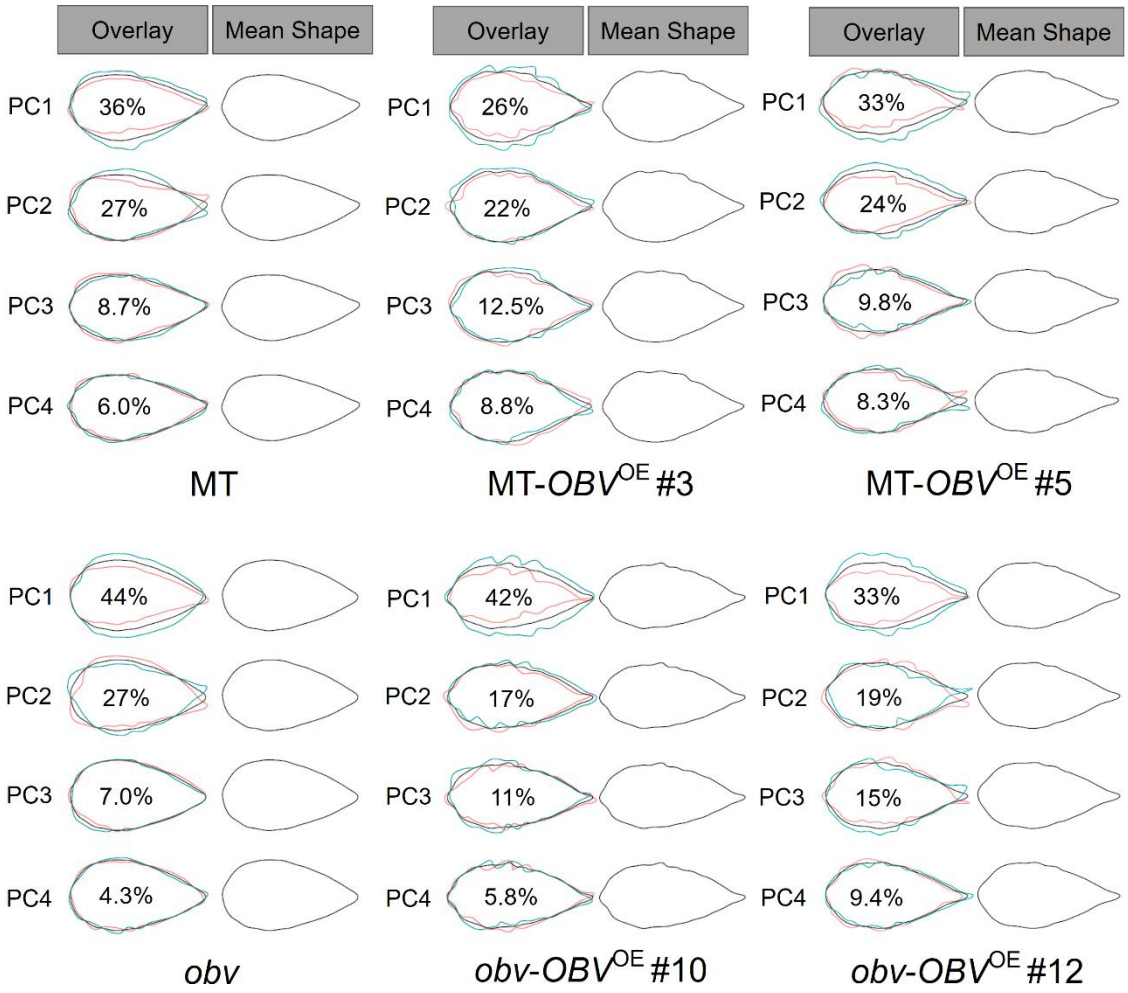

Supplementary Figure 8. *OBV* levels alters leaflets shape in Micro-Tom (MT), *obv* mutant and overexpression lines. The first column shows overlap of the mean leaflet shape in black, -2 SD in orange and +2 SD in green. The second column shows only mean shape of the leaflets. The sum of the principal components (PCs) represents about 74% of all variation found in the leaflets (the lowest PC value found was 67% and the highest 81%). The percentages of each PC are indicated in the overlapping shapes. Values were obtained by evaluating 20 terminal leaflets per genotype.

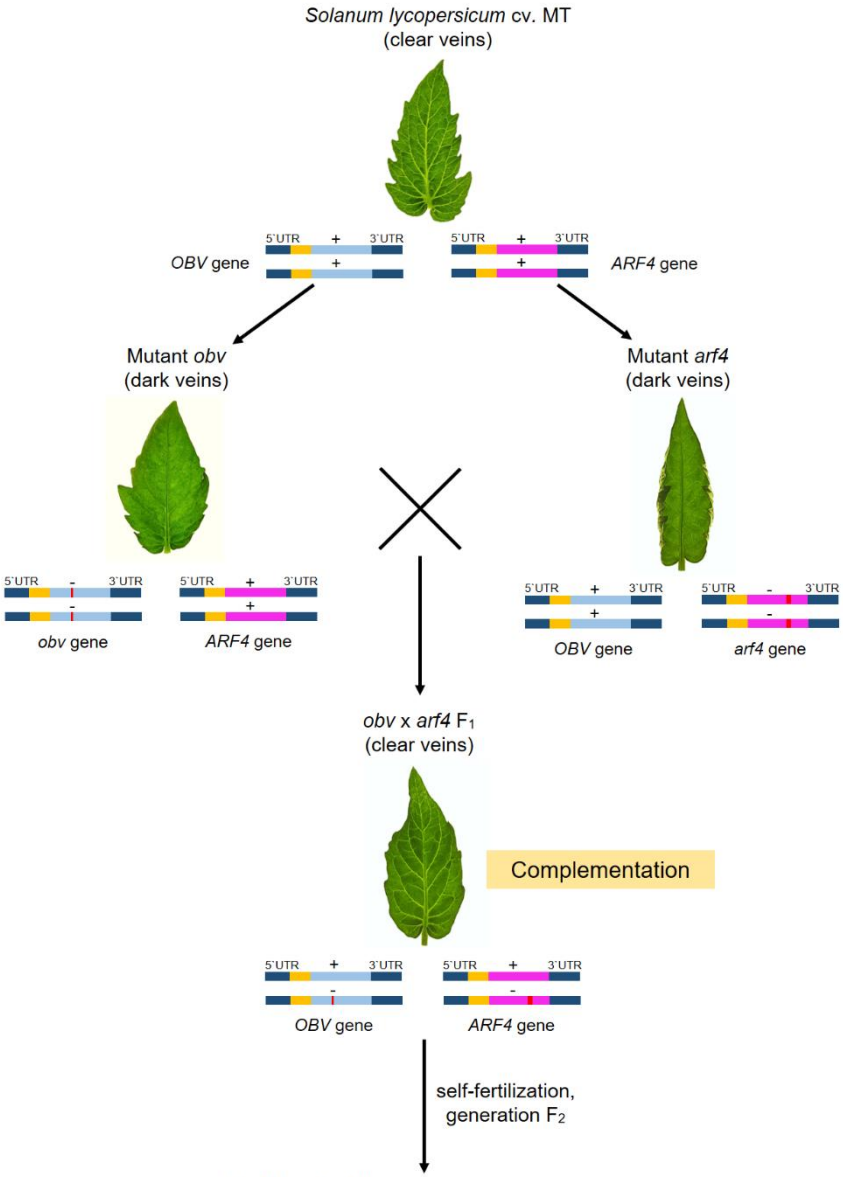

Aa-Bb x Aa-Bb

Gametes	AB	Ab	aB	ab
AB	AA-BB	AA-Bb	Aa-BB	Aa-Bb
Ab	AA-Bb	AA-bb	Aa-Bb	Aa-bb
aB	Aa-BB	Aa-Bb	aa-BB	aa-Bb
ab	Aa-Bb	Aa-bb	aa-Bb	aa-bb

* A: *OBV*, a: *obv*, B: *ARF4*, b: *arf4*

Genotypic segregation:
A — B — 9/16
A — b b 3/16
a a B — 3/16
a a b b 1/16

Phenotypic segregation:
9 - wild-type (clear veins and serrated leaf)
3 - *obv* (dark veins and rounded leaf, less serrated)
3 - *arf4* (dark veins, but with clear regions and rolled leaf)
1 - *obv*/*arf4* (dark veins and rolled leaf)

=

N = 96 plants
A — B — 54
A — b b 18
a a B — 18
a a b b 6

(1): Phenotypic segregation in the F_2 population follows the patterns of mendelian segregation 9:3:3:1 for monogenic inheritance without genetic interactions.
(2): Distortions in the 9:3:3:1 segregation pattern indicate occurrence of genetic interaction = Epistasis.
Example: 12:3:1 dominant epistasis
9:3:4 recessive epistasis
15:1 dominant double epistasis
9:7 recessive double epistasis

Chi-square test:

$$X^2 = \frac{(F0-Fe)^2}{Fe}$$

$X^2_{cal} < X^2_{tab}$ F0 = Fe **(1)**

$X^2_{cal} \geq X^2_{tab}$ F0 ≠ Fe **(2)**

Supplementary Figure 9. Pipeline for the complementation test between *OBV* and *ARF4*. *Solanum lycopersicum* cv. Micro-Tom was considered a wild-type for vein traits and leaf shape. From that background there are two mutants with dark vein phenotype. The *obv* mutant, whose recessive mutation in *OBV* gene confers dark veins phenotype and rounded leaf with little serration at the margins, and *arf4* mutant whose mutation in *ARF4* gene also confers dark veins and leaf winding. These two mutants, both homozygous, were crossed with each other and a population of F_1 plants was generated, all with complemented mutant phenotype. The F_1 generation plants were self-pollinated to generate the segregating F_2 population. In generation F_2, more than 100 plants were germinated and 96 were randomly selected for screening. In the screening, plants were grouped into four phenotypic classes: plants with wild-type (MT) leaves; plants with *obv* leaves; plants with *arf4* leaves and plants that had traits of *obv* and *arf4* together. Finally, the observed phenotypic frequencies were tested with a chi-square test and leaf winding values were quantified.

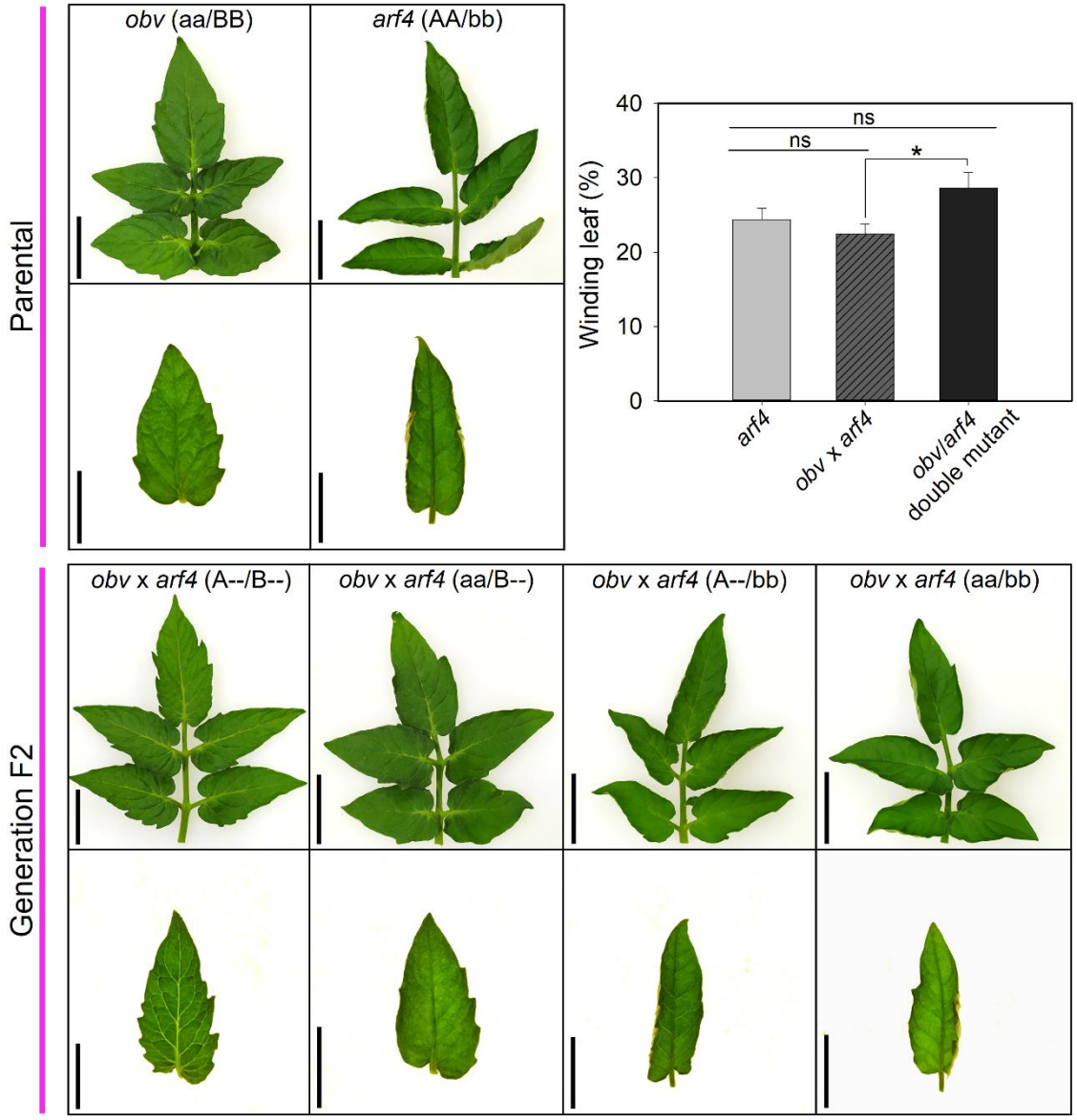

Supplementary Figure 10. Interaction between *OBV* and *ARF4* genes. Representative leaves and leaflets of *obv* mutant, *arf4* mutant (parental) and F_2 progeny 60 days after germination. The leaf winding rate was evaluated in expanded terminal leaflet of the *arf4* mutant, in segregating plants that presented *arf4* phenotype and in the double mutant, respectively. Asterisk indicates statistical difference by T test at 5% probability. ns: not significant. The results show a non-additive effect for leaf winding in the segregating plants in relation to the parental plants. AA = *OBV* functional, aa = *obv* mutant, BB = *ARF4* functional, bb = *arf4* mutant.

Supplementary Table. Observed and expected phenotypic frequencies for F_2 population of the cross between *obv* mutant and *arf4* mutant. A total of 96 plants were screened. For the chi-square calculation was stated a G.L. of 3 with 5% probability.

Phenotypes	**OF**	**EF**	**(OF-EF)**	**$(OF-EF)^2$**	**$X^2 = (OF-EF)^2/EF$**
wild-type leaf	26	18	8	64	3.55
arf4 leaf	38	36	2	4	0.11
obv leaf	16	18	-2	4	0.22
obv/*arf4* leaf	16	24	-8	64	2.66
Total	96	96	---	---	$X^2_{cal} = 6.54$
					$X^2_{tab} = 7.815$

* OF = observed frequency; EF = expected frequency. The EF used for a semi-dominant gene is 3:6:3:4.

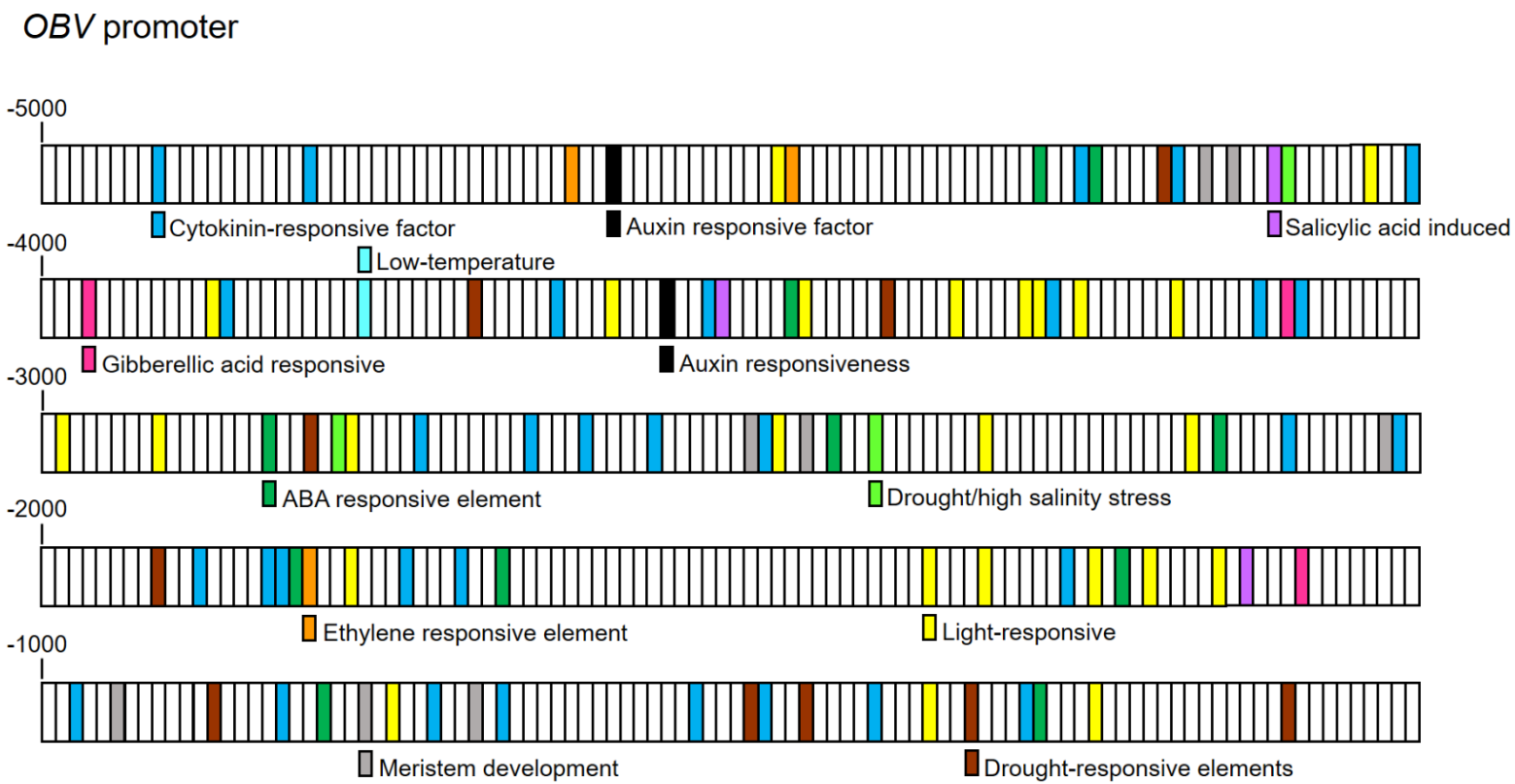

Supplementary Figure 11. Analysis of the *OBV* promoter region (5000 pb upstream from the ATG codon) from *Solanum lycopersicum* cv Heinz. Some interesting cis-elements have been found, such as elements associated with hormones and elements involved with stress conditions. Cis-elements auxin responsive are marked in black. The presence of these elements provides important information about possible functions for the *OBV* gene and its relationship with auxin. Each box in the figure illustrates 10 bp of the promoter region. Source: https://www.dna.affrc.go.jp/PLACE/?action=newplace

CHAPTER 3: Impacts of the *OBV* gene on commercial tomato cultivars

1. INTRODUCTION

Leaf is the organ that coordinates two central processes for plant growth and development, namely photosynthesis and hydraulic relations. Over millions of years, leaves have evolved to optimize these two processes, creating strategies to improve light capture and balance between CO_2 assimilation and loss of water vapor to the atmosphere (Nicotra et al., 2008; Nicotra et al., 2011). Studies hypothesize that evolution towards a more efficient water transport system was the basis for improvements in photosynthetic capacity allowing distribution of the plants in different ecosystems (Cowan and Farquhar, 1977; Brodribb et al., 2007).

The leaves structure and function are closely linked and together with phenotypic plasticity allows plants to explore environments with totally different conditions (Abrams, 1994; Sack et al., 2006; Scoffoni et al., 2015). Hydraulic function is determined by the structural diversity of veins (number, length and diameter) and mesophyll cells anatomy including cell size, intercellular spaces, deposition of hydrophilic substances, lignification, aquaporins number and bundle sheath structure (Scoffoni et al., 2016; Brodribb et al., 2007). The veins structure will determine hydraulic conductance of the xylem (K_x), which can be defined as ease with which water is transported through xylem conduits, from root to leaf. The anatomical and biochemical constitution of mesophilic cells will contribute for conductance outside the xylem (K_{ox}). This extra xylemic route represents most of all resistance that liquid water faces to be distributed along leaf blade. Together, K_x and K_{ok} make up leaf hydraulic conductance (K_{leaf}) (Scoffoni et al., 2015; Scoffoni et al., 2016). The Water flow through plant occurs via xylem within the vascular bundles, which upon entering in leaf blade from the petiole, rearrange into major and minor veins. Upon leaving the xylem, water starts the extra xylemic route and get in touch with first component, the bundle sheath, a layer of parenchymal cells compactly arranged around vasculature (Scoffoni et al., 2017; Trifiló and Nardini, 2016).

Bundle sheaths function as water flux sensors in the leaf and exhibit a diverse anatomical structure (Ohtsuka et al., 2018). In many species, cells in the bundle sheath form an extension that connects the vascular region with upper, lower epidermis, or both. This structure is known as bundle sheath extension (BSE), can occur in veins of any order

and is composed of one or more columns of parenchymatic cells, compact and devoid of pigments (Esau, 1977; Wylie, 1943; Wylie, 1952). The presence of BSE in leaves contribute directly to the increments in K_{leaf} and photosynthetic performance. In the first case, BSEs promote better hydraulic integration, creating a route of less resistance for the liquid water path between supply structures (veins) and water outlets (stomata) (Zwieniecki et al., 2007). The second is attributed to the optical properties of BSEs in the distribution of light within leaf, enriching mesophyll layers with photosynthetically active radiation (Karabourniotis et al., 2000; Nikolopoulos et al., 2002). The presence of BSEs obstructs lateral diffusion of gases, creating compartments with potentially different partial pressures of gases (water vapor and CO_2) along the leaf blade. The species with BSEs in leaves are therefore called *heterobaric*, while in leaves without BSEs (*homobaric*), lateral circulation of gases in the intercellular spaces of the mesophyll occurs freely (Neger, 1918; Terashima, 1992; Pieruschka et al., 2006).

In a previous study done with heterobaric and homobaric tomato leaves (*Solanum lycopersicum* cv. Micro-tom), was showed that homobaric mutant *obscuravenosa* (*obv*, whose mutation takes loss of BSEs) reduces K_{leaf} and stomatal conductance, but does not affect assimilation photosynthetic (Zsogon et al., 2015). In a second study, plants with heterobaric and homobaric leaves were grown under two contrasting irradiance levels (sun and shade) and both leaves showed different plastic responses. In the shaded environment, heterobaric leaves reduced K_{leaf} and vein density. In homobaric leaves, these parameters remained unchanged. Shading in homobaric leaves induced an increase in another set of traits, including photosynthetic assimilation and leaf intercellular air spaces (Barbosa et al., 2019). It was also evidenced that *obv* mutant cultivated under a condition of hydric restriction presented higher values of hydric potential and lower rate of leaf rolling, compared to Micro-tom (heterobaric) (Barbosa, 2017). These responses suggest that homobaric leaves may have a particular tolerance mechanism that provides advantages for environments where water is a limiting factor.

In addition to the physiological impacts caused by presence or lack BSEs in leaves, the distribution of this structure among commercial tomato cultivars is quite interesting. Homobaric leaves are more frequent in industrial tomato varieties, grown in field, while heterobaric leaves are typical of table tomato varieties, grown in greenhouse (Jones et al., 2007). From these observations, we questioned if variation between heterobaric and

homobaric characters, until then unconsciously selected by breeding programs may actually have a relevant agronomic to tomato crop.

To assess a possible agronomic impact of the heterobaric and homobaric tomato leaves, we choose two commercial homobaric cultivars (M82 and VFN8) harboring *obv* mutation, and we confirmed by complementation that loss of BSEs in these cultivars was also caused by *OBV* allele loss of function. Then, we selected M82 cultivar to perform the introgression of *OBV* functional allele (from MT wild-type) and in parallel we conducted the introgression of transgene *obv-OBV*^{OE} (from complemented lines #10 and #12) to generate M82 near-isogenic lines carrying *OBV* allele at distinct expression levels. The introgressed lines generated here provide a material of study appropriate, for being a background with already known productivity and with variations focused only on the leaf structure.

2. MATERIAL AND METHODS

Plant material, growth conditions and breeding

Tomato seeds (*Solanum lycopersicum* cv Micro-Tom and M82) were seeded in polyethylene trays containing Tropostrato® commercial substrate and kept under greenhouse conditions, ~800 µmol m^{-2} s^{-1}, photoperiod 12/12-h and temperature 26/18°C day/night. Upon appearance of the first true leaf, seedlings of each cultivar were transplanted to pots with capacity of 350 ml and 3000 ml respectively. The basic fertilizing was done with NPK 2 g L^{-1} (10-10-10) and limestone 4 g L^{-1}.

OBV functional allele from MT (wild-type) or transgene *obv-OBV*^{OE} from complemented lines #10 and #12 were introgressed into M82 cultivar following the scheme illustrated in Supplementary Figure 3. Briefly, plants were grown in greenhouse under conditions described above. M82 and MT were crossed using the first as female receiver and the second as pollen donor. F_1 plants were self-pollinated, generating a segregating F_2 progeny. The F_2 seedlings resulting were screened looking for translucent veins and bigger stature of M82. Selected plants were backcrossed with M82 parental to remove gradually MT genes, producing F_2BC1 seeds. This procedure of crossing and screening was carried until BC3.

Phenotypic characterization

The morphological measurements and leaf characterization were made in M82 and M82 near-isogenic lines with *OBV* functional (from MT or *obv-OBV*^{OE} #10/#12), after anthesis of the first flower. The height was taken through of the plant measurement from ground level to first inflorescence. The length and diameter of the internodes were obtained by measuring 4th and 5th internodes counted from ground level. Stem diameter was obtained using a mechanical pachymeter (Mitutoyo® Vernie Caliper model, Japan) and measurements were made on level above the cotyledons. Leaves number until first inflorescence was obtained upwards by counting the number of leaves on main stem. Leaf insertion angle was determined with aid of a protractor, based on insertion of the 4th and 5th leaf. All these growth measurements were evaluated in seven plants per treatment, in F_1 generation and repeated in BC2 plants. For leaf characterization, four terminal leaflets were selected per plant, in six plants per genotype. The leaflets were digitized using an HP Scanjet G2410 scanner (Hewlett-Packard, Palo Alto, California, USA) and measures of perimeter, leaflet area, circularity and serration number were obtained using Image-Pro Plus software (version 4.5, Media Cybernetics, Silver Spring, USA).

Agronomic parameters (yield and Brix)

Fruit agronomic parameters were determined in M82 cultivar and M82 near-isogenic lines with *OBV* functional (from MT or *obv-OBV*^{OE} #10/#12), in BC3. The number of fruits per plant was obtained by total fruit count and frequency of green and mature fruits, determined separately. The yield fruits per plant was obtained after weighing all fruits, using a semi analytical balance with sensitivity of 0.01 g (AUY220, Shimadzu, Kyoto, Japan). The analyses were performed in 10 plants per genotype. The length and diameter of the fruits were evaluated in six fruits per plant (10 plants per genotype). The determination of the soluble solids content (°Brix) was measured in six fruits per plant (10 plants) with a digital refractometer (model RTD 45, Instrutherm®, São Paulo, Brazil).

Statistical analysis

The experimental design was completely randomized. The data were submitted to analysis of variance (ANOVA) using Sisvar® version 5.6 and the means were compared by Tukey test at 5% level of significance ($P \leq 0.05$).

3. RESULTS

A hitherto unexplained observation in tomato agronomy is widespread distribution of the *obv* mutation in field tomato varieties, which is nevertheless conspicuously absent in most glasshouse varieties. We selected two field tomato varieties traditionally used in research, VFN8 and M82, both harboring the *obv* mutation, and crossed them to MT and *obv*-*OBV*^{OE} #10/#12 lines (Figure 1). All F_1 hybrids showed recovery of clear veins in leaf, wild-type phenotype, indicating complementation of the genetic alteration in *obv* by functional allele derived from MT and *OBV*^{OE} transgene (Supplementary Figure 1). We also observed and quantified the pleiotropic effects caused by *OBV* and we saw that some of these effects are consistent with observed in MT background, while others were less expressive. There was an increase in the perimeter and reduction in leaf circularity (Figure 2A-C). The increase in the serration number was not well evidenced in hybrids (Figure 2D). Other growth parameters evaluated such as plant height, number of leaves and leaflets, length of internodes, leaf angle and fruit shape were not impacted by *OBV* allele, in F_1 plants (Supplementary Table 1 and 2).

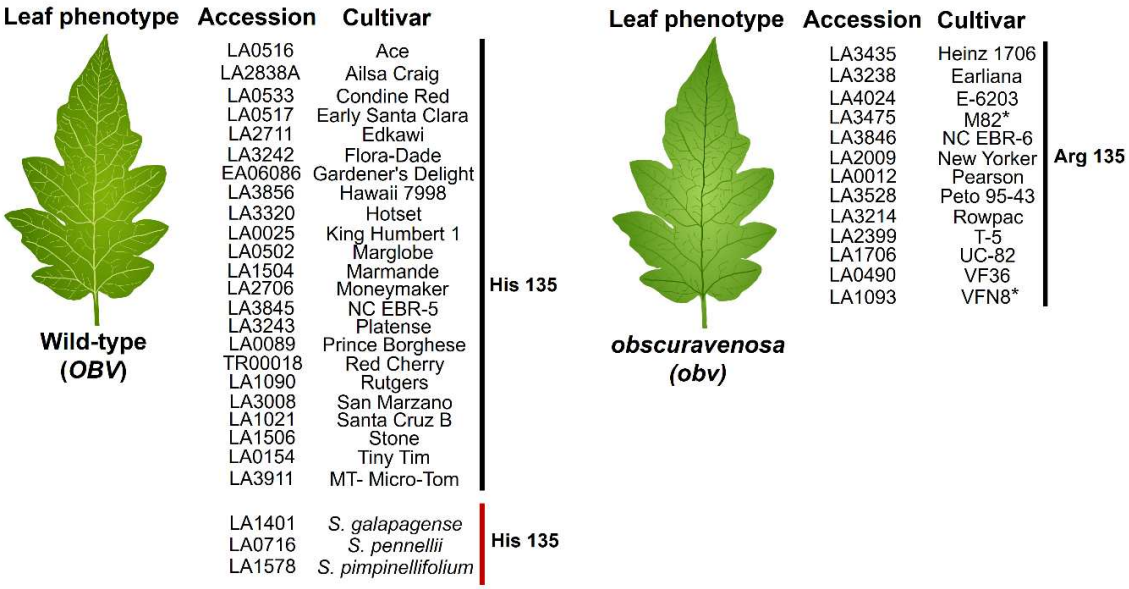

Figure 1. Leaf phenotype of some commercial tomato cultivars with their corresponding amino acid polymorphism. Most greenhouse cultivars, such as those shown on the right, and wild tomato species (in red) have clear veins. This phenotype is associated with presence of BSEs in the leaves. In tomato, one of the key regulators of BSEs is the transcription factor *OBV*, which in its functional form encodes a zinc finger protein containing a histidine at 135 position. In contrast, most field cultivars, on the left, have the *obscuravenosa* mutation resulting in a phenotype of dark veins as consequence of the BSEs loss in the leaves. *obv* mutation is caused by a SNP (A→G) conserved in *OBV* gene that promotes exchange to histidine for arginine at 135 position. The asteristic indicates both cultivars (M82 and VFN8) selected for complementation and introgression of *OBV* functional allele.

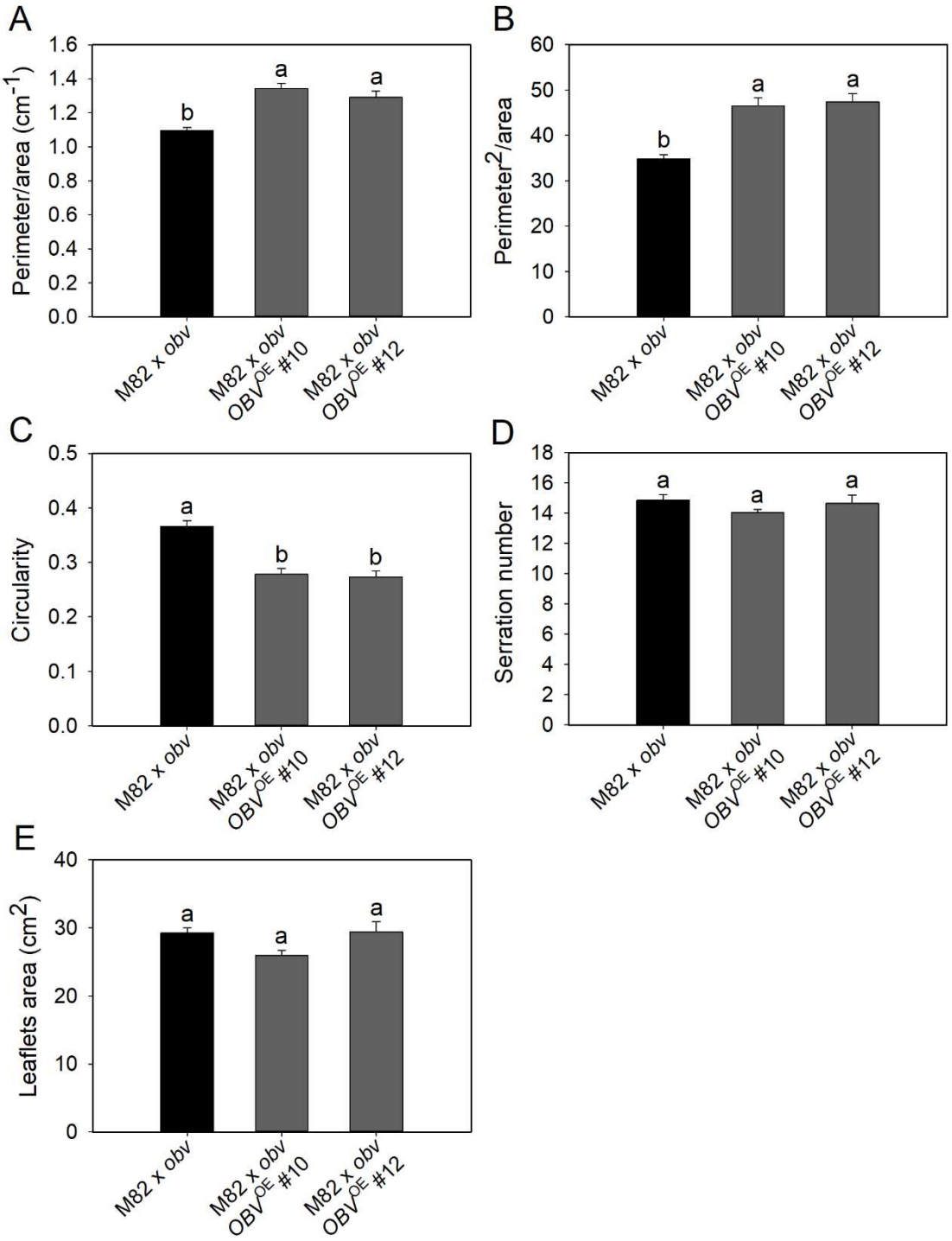

Figure 2. *OBV* overexpression alters leaf morphology in M82 hybrids. Morphological parameters: (A) relationship between perimeter/area; (B) perimeter^2/area; (C) Circularity; (E) Serration number and (D) leaflets area. Measurements were made in F_1 generation plants. Bars are mean values ± s.e.m. (n=23 terminal leaflets per genotype). Different letters indicate significant differences by Tukey's test at 5% probability.

Next, we made backcrosses to create M82 near-isogenic lines displaying BSEs. (Supplementary Figure 3). We conducted two rounds of backcrossing (BC_1 and BC_2). The plants generated after each backcross were selected based on bigger stature (a trait from M82, whose alleles complement the dwarfing alleles of MT) and leaves with clear veins, indicating presence of the *OBV* wild-type allele or OBV^{OE} transgene. Plants derived from introgression showed similar to parental M82 in some morphological traits such as plant height, internodes size, stem diameter and number of leaves (Table 1). Leaf insertion angle was slightly changed in plants introgressed with OBV^{OE} transgene. The plants showed a subtle reduction in the angle, however, due to great variation in this trait we did not find significant differences between genotypes. In BC2, we could see that OBV^{OE} promoted a noticeable increase in leaf serration, forming margins cutout deeply with the leaflet tip acute (Supplementary Figure 4). On the other hand, in plants introgressed with *OBV* wild allele from MT the cutout of the leaf margin was similar to M82 parental (Figure 3B, C).

Table 1. Growth parameters in M82 cultivar harboring *OBV* functional allele.
Parameters are as follows: height of the primary shoot (cm); length of the two internodes (cm); diameter of the two internodes (cm); stem diameter (cm); leaves number on primary shoot (leaves number up to first inflorescence) and leaf insertion angle in two leaves (°). Measurements were performed at 70 DAG in BC2 plants. Data are means ± se (n = 7 plants). Different letters indicate statistically significant differences (Tukey's test, $P < 0.05$).

Parameters	**M82**	**M82 x MT**	**M82 x *obv* *OBV*^{OE} #10**	**M82 x *obv* *OBV*^{OE} #12**
Plant height (cm)	26.7 ± 3.9a	28.2 ± 4.3a	29.1 ± 4.1a	31.7 ± 5.3a
Length of the internodes (cm)				
Internode 4th	2.92 ± 0.54a	2.75 ± 0.57a	3.08 ± 0.51a	3.27 ± 0.82a
Internode 5th	3.62 ± 0.78a	3.53 ± 0.91a	3.65 ± 0.47a	4.03 ± 0.69a
Diameter of the internodes (cm)				
Internode 4th	1.06 ± 0.07a	1.02 ± 0.06a	1.09 ± 0.08a	1.11 ± 0.07a
Internode 5th	1.02 ± 0.06a	1.01 ± 0.07a	1.12 ± 0.11a	1.06 ± 0.09a
Stem diameter (cm)	1.07 ± 0.05a	0.98 ± 0.1b	1.13 ± 0.08a	1.12 ± 0.09a
Leaves number	7 ± 0.8a	6.8 ± 0.6a	7.5 ± 1.2a	7.4 ± 0.7a
Leaf insertion angle (°)				
Leaf 5th	84.4 ± 5.7a	88.2 ± 5.1a	88.2 ± 8.4a	81.8 ± 11.1a
Leaf 6th	87.7 ± 5.7a	89.2 ± 5.8a	87.2 ± 6.5a	84.2 ± 5.4a

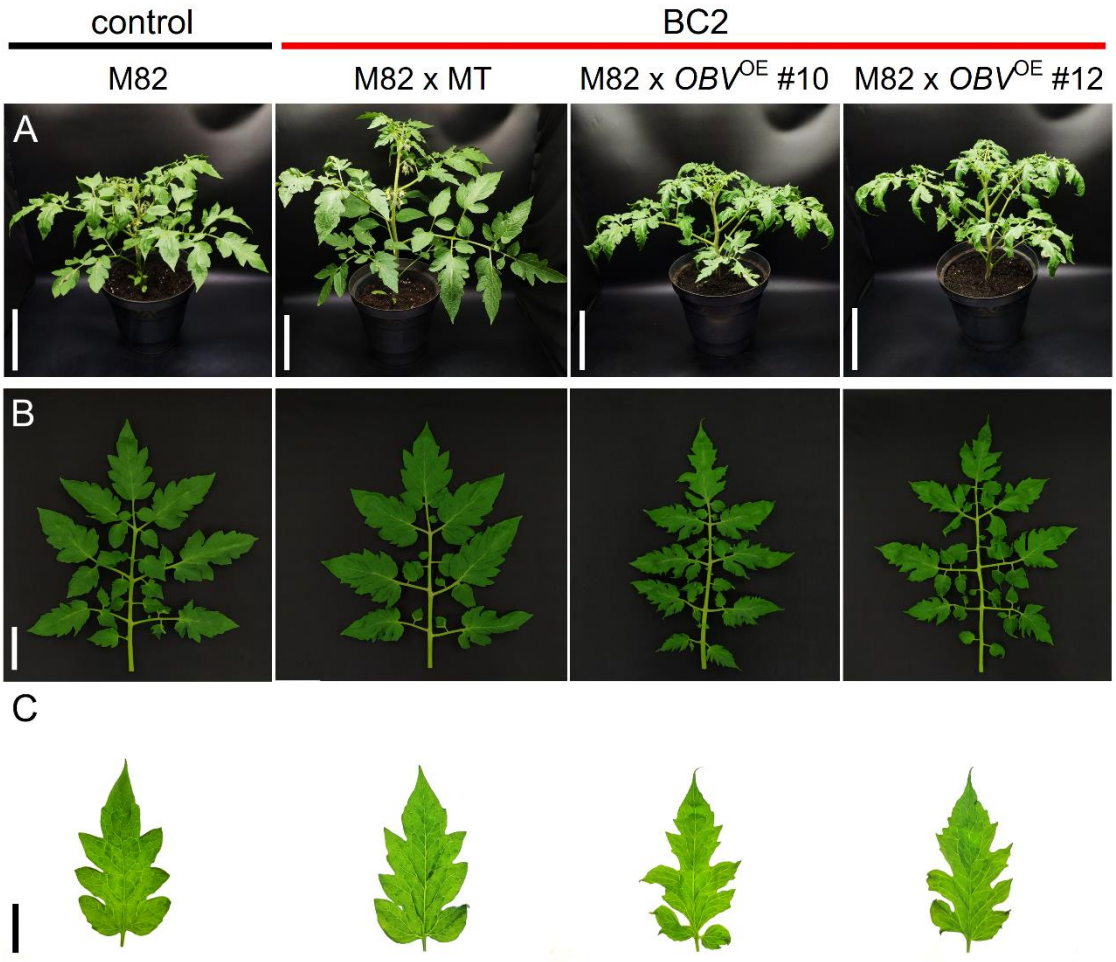

Figure 3. Impact of *OBV* on phenotypic characteristics of M82 near-isogenic lines. (A) Representative plants of M82 (*obv* mutant), BC2 plants introgressed with *OBV* wild allele from MT and introgressed plants with transgene *obv*-*OBV*^{OE} #10/#12. (B and C) Leaves and leaflets of M82 (dark veins) and introgressed plants (clear veins).

4. CONCLUSION

Our results suggest that *OBV* could have strong impact on relevant agronomic traits in the tomato. Whether different alleles of *OBV* where deliberately selected by breeders in tomato cultivars still remains an open question. In future work, and to investigate possible impacts of the leaf structure on productivity of the M82 cultivar, we will evaluate, in more advanced BC_3 plants, quantitative and qualitative parameters related to production, such as number of fruits per plant, fresh weight, length and diameter of fruits, index of harvest and brix. These results will elucidate if the presence of the *OBV* gene in field tomato can have any potential agricultural impact whether in the productivity, in plant performance under controlled conditions or even under restrictive environmental conditions.

5. REFERENCES

Abrams MD, Kubiske ME, Mostoller SA (1994) Relating wet and dry year ecophysiology to leaf structure in temperate tree species. Ecology **75**: 123-133

Barbosa MAM (2017) Homobaric and heterobaric leaves in tomato (*Solanum lycopersicum* L.): morphological, anatomical and physiological implications in different environmental conditions. MSc Thesis, Universidade Federal de Viçosa

Barbosa MAM, Chitwood DH, Azevedo AA, Araújo WL, Ribeiro DM, Peres LE, Zsögön A (2019) Bundle sheath extensions affect leaf structural and physiological plasticity in response to irradiance. Plant Cell and Environment **42**: 1575-1589

Brodribb TJ, Feild TS, Jordan GJ (2007) Leaf maximum photosynthetic rate and venation are linked by hydraulics. Plant Physiology **144**: 1890-1898

Cowan IR, & GD, F (1977) Stomatal function in relation to leaf metabolism and environment.

Esau K (1977) Anatomy of Seed Plants, 2nd ed. John Wiley & Sons, Inc., New York

Inoue Y, Kenzo T, Tanaka-Oda A, Yoneyama A, Ichie T (2015) Leaf water use in heterobaric and homobaric leafed canopy tree species in a Malaysian tropical rain forest. Photosynthetica **53**: 177-186

Jones CM, Rick CM, Adams D, Jernstedt J, Chetelat RT (2007) Genealogy and fine mapping of *obscuravenosa*, a gene affecting the distribution of chloroplasts in leaf veins, and evidence of selection during breeding of tomatoes (*Lycopersicon esculentum*; Solanaceae). American Journal of Botany **94**: 935-47

Karabourniotis G, Bornman JF, Nikolopoulos D (2000) A possible optical role of the bundle sheath extensions of the heterobaric leaves of *Vitis vinifera* and *Quercus coccifera*. Plant Cell and Environment **23**: 423-430

Kenzo T, Ichie T, Watanabe Y, Hiromi T (2007) Ecological distribution of homobaric and heterobaric leaves in tree species of Malaysian lowland tropical rainforest. American Journal of Botany **94**: 764-775

Neger F (1918) Wegsamkeit der Laubblatter fur gase. Flora **111**: 152-161

Nicotra AB, Cosgrove MJ, Cowling A, Schlichting CD, Jones CS (2008) Leaf shape linked to photosynthetic rates and temperature optima in South African Pelargonium species. Oecologia **154**: 625-35

Nicotra AB, Leigh A, Boyce CK, Jones CS, Niklas KJ, Royer DL, Tsukaya H (2011) The evolution and functional significance of leaf shape in the angiosperms. Functional Plant Biology **38**: 535-552

Nikolopoulos D, Liakopoulos G, Drossopoulos I, Karabourniotis G (2002) The relationship between anatomy and photosynthetic performance of heterobaric leaves. Plant Physiology **129**: 235-243

Ohtsuka A, Sack L, Taneda H (2018) Bundle sheath lignification mediates the linkage of leaf hydraulics and venation. Plant Cell and Environment **41**: 342-353

Pieruschka R, Schurr U, Jensen M, Wolff WF, Jahnke S (2006) Lateral diffusion of CO_2 from shaded to illuminated leaf parts affects photosynthesis inside homobaric leaves. New Phytologist **169**: 779-788

Sack L, Frole K (2006) Leaf structural diversity is related to hydraulic capacity in tropical rain forest trees. Ecology **87**: 483-491

Scoffoni C, Albuquerque C, Brodersen CR, Townes SV, John GP, Bartlett MK, Sack L (2017) Outside-xylem vulnerability, not xylem embolism, controls leaf hydraulic decline during dehydration. Plant Physiology **173**: 1197-1210

Scoffoni C, Chatelet DS, Pasquet-kok J, Rawls M, Donoghue MJ, Edwards EJ, Sack L (2016) Hydraulic basis for the evolution of photosynthetic productivity. Nature Plants **2**: 1-8

Scoffoni C, Kunkle J, Pasquet-Kok J, Vuong C, Patel AJ, Montgomery RA, Sack L (2015) Light-induced plasticity in leaf hydraulics, venation, anatomy, and gas exchange in ecologically diverse *Hawaiian lobeliads*. New Phytologist **207**: 43-58

Terashima I (1992) Anatomy of non-uniform leaf photosynthesis. Photosynthesis Research **31**: 195-212

Trifiló P, Raimondo F, Savi T, Lo Gullo MA, Nardini A (2016) The contribution of vascular and extra-vascular water pathways to drought-induced decline of leaf hydraulic conductance. Journal of Experimental Botany **67**: 5029-5039

Wylie RB (1943) The role of the epidermis in foliar organization and its relations to the minor venation. American Journal of Botany **30**: 273-280

Wylie RB (1952) The bundle sheath extension in leaves of dicotyledons. American Journal of Botany **39**: 645-651

Zsögön A, Alves Negrini AC, Peres LEP, Nguyen HT, Ball MC (2015) A mutation that eliminates bundle sheath extensions reduces leaf hydraulic conductance, stomatal conductance and assimilation rates in tomato (*Solanum lycopersicum*). New Phytologist **205**: 618-626

Zwieniecki MA, Brodribb TJ, Holbrook NM (2007) Hydraulic design of leaves: insights from rehydration kinetics. Plant Cell and Environment **30**: 910-921

6. SUPPLEMENTARY MATERIAL

Supplementary Table 1. Growth parameters in M82 hybrids harboring different *OBV* alleles

Parameters are as follows: height of the primary shoot (cm); length of the three internodes (cm); diameter of the three internodes (cm); stem diameter (cm); leaves number on primary shoot (leaves number up to first inflorescence); leaf insertion angle in three leaves (°) and leaflets number. Measurements were performed at 70 DAG in F_1 generation plants. Data are means ± se (n = 6 plants). Different letters indicate statistically significant differences (Tukey's test, $P < 0.05$).

Parameters	**M82 x *obv***	**M82 x *obv* *OBV*^{OE} #10**	**M82 x *obv* *OBV*^{OE} #12**
Plant height (cm)	44.60 ± 2.98a	52.38 ± 3.29a	48.38 ± 1.31a
Length of the internodes (cm)			
Internode 4th	3.89 ± 0.33a	3.41 ± 0.18a	3.32 ± 0.33a
Internode 5th	4.20 ± 0.48a	4.17 ± 0.21a	3.43 ± 0.09a
Internode 6th	4.86 ± 0.66a	5.47 ± 0.53a	3.87 ± 0.21a
Diameter of the internodes (cm)			
Internode 4th	0.88 ± 0.05b	1.17 ± 0.04a	1.09 ± 0.06a
Internode 5th	0.88 ± 0.06b	1.10 ± 0.04a	1.12 ± 0.07a
Internode 6th	0.89 ± 0.05b	1.02 ± 0.03ab	1.10 ± 0.08a
Stem diameter (cm)	0.97 ± 0.03b	1.26 ± 0.03a	1.23 ± 0.06a
Leaves to 1st inflorescence	9 ± 0.68a	9 ± 0.33a	10 ± 0.42a
Leaf insertion angle (°)			
Leaf 5th	84 ± 2.59a	85 ± 2.06a	93 ± 2.08a
Leaf 6th	84 ± 2.33a	86 ± 0.72a	82 ± 1.60a
Leaf 7th	86 ± 2.19a	84 ± 1.26a	83 ± 1.32a
Leaflets number			
Leaf 5th	14 ± 1.70a	16 ± 0.93a	12 ± 0.77a
Leaf 6th	19 ± 1.45a	21 ± 1.06a	17 ± 1.23a
Leaf 7th	17 ± 1.21b	27 ± 0.72a	23 ± 1.41a

Supplementary Table 2. Agronomic parameters in M82 hybrids Parameters are as follows: average length of fruits (mm); average diameter of fruits (mm) and fruit shape obtained by relationship between length and diameter. Measurements were performed at 10; 17; 24; 31; 38; 45; 52 and 59 days after anthesis (DAA) in F_1 generation plants. Data are means ± se (n = 24 fruits). Different letters indicate statistically significant differences (Tukey's test, $P < 0.05$).

Parameters	**M82 x *obv***	**M82 x *obv* *OBV*^{OE} #10**	**M82 x *obv* *OBV*^{OE} #12**
Fruit length (mm)			
10 DAA	9.72 ± 0.54a	9.77 ± 0.32a	8.48 ± 0.42a
17 DAA	16.55 ± 0.78a	16.30 ± 0.55a	14.92 ± 0.74a
24 DAA	26.65 ± 1.08a	23.90 ± 0.85a	24.58 ± 0.69a
31 DAA	31.75 ± 1.38a	30.86 ± 0.68a	30.36 ± 0.77a
38 DAA	37.24 ± 1.15a	35.57 ± 0.63ab	33.79 ± 0.76b
45 DAA	40.76 ± 0.89a	36.78 ± 0.79b	35.60 ± 1.04b
52 DAA	42.72 ± 1.01a	38.09 ± 1.03b	37.92 ± 0.93b
59 DAA	43.59 ± 1.12a	39.80 ± 1.04b	37.88 ± 0.82b
Fruit diameter (mm)			
10 DAA	7.66 ± 0.46a	8.76 ± 0.30a	7.60 ± 0.37a
17 DAA	15.44 ± 0.75a	16.36 ± 0.62a	14.91 ± 0.74a
24 DAA	25.88 ± 1.03a	23.90 ± 0.90a	24.70 ± 0.66a
31 DAA	31.67 ± 1.34a	31.11 ± 0.70a	30.68 ± 0.77a
38 DAA	37.07 ± 0.96a	36.90 ± 0.71ab	34.15 ± 0.78b
45 DAA	40.92 ± 0.78a	37.73 ± 0.96ab	36.00 ± 1.08b
52 DAA	42.77 ± 0.92a	38.53 ± 1.07b	38.32 ± 0.93b
59 DAA	42.47 ± 1.00a	40.39 ± 1.07ab	37.96 ± 0.79b
Fruit shape			
10 DAA	1.29 ± 0.03a	1.12 ± 0.01b	1.12 ± 0.01b
17 DAA	1.08 ± 0.02a	1.00 ± 0.01b	1.00 ± 0.01b
24 DAA	1.04 ± 0.02a	1.00 ± 0.01a	0.99 ± 0.01a
31 DAA	1.00 ± 0.01a	0.99 ± 0.01a	0.99 ± 0.01a
38 DAA	1.00 ± 0.02a	0.97 ± 0.01b	0.99 ± 0.004ab
45 DAA	1.00 ± 0.01a	0.98 ± 0.01a	0.99 ± 0.004a
52 DAA	1.00 ± 0.02a	0.99 ± 0.01a	0.99 ± 0.005a
59 DAA	1.03 ± 0.02a	0.99 ± 0.01b	1.00 ± 0.01ab


M82 x obv
M82 x obv-OBV^OE #10
M82 x obv-OBV^OE #12
VFN8
VFN8 x MT-OBV^OE #3
VFN8 x obv-OBV^OE #10

Supplementary Figure 1. **Morphology of M82, VFN8 and *OBV*-complemented plants.** Representative F_1 generation plants from crossing of M82 x *obv*, M82 x *obv*-*OBV*^{OE} #10, M82 x *obv*-*OBV*^{OE} #12, VFN8, VFN8 x MT-*OBV*^{OE} #3 and VFN8 x *obv*-*OBV*^{OE} #10. Below are shown leaves and terminal leaflets. Cultivars M82 and VFN8 (*obv* mutant) has dark veins and the complemented plants with *OBV*^{OE} allele recovered light veins phenotype. The illustrated plants have 70 days after germination. Scale bars represents 30 cm for plants and 4 cm for leaves and leaflets.

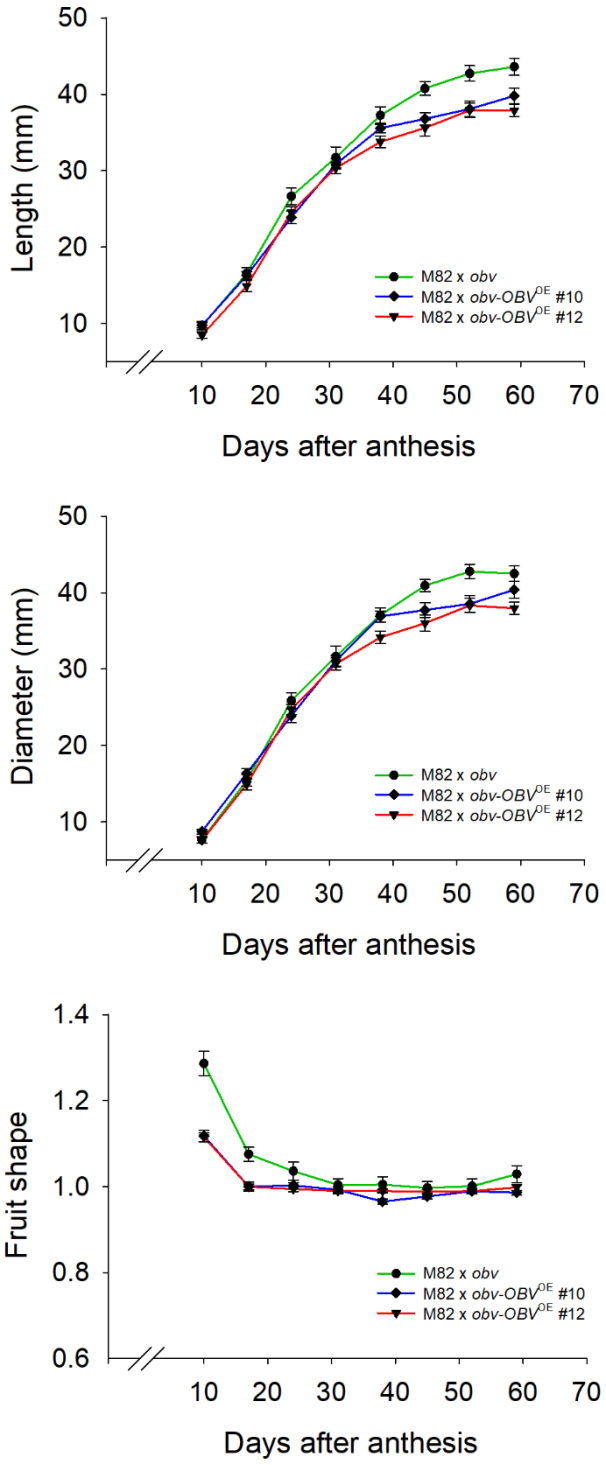

Supplementary Figure 2. **Agronomic parameters in M82 hybrids harboring different *OBV* alleles**. The histograms show the length of fruits (mm); diameter of fruits (mm) and fruit shape (obtained by the relationship between length and diameter) evaluated in M82 x MT-*obv*, and M82 x *obv-OBV*^{OE} #10/#12, F_1 generation. Measurements were performed at 10; 17; 24; 31; 38; 45; 52 and 59 days after anthesis (DAA). Data are mean values ± s.e.m. (n=24 fruits).

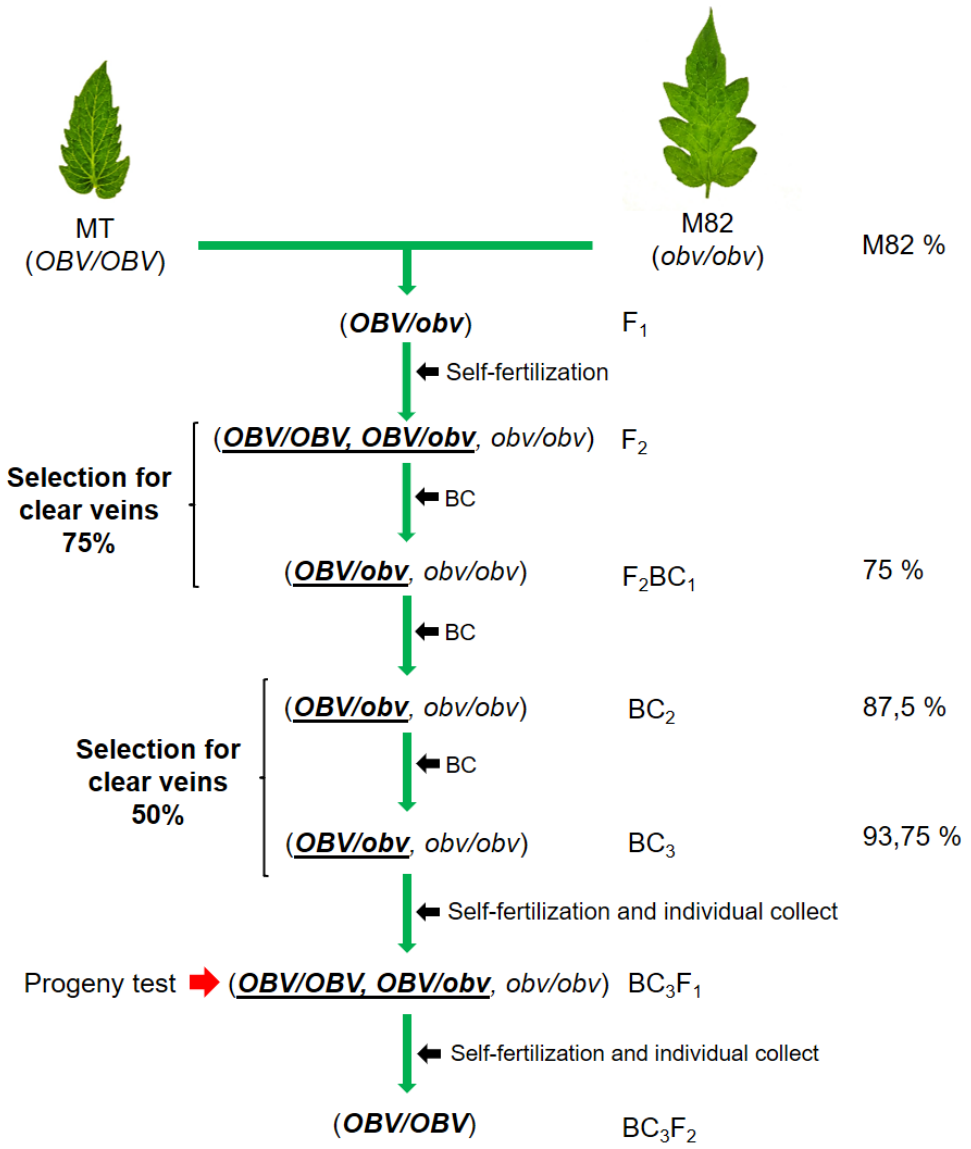

Supplementary Figure 3. **Pipeline for introgression of *OBV* functional allele into M82 background.** This pipeline shows the steps performed to obtain a near-isogenic line of M82 carrying *OBV* functional allele from MT (wild-type). The same steps were performed to obtain introgression lines with transgene (*obv*-*OBV*^{OE} #10 and #12, generation T4, homozygous). The selection of plants was made by choosing plants with clear veins and larger size. Progeny test was conducted at the end of introgression process and populations with 100% of individuals presenting clear veins were considered homozygous. BC = backcross.

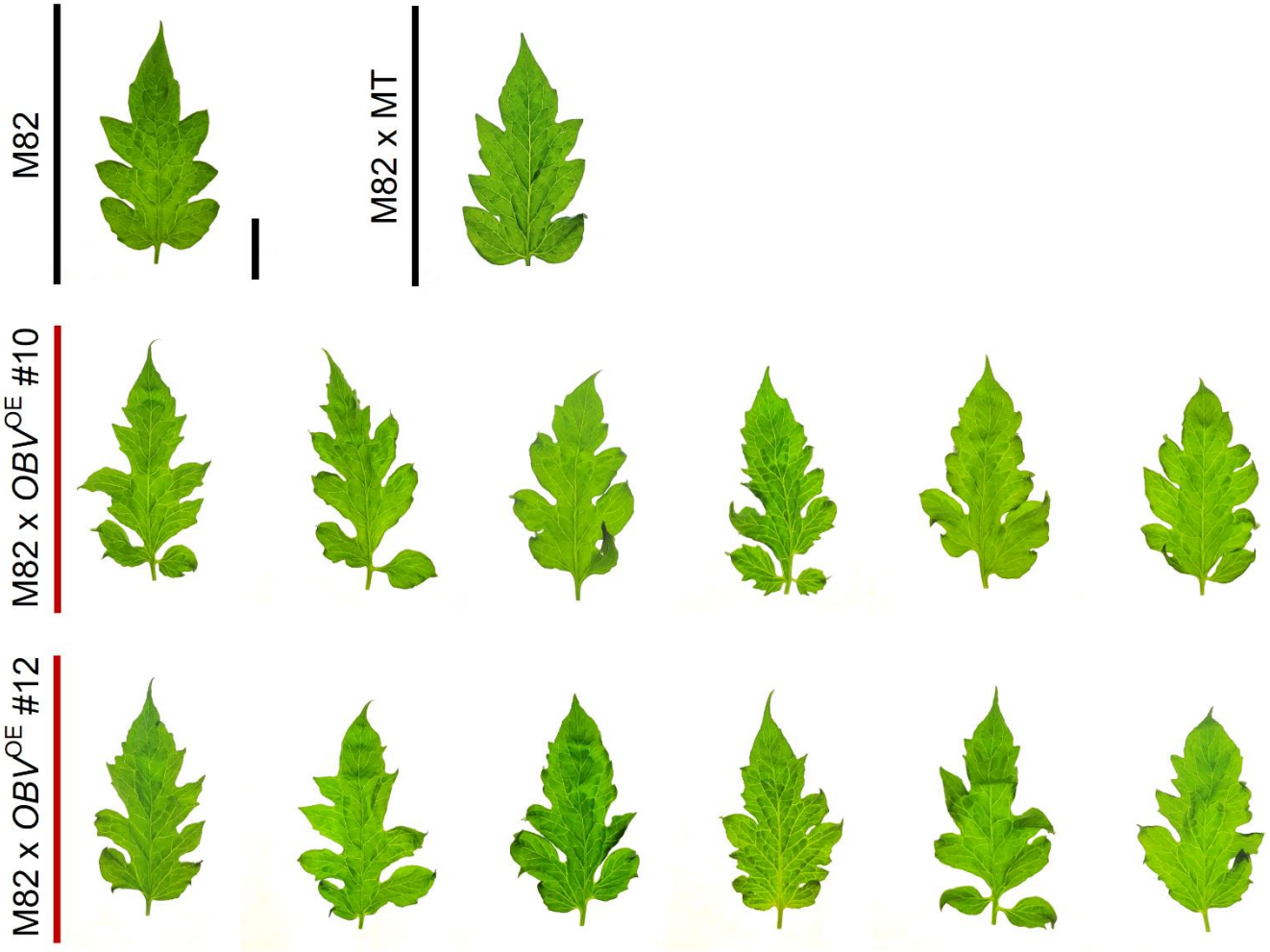

Supplementary Figure 4. Phenotypic variation in leaflets from introgressed lines with *obv-OBV*^{OE} transgene. Representative leaflets of M82 (*obv* mutant), BC2 plants introgressed with *OBV* wild allele from MT and introgressed plants with transgene *obv-OBV*^{OE} #10/#12, BC2.

GENERAL CONCLUSION

Through studies of genotype × phenotype association, we have identified a strong candidate for the *obv* mutation in tomato. The Solyc05g054030 locus has a SNP (A→G) conserved in the third exon of the gene and with high penetrance among homobaric tomato cultivars. The SNP causes the exchange of a histidine residue for arginine at position 135 of the protein. Target gene encodes a zinc-finger transcription factor C2H2 type. We have shown through predictions that the OBV protein has three classic zinc finger domains, which allow interaction in DNA. In the *obv* mutant, the exchange of histidine for arginine led to the elimination of one zinc finger motif, resulting in a probable loss protein function. We complemented the *obv* mutant with the *OBV* functional allele and recovered the clear veins phenotype. In addition, we transformed the *obv* mutant with the mutant *obv* allele and showed that phenotype was not reversed. We also generated interference RNA silenced lines (OBV^{RNAi}), in which we observed the total elimination of BSE in the wild-type background (MT-OBV^{RNAi} #3). Through these assays, we confirmed that *OBV* is responsible for the *obv* mutation in tomato and have thus discovered a key component involved in the development of BSEs in angiosperm leaves. Besides regular the formation of BSEs, *OBV* has a series of pleiotropic effects, such as the control of leaf insertion angle, serration leaf, vein density and fruit shape. We found that *OBV* coordinates the development of BSEs through an auxin-mediated mechanism, specifically by changes in auxin signaling members (ARFs and Aux/IAAs). We identified a potential link between *OBV* and *ARF4*, whereby these two transcriptional regulators could be involved in the same genetic pathway to regulate the formation of BSEs in tomato. The discoveries reported here will assist in the identification of other components of the molecular pathway of BSEs development in leaves. With a better understanding of the regulation and function of BSEs in tomato, we can, in the future, manipulate this structure in other crops of agricultural interest to develop cultivars with better fitness in adverse environmental conditions.